Volume 46 | Number 16 | 21 August 2017 | Pages 4811–5174

Chem Soc Rev

Chemical Society Reviews
rsc.li/chem-soc-rev

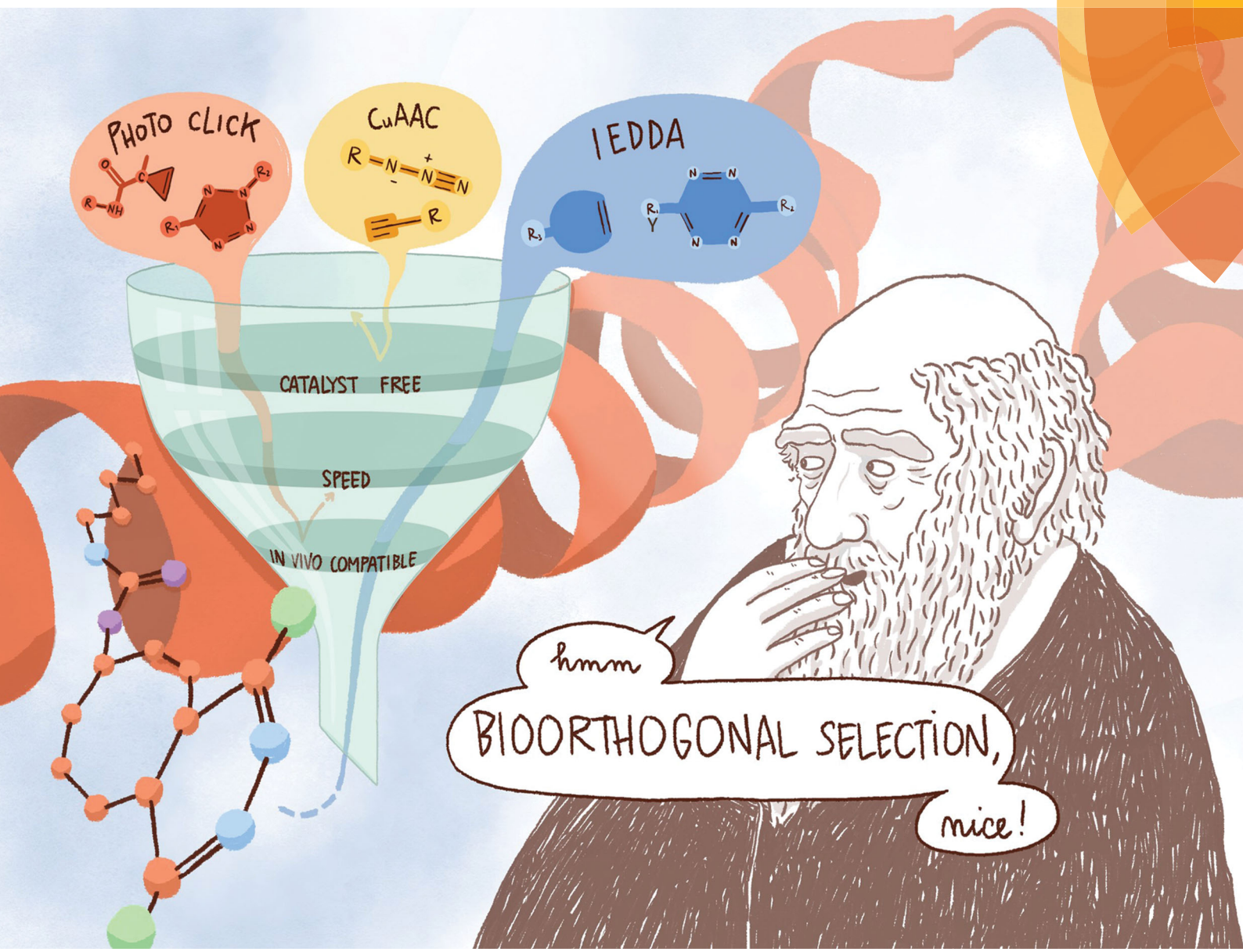

ISSN 0306-0012

ROYAL SOCIETY OF CHEMISTRY

REVIEW ARTICLE
B. L. Oliveira, G. J. L. Bernardes *et al.*
Inverse electron demand Diels–Alder reactions in chemical biology

Chem Soc Rev

REVIEW ARTICLE

View Article Online
View Journal | View Issue

Cite this: *Chem. Soc. Rev.*, 2017, **46**, 4895

Inverse electron demand Diels–Alder reactions in chemical biology

B. L. Oliveira,†*[a] Z. Guo†[a] and G. J. L. Bernardes *[ab]

The emerging inverse electron demand Diels–Alder (IEDDA) reaction stands out from other bioorthogonal reactions by virtue of its unmatchable kinetics, excellent orthogonality and biocompatibility. With the recent discovery of novel dienophiles and optimal tetrazine coupling partners, attention has now been turned to the use of IEDDA approaches in basic biology, imaging and therapeutics. Here we review this bioorthogonal reaction and its promising applications for live cell and animal studies. We first discuss the key factors that contribute to the fast IEDDA kinetics and describe the most recent advances in the synthesis of tetrazine and dienophile coupling partners. Both coupling partners have been incorporated into proteins for tracking and imaging by use of fluorogenic tetrazines that become strongly fluorescent upon reaction. Selected notable examples of such applications are presented. The exceptional fast kinetics of this catalyst-free reaction, even using low concentrations of coupling partners, make it amenable for *in vivo* radiolabelling using pretargeting methodologies, which are also discussed. Finally, IEDDA reactions have recently found use in bioorthogonal decaging to activate proteins or drugs in gain-of-function strategies. We conclude by showing applications of the IEDDA reaction in the construction of biomaterials that are used for drug delivery and multimodal imaging, among others. The use and utility of the IEDDA reaction is interdisciplinary and promises to revolutionize chemical biology, radiochemistry and materials science.

Received 10th March 2017

DOI: 10.1039/c7cs00184c

rsc.li/chem-soc-rev

[a] *Department of Chemistry, University of Cambridge, Lensfield Road, Cambridge, CB2 1EW, UK. E-mail: bljp2@cam.ac.uk, gb453@cam.ac.uk*
[b] *Instituto de Medicina Molecular, Faculdade de Medicina, Universidade de Lisboa, Avenida Professor Egas Moniz, Lisboa, 1649-028, Portugal. E-mail: gbernardes@medicina.ulisboa.pt*
† These authors contributed equally to this work.

B. L. Oliveira

Dr Bruno Oliveira received his PhD from the University of Lisbon in 2012 under the guidance of Profs João Galamba and Isabel Santos. His PhD work involved collaborative visits to the groups of Prof. Roger Alberto (University of Zurich, Switzerland), Prof. Maria João Ramos (University of Porto, Portugal) and Prof. Francisco Blanco (CNIO, Spain). In 2013 he moved to Boston, USA to work with Prof. Peter Caravan (Massachusetts General Hospital/Harvard Medical School) in the development of PET/SPECT nuclear probes for thrombus detection. Since 2015 he has been working with Dr Gonçalo Bernardes, University of Cambridge, where he develops new bioorthogonal methods for protein modification and imaging.

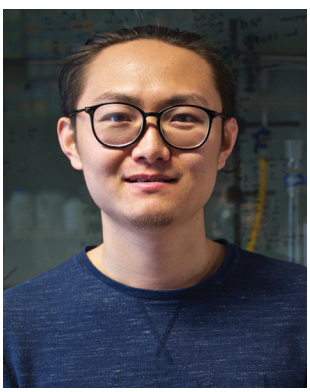

Z. Guo

Zijian Guo received his Bachelor of Science degree in Fundamental Science (Chemistry and Biology) from Tsinghua University (Beijing, China) in 2014. He is currently a PhD candidate under the supervision of Dr Gonçalo Bernardes in the Department of Chemistry, University of Cambridge (Cambridge, UK). His research is focusing on developing novel bioorthogonal chemistry methodologies for protein and cell labelling.

Introduction

Chemical site-selective protein modification has become increasingly popular for probing and controlling protein functions *in vitro* and in living systems. The progressive developments of the last decade in genetic encoding[1] and aqueous chemoselective reactions for protein modification[2] have provided tools to ''decorate'' biomolecules with the desired functionality (affinity probes, fluorophores, reactive tags, post-translational protein modifications – PTMs, *etc.*) without significantly perturbing their native functions (Fig. 1).[3–6]

These transformations have been used, for example, for the spatial and temporal control of biomolecules *in vivo*,[7] for super-resolution imaging,[8] and for the elucidation of the role of post-translational modifications,[9] among others. Ideally, such bioorthogonal reactions must be (1) selective over other potential reactive functional groups present on biomolecules, (2) proceed in aqueous media at (3) near physiological pH and (4) have fast reaction rates at room temperature (or up to 37 °C) using low reactant concentrations, all to ensure high modification efficiency. However, the existing bioorthogonal reactions are not yet able to meet all the bioorthogonal requirements simultaneously, and thus, the specific labelling of biomolecules in their native environment using chemical reactions is still a very challenging task.[1,2]

For instance, the requirement of Cu(I) to catalyse the 1,3 dipolar cycloaddition between azides and alkynes raises toxicity issues for its direct utilization in living cells due to Cu(I)-mediated generation of reactive oxygen species (ROS) from O_2.[16,17] To circumvent this issue, a strain-promoted azide–alkyne cycloaddition version that does not require the use of copper was developed.[18] However, the bioorthogonality of this approach remains an issue, since the cyclooctyne reagents may undergo side reactions with cellular and plasma nucleophiles (*e.g.* the sulphydril side chain of free Cys) limiting the number of targets this approach may be used for.[19,20] Amongst all bioorthogonal reactions developed to date, the [4+2] cycloaddition of 1,2,4,5-tetrazines (s-tetrazines, Tz) and various dienophiles, referred as inverse electron demand Diels–Alder (IEDDA) reaction, is the one that satisfies most of the bioorthogonal criteria (*e.g.* fast, selective, biocompatible and catalyst-free) necessary for use in applications from protein labelling to cancer imaging or materials science.

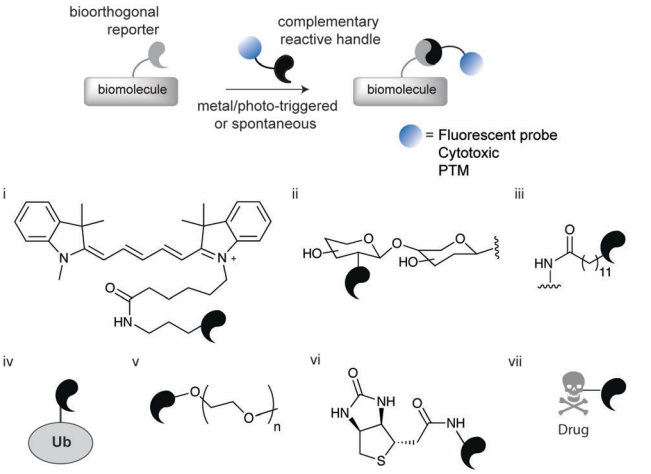

Fig. 1 Schematic representation of chemical biology approaches for protein labelling and/or engineering through bioorthogonal chemistry. The first step involves the introduction of a bioorthogonal reporter on a protein either by genetic, enzymatic or chemical methods. In a second step the bioorthogonal reporter reacts with a molecule of interest bearing a complementary reactive handle. This approach has been used to install a diverse array of molecules for (i) fluorescent labelling,[8] (ii) glycosylation,[10] (iii) lipidation,[11] (iv) ubiquitination,[12] (v) PEGylation,[13] (vi) biotinylation,[14] and (vii) drugs.[15]

In this review, we present recent developments of this fast and robust bioorthogonal reaction and highlight its recent applications in the abovementioned fields. We begin in Section 1 by presenting a general overview of the most representative bioorthogonal reactions with a focus on their general utilities and challenges. The IEDDA reaction has emerged as an important tool for probing the mechanism and function of bioactive molecules in living systems. For such applications, the rate constant is of critical importance as very fast kinetics are required for labelling cellular processes that occur on biological time scales. In this regard, the exceptional speed of the IEDDA reaction revolutionised our ability to explore such demanding applications. In Section 2 the key factors that are behind the fast kinetics of the reaction will be discussed. In addition, the increased use of the IEDDA reaction has triggered the development of new tetrazine and dienophile precursors to create more stable and reactive partners. As such, a brief summary of the methodologies recently described for the synthesis of ''IEDDA precursors'' will be also presented. As the reaction rates depend directly on the reaction partners, Section 3 presents an overview of the most relevant tetrazines and dienophiles, their stability and their reactivity. Another beneficial aspect of using tetrazines as coupling partners is the increase of fluorescence

G. J. L. Bernardes

Dr Gonçalo Bernardes is a Group Leader at the Department of Chemistry, University of Cambridge, U.K. He is also the Director of the Chemical Biology and Pharmaceutical Biotechnology Unit at the Instituto de Medicina Molecular, Portugal. After completing his DPhil degree in 2008 at the University of Oxford, U.K., he undertook postdoctoral work at the Max-Planck Institute of Colloids and Interfaces, Germany, and the ETH Zürich, Switzerland, and worked as a Group Leader at Alfama Lda in Portugal. He started his independent research career in 2013, and his research group interests focus on the development of site-selective chemical protein modification for basic biology and drug development. He is a Royal Society University Research Fellow and the awardee of a Starting Grant from the European Research Council (TagIt).

observed after bioorthogonal reaction, resulting in a ''turn-on system'' useful for example for cell imaging applications. In this section, we also provide some representative examples of highly fluorogenic tetrazines for IEDDA labelling. Over the years numerous tetrazine and dienophile functionalities have been incorporated into proteins *via* genetic, enzymatic and chemical approaches. These methods are presented and discussed in Section 4. In Section 5 we present some selected examples where the appealing features of the tetrazine ligation provide a step-change in biological applications beyond the reach of other bioorthogonal chemical reactions. One of the most challenging and important applications of the tetrazine ligation is the selective labelling of biomolecules inside living organisms for imaging and therapy using pretargeting approaches. These applications, which are extensively explored by radiochemists, are summarized in Section 6. The major focus of bioorthogonal chemistry in the past two decades has been largely centred on 'bond formation' reactions for protein modification. Just very recently, focus has been placed on reactions that can instead cleave specific bonds under bioorthogonal conditions. Section 7 will focus on recent developments in IEDDA elimination reactions for accurate spatiotemporal control over protein function and drug activity. Section 8 outlines the potential of the IEDDA reactions in the development of biomaterials for applications in biology and medicine such as 3-D cell culture, drug delivery, multimodal imaging and clinical diagnostics. Finally, we draw conclusions and present a brief prospect of the role of IEDDA reactions in the field of bioorthogonal chemistry.

1. Meeting the candidates: a brief introduction to bioorthogonal chemistry

Arguably the most quoted example of a click reaction is the Cu(I)-catalysed [3+2] azido–alkyne cycloaddition (CuAAC) between an azide and alkyne, which was discovered independently by Sharpless *et al.* and Meldal *et al.* (Fig. 2i).[16,17] Since these initial findings the CuAAC has been shown to be suitable for protein labelling in living systems, however, the wide use of CuAAC chemistry has been hindered by the potential toxicity induced by copper. In fact, Bertozzi *et al.* reported that mammalian cells could only survive to low concentrations (<500 μM) of Cu(I), leading to very slow CuAAC reaction rates at such concentrations that are not compatible with biological time scales. In addition, Zebrafish embryos also exhibited a similar sensitivity to Cu(I) limiting its use for *in vivo* applications.[21] To improve the biocompatibility of the CuAAC reactions, the toxicity of Cu(I) was addressed by use of water-soluble Cu(I) ligands that stabilize the metal oxidation state and so, prevent the release of free copper ions that generate toxic reactive oxygen species.[22,23] Notably, these biocompatible ligands have allowed the labelling

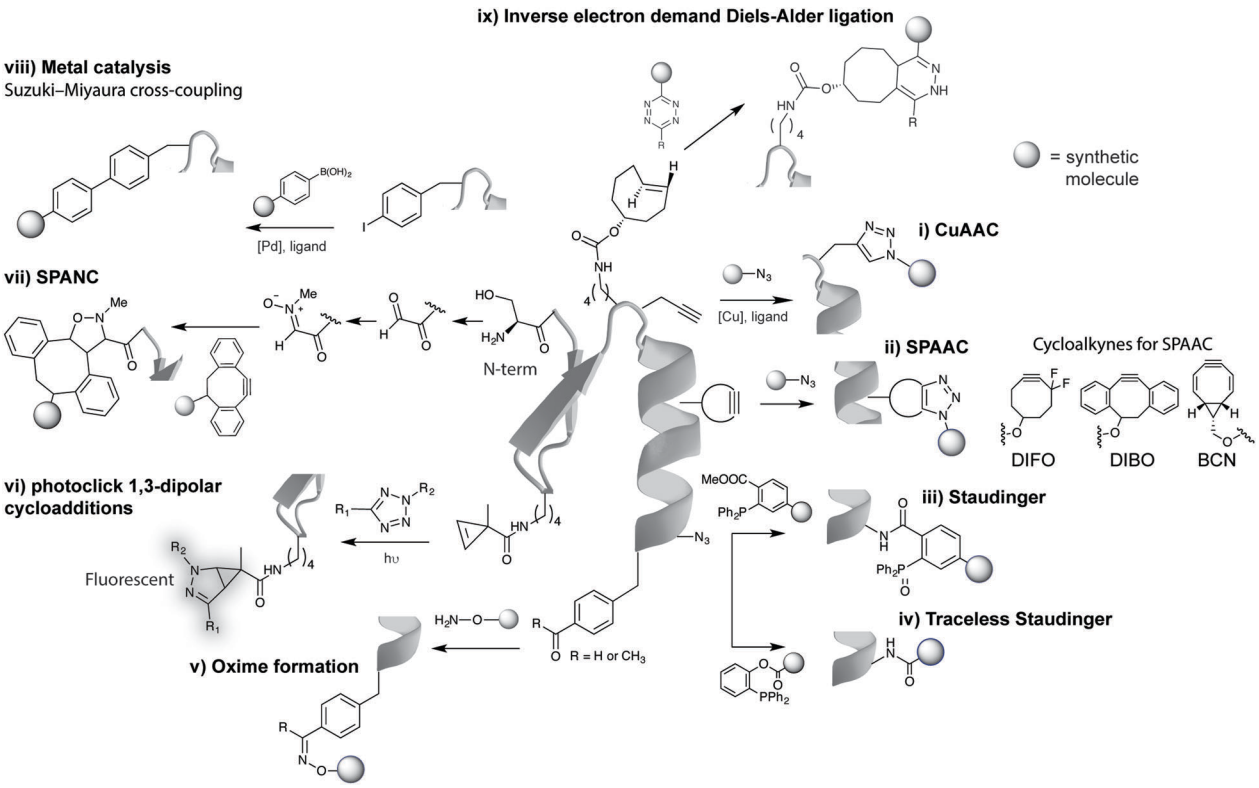

Fig. 2 Representative examples of bioorthogonal reactions for protein modification. (i) CuAAC,[22,23] (ii) SPAAC,[24] (iii) Staudinger,[25] (iv) traceless Staudinger,[26,27] (v) hydrazones and oximes formation,[29] (vi) photoclick reactions,[30,31] (vii) strain-promoted alkyne-nitrone cycloaddition (SPANC) reactions,[32] (viii) transition metal catalysis,[33] and (ix) IEDDA reactions. Reactive handles installed site selectively into proteins by genetic encoding techniques except for (vii).

of glycans in developing zebrafish embryos.[23] The Cu(I) catalyst toxicity could be also obviated by use of strained alkyne substrates. The strain-promoted [3+2] azide–alkyne cycloaddition (SPAAC) developed by Bertozzi *et al.* in 2004 proceeds under physiological conditions without the need for a catalyst, however, in relatively slower kinetics when compared to the Cu(I) catalysed reaction (Fig. 2ii).[18] Further enhancements in the rate constant of SPAAC additions have been reported using novel cyclooctyne analogues (*e.g.* DIBO, DIFO and BCN).[24] The use of azides as chemical reporters has been also explored by the Staudinger ligation with phosphines (Fig. 2iii).[25] Whereas azides produce a stable triazole linkage in CuAAC and SPAAC reactions, the Staudinger ligation generates a stable amide bond. Soon after the publication on the Staudinger ligation, Raines *et al.*[26] and Bertozzi *et al.*[27] simultaneously reported the so-called traceless Staudinger ligation (Fig. 2iv). Although this click reaction has sufficient biocompatibility to be performed in living systems it suffers from phosphine oxidation and very slow kinetics.[28] A wider list of bioorthogonal reactions includes other chemical transformations such as aldehyde/ketone-amine ligations[29] (Fig. 2v), photoclick 1,3-dipolar cycloadditions between tetrazoles and substituted alkenes[30,31] (Fig. 2vi) and, strain-promoted cycloadditions involving nitrones and alkynes[32] (Fig. 2vii). These bioorthogonal reactions, however, have been used mainly for *in vitro* bioconjugation because of the reaction conditions (*e.g.* requirement of an acidic pH and a light source in the case of ketones/aldehydes and tetrazoles, respectively). Recently, transition metal catalysis has been considered a powerful tool for the continued expansion of the bioconjugation toolkit (Fig. 2viii). Several emerging examples for forming new carbon–carbon bonds have been described including Suzuki[33] and Sonagashira couplings[34] or olefin metathesis.[35] This "new class" of bioorthogonal reagents have been explored for labelling of proteins *in vitro* and on the cell surface.[36]

A breakthrough was achieved with the IEDDA reaction between tetrazines and strained dienophiles (Fig. 2ix), arguably the most optimal bioorthogonal reaction developed to date. A general overview of the features of the abovementioned bioorthogonal chemical reactions is presented in Fig. 3 with a focus on the general utility of each reported bioorthogonal reaction in terms of their reaction rates and labelling efficiency but also their various biological applications. The non-metal nature and physiological pH makes IEDDA more cell-friendly than CuAAC and oxime ligation. Superfast kinetics (10 000-fold

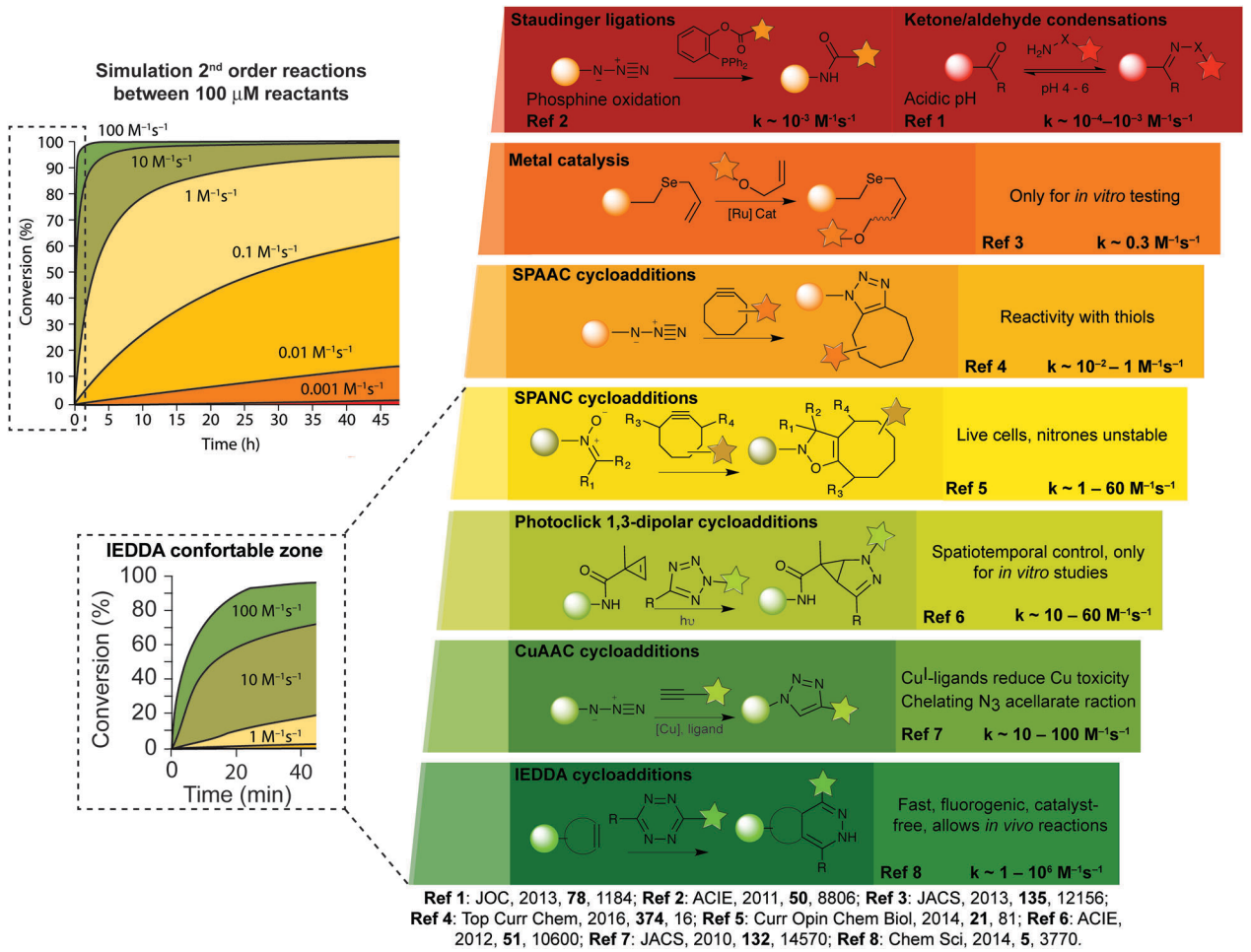

Ref 1: JOC, 2013, **78**, 1184; **Ref 2**: ACIE, 2011, **50**, 8806; **Ref 3**: JACS, 2013, **135**, 12156; **Ref 4**: Top Curr Chem, 2016, **374**, 16; **Ref 5**: Curr Opin Chem Biol, 2014, **21**, 81; **Ref 6**: ACIE, 2012, **51**, 10600; **Ref 7**: JACS, 2010, **132**, 14570; **Ref 8**: Chem Sci, 2014, **5**, 3770.

Fig. 3 Examples of bioorthogonal reactions useful for bioconjugation and general comments about their utility and challenges.

faster than CuAAC) allows IEDDA to proceed with low concentrations, similar to the concentrations of intracellular proteins. This click reaction endows itself an irreplaceable tool to study cellular functions and dynamic processes. Indeed, this reaction meets the need for demanding biological applications, *i.e.*, has high selectivity, is compatible with mild reaction conditions in water and has impressive fast kinetics. Such assets have never been achieved with other site-selective reactions, highlighting the importance of IEDDA ligations in bioorthogonal chemistry.

2. Principles of IEDDA reaction

2.1 Mechanism

Diels–Alder [4+2]-cycloaddition describes the reaction between a diene (*e.g.* 1,2,4,5-tetrazines) and a dienophile (alkene or alkyne) to form a six-membered ring in a π4s + π2s fashion (Fig. 4a), *via* suprafacial/suprafacial interaction of 4π-electrons of the diene with the 2π-electrons of the dienophile (Fig. 4b). In contrast to a normal electron demand Diels–Alder reaction, where an electron-rich diene reacts with an electron-poor dienophile, in an inverse-electron-demand Diels–Alder reaction (IEDDA), an electron-rich dienophile reacts with an electron-poor diene (Fig. 4b). The ability of tetrazines to react with unsaturated compounds was first revealed in 1959 by Lindsey *et al.*[37] This Diels–Alder reaction proceeds *via* the 1,4-addition of the –C═N–N═C– diene system of the tetrazine to an appropriate alkene, yielding a highly strained bicyclic intermediate (Fig. 4a). Upon the evolution of 1 equivalent of nitrogen, the adduct undergoes a retro-Diels–Alder reaction to afford the corresponding 4,5-dihydropyridazine, which either isomerises to the corresponding 1,4-dihydro-isomers or is oxidized to give a pyridazine product (Fig. 4a). Alkyne dienophiles directly yield the respective pyridazine upon reaction.

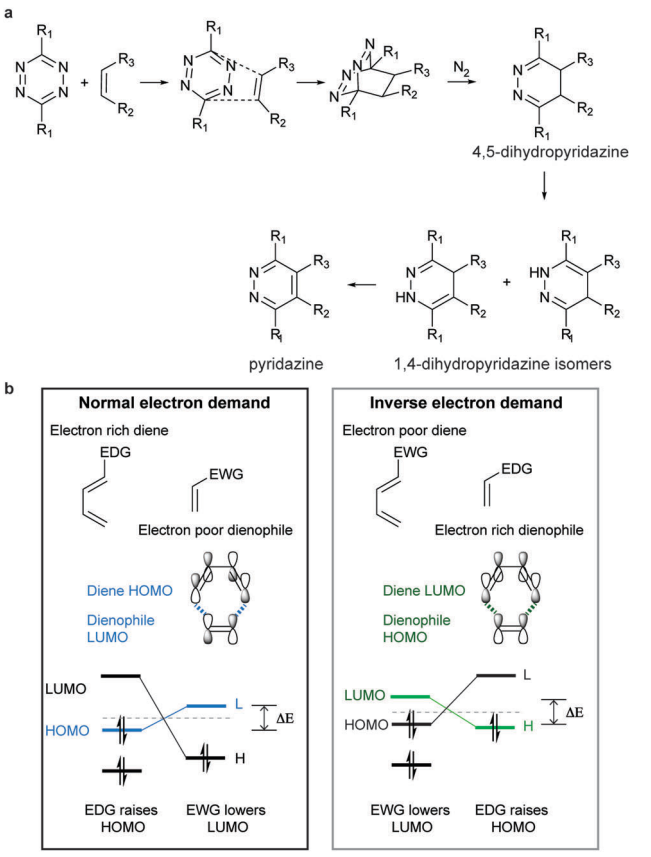

Fig. 4 Mechanism of IEDDA reaction. (a) Schematic representation of the reaction between a dienophile and a tetrazine. (b) Frontier molecular orbital of normal and inverse electron demand Diels–Alder reaction. EDG = electron-donating group, EWG = electron-withdrawing group.

2.2 Features for reactivity of IEDDA reactants

Based on the frontier molecular orbital theory (FMO), the IEDDA reaction kinetics is governed by the energy gap between the corresponding HOMO and LUMO of the reactants (Fig. 4b). In particular, any pairs of diene/dienophile with a smaller $HOMO_{dienophile}$–$LUMO_{diene}$ energy difference would react faster in IEDDA reactions. Since the earlier comprehensive kinetics studies in organic solvents performed by Sauer and Boger, efforts have been made to find fast IEDDA reactants for rapid bioorthogonal reaction in aqueous media. Indeed, by fine-tuning the tetrazine and dienophile pairs considerable rate enhancements and bioorthogonality have been achieved. The different factors tuning the IEDDA kinetics are discussed as follows.

2.2.1 Electronic effects of the substituents in the IEDDA partners. Electron-donating groups (EDG) raise both HOMO and LUMO energy of the cycloaddends, whereas electron-withdrawing groups (EWG) act conversely. Therefore, by electronically tuning the cycloaddends it is possible to manipulate the $LUMO_{diene}$–$HOMO_{dienophile}$ energy gap and enhance their reactivity. In terms of the diene partner, electron deficiency lowers the $LUMO_{diene}$ energy, accelerating the IEDDA reaction (Fig. 5a). Early efforts from Boger *et al.* compared the reactivity of several 3,6-disubstituted-1,2,4,5-tetrazines towards *N*-vinyl

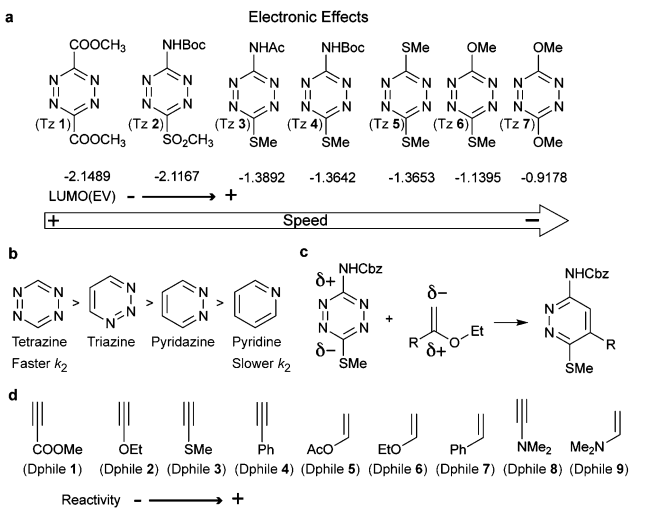

Fig. 5 (a) Dependence of reactivity against LUMO energy of tetrazine. (b) Reactivity of heterocyclic ring bearing various numbers of nitrogen atoms. (c) Electronic effects on regioselectivity. (d) Electronic effects on olefinic and acetylenic dienophiles.

pyrrolidinone. Consistent with the experiments, their computational studies revealed that the more reactive tetrazines always have a lower LUMO energy (Fig. 5a).[38,39] For instance, tetrazines attached to carboxylate EWGs (Tz **1**) present faster kinetics than tetrazines bearing methoxy groups (Tz **7**, Fig. 5a).[38,39] The same effect is observed for tetrazines with stronger EWGs (6-pyrimidyl), which present faster kinetics than methyl-bearing tetrazines (EDGs).[40,41] Similarly, decreasing the electron density of the tetrazine ring by substituting positions C3 and C6 with aromatic heterocycles with different pendant EWGs increases the reaction rate against dienophiles.[42,43] The electronic effect of the number of N-heteroatoms in the heterocyclic ring was also studied by Sauer *et al.*[44] The authors showed that tetrazine reacts significantly faster than, for example, triazine (K_2 tetrazine > K_2 triazine > K_2 pyridazine > K_2 pyridine; Fig. 5b).[44] Importantly, the steric substituent effects are approximately the same for all the heterocycles.[44]

Very recently, 1,2,4-triazines have been described as a new class of bioorthogonal reagent for IEDDA reactions, however, they are less reactive than 1,2,4,5-tetrazines.[45,46] Boger *et al.* and Saez *et al.* also showed that the electronic properties of the substituent not only influence tetrazine's reactivity but also affect the regioselectivity of the cycloadditions (Fig. 5c). Accordingly, the authors demonstrated experimentally and theoretically that it is possible to predict the product formation by analysing the partial net charge on C3 and C6 positions (Fig. 5c).[38,39,47]

An even more pronounced impact on the IEDDA kinetics arises from the type of dienophile. In this case, dienophiles with electron-rich substituents are preferred to achieve fast kinetics. So far, a large number of papers, mostly by Sauer and co-workers,[48] have been devoted to discussing the reactivity of different substituted unstrained dienophiles and several principal rules have been summarized based on the electronic effect.[49–55] Briefly, olefinic dienophiles surpass acetylenic dienophiles in terms of reaction rates, (Dphile **1–4** *versus* Dphile **5–7**, Fig. 5d) due to the increased electron withdrawing character of the triple bond, therefore lowering the energy of the HOMO.[49,55] Introduction of EDGs, such as dialkylamino, make enamines (Dphile **8**) and ynamines (Dphile **9**) highly reactive dienophiles. Similar dependence between electronic properties and kinetics are also observed with phenylacetylenes (Dphile **4**) and styrene (Dphile **7**) if EDGs are introduced in either the phenyl group or in the olefinic/acetylenic part.[49,55]

2.2.2 Strain effect. Independent from the electronic effect of the dienophile substituents, ring strain plays the most important role in the IEDDA reaction rate by raising the $HOMO_{dienophile}$. Sauer *et al.* described the reaction kinetics between various tetrazines and a number of dienophiles and quantitatively demonstrated that the rate constant increases with increasing ring strain according to the following order: cyclopropene > cyclobutene > cyclopentene > cyclohexene > cyclooctene (Fig. 6a). Furthermore, it was observed that the use of *trans*-cyclooctene (TCO) as a precursor gave a tremendous rate difference compared to *cis*-cyclooctene and most importantly to the other cyclic alkenes with higher ring strain (*e.g.* cyclopropene).[56] This higher reactivity is attributed to a 'crown' conformation

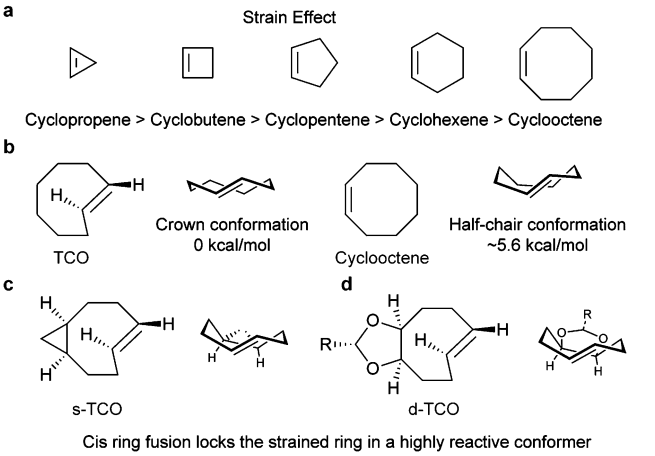

Fig. 6 Influence of the strain effect on the IEDDA reaction. (a) Degree of ring strain along a series of cyclic alkenes. Similar strain effects are also observed for cyclo-enamines and cyclic enol ethers.[49] (b) The crown conformation of TCO makes it 7 orders of magnitude more reactive than *cis*-cyclooctene towards 3,6-bismethyoxycarbonyl-1,2,4,5-tetrazine and 3,6-bistrifluoromethyl-1,2,4,5-tetrazine.[56] (c and d) *Via* strained ring fusion, the crown conformation was furthered locked, resulting in rate enhancement against TCO.

adopted by TCO, which is lower in energy than the 'half-chair' conformation of *cis*-cyclooctene as predicted by *ab initio* calculations (Fig. 6b). Indeed, computational studies have emerged as an important tool for understanding and predicting the reactivity of IEDDA partners. Studies performed by Houk *et al.* revealed that strained dienophiles are more reactive due to their pre-distorted conformation towards the transition structures. Therefore, less distortion energies are needed for the dienophile to react.[57,58] Additional insights on designing more reactive dienophiles were obtained with the help of computers. Based on *ab initio* calculations, the fusion of a cyclopropane ring with *trans*-cyclooctene to form s-TCO was proposed as a strategy to induce the formation of a non-crown conformer which was expected to increase the reactivity towards tetrazines (Fig. 6c). The resulting more highly strained, fused TCO was found to have a lower computed barrier, which makes the reaction 160 times faster than the original TCO, as verified by experimental $\Delta\Delta G^{\ddagger}$ (3.0 kcal mol^{-1}) and calculated $\Delta\Delta G^{\ddagger}$ (3.34 kcal mol^{-1}).[59] Similarly, in order to increase the stability and hydrophilicity, while maintaining the ring strain, a *cis*-dioxolane-fused TCO (d-TCO) was proposed to display high reactivity towards tetrazine (Fig. 6d). Compared with the original TCO, 27-fold rate enhancement was observed towards diphenyl-s-tetrazine, which is in good alignment with the computationally predicted $\Delta\Delta G^{\ddagger}$.[60] Similarly, a high dependence between the degree of ring strain and reactivity is observed for the IEDDA reaction of cyclooctynes and tetrazines. As previously described for cyclooctenes there is a decrease in the activation energy by raising the HOMO of the cyclooctyne-dienophile.[61]

2.2.3 Stereochemistry effect. Recently, stereochemistry of strained dienophiles also emerged to be a crucial determinant towards the reaction rate. The axial isomer of a functionalized TCO (RO-TCO) was found to be more reactive than the corresponding equatorial isomer by 1.1 kcal mol^{-1} ($\sim 4\times$) (Fig. 7a).[60,62–65]

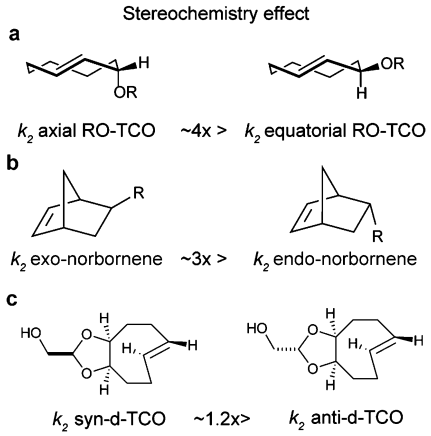

Fig. 7 Effect of stereochemistry on stereoisomers of (a) TCO, (b) norbornene and (c) d-TCO.

The influence of the stereochemistry is also presented in others dienophiles. The *exo*-norbornene reacts with tetrazines 3 times faster than the *endo* one (Fig. 7b).[66] The same trend is observed for syn-d-TCO that has a slightly higher rate constant (1.2×) compared with the anti-diastereomer (Fig. 7c).[60] Finally, the cyclooctyne *endo*-BCN isomer is slightly faster than its *exo* isomer in reaction with tetrazines.[67]

2.2.4 Steric effect. In the dienophile, any substituent exchanging hydrogen, in principle, results in an increase of the steric effects hampering its reactivity. Therefore, terminal alkenes and alkynes dienophiles are more reactive than the corresponding internal ones. Consequently, introducing EDGs into dienophiles needs to compensate for the impeding steric effects, which sometimes leads to only comparable or even lower reactivity.[49] The reactivity of tetrazines can be similarly altered *via* steric modifications. For instance, several groups have reported that mono substituted tetrazines participate in IEDDA reactions with faster kinetics than di-substituted tetrazines, even with strong EWG.[40,44,68] This important observation has been used to design mutual orthogonal IEDDA reactants. In a pioneering study Devaraj group elegantly demonstrated that a mono-substituted tetrazine undergoes IEDDA ligation with TCO more than 30 times faster than cyclopropene (Fig. 8a). In contrast, if the tetrazine is substituted with a bulky *tert*-butyl group, the unfavourable steric repulsion between TCO and the "bulky tetrazine" slows the reaction, leaving the cyclopropene tag with faster reaction rates.[69] In a concurrent study, H-tetrazine (H-Tz) was proved to be more reactive than Me-tetrazine (Me-Tz),[62] due to electronic effects, and mostly, due to additional distortion energies from the methyl group. Thus, under certain reaction conditions and time scale, Lemke *et al.* showed that some dienophiles could react quickly with the reactive Me-Tz but not with the Met-Tz. Specifically, it was observed that SCO exclusively reacts with H-Tz, due to steric constrains, while TCO reacts with nearly both tetrazines (Fig. 8b). The authors applied these exclusive reactivities for the dual labelling of cell surface proteins (more details in Section 5).[8] Importantly, the orthogonality of this system to azides renders multi-colour labelling of biological systems possible *via* Diels–Alder and SPAAC click reactions.[8] Recent DFT studies revealed

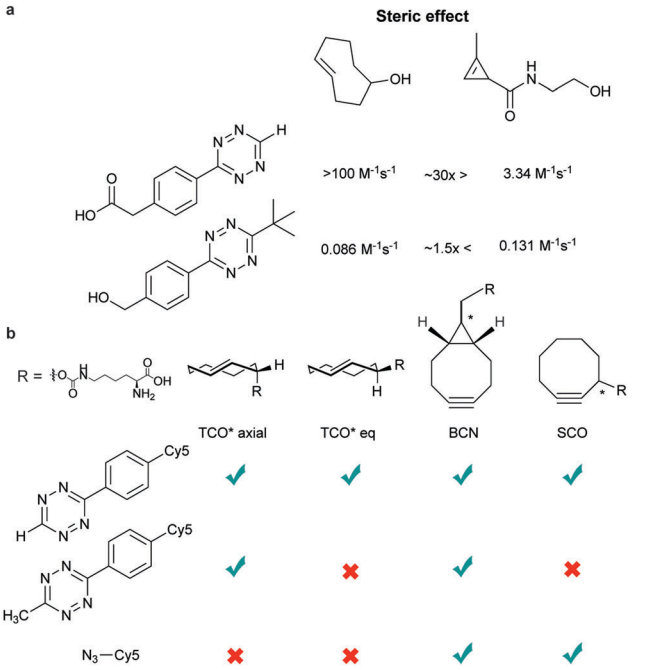

Fig. 8 Influence of the steric effect on the IEDDA reaction (a) bulky tetrazine reverse the reactivity of TCO and cyclopropene compared with less bulky tetrazine. (b) Reactivities of TCO*, SCO, and BCN with azide, H-Tz, and Me-Tz. By fine-tuning the reaction partners mutual bioorthogonality could be obtained.

that SCO undergoes normal electron demand Diels–Alder reactions with both H-Tz and Me-Tz instead of inverse reactions.[62] These results should be highlighted since the type of reaction may switch upon minimal chemical changes, which may have direct consequences for the rational design of orthogonal dienophiles, in this particular case, or in the optimization of the IEDDA reaction.[62]

2.2.5 Solvent and pH effect. Protic solvents are described to accelerate the IEDDA reaction and this effect is even more pronounced when reactions are performed in water. This effect is attributed to the stabilized interaction between the activated complex and water but also to an enhanced hydrophobic interaction between cycloaddends, which is facilitated in water.[70] Additionally, hydrogen-bonding with tetrazines, similar to electron-withdrawing substituents, induces polarity and lowers the HOMO–LUMO energy gap, enhancing the reaction rate.[42,54,71,72] It should be noted that the reaction solvent may also affect the product formation in IEDDA reactions. For instance, when ketene acetals are used as dienophiles, increasing polarity of the solvent favours the *meta*-isomer whereas ethanol exclusively affords the *ortho*-isomer.[54] The formation of stable hydrogen-bonded complexes between tetrazine and protic solvents is also described to guide the reaction route.[73] The dependence of reaction rate on pH was found to be minor. A lower pH is expected to accelerate the reaction possibly by protonation of the pyridine rings.[40,71]

2.3 Synthesis of tetrazine derivatives

Conventionally tetrazines are obtained *via* the synthesis of dihydrotetrazines by reacting the appropriate precursors

(*e.g.* aromatic/aliphatic nitriles and imidoesters) with hydrazine, followed by oxidation to afford the reactive tetrazine cores. Since recently, new methodologies based on carbon–carbon bond formation have been explored in the generation of various tetrazines, especially tetrazines functionalized with fluorescent dyes. In the following sections these methods are presented and discussed in detail.

2.3.1 Classic methods for the preparation of tetrazines. A well-developed method for the synthesis of tetrazines was first reported by Adolf Pinner in 1893.[74] Typical Pinner conditions involve the reaction of imidoesters with hydrazine, leading to the formation of amidrazone intermediates, which undergo further reaction with excess of hydrazine to give dihydrotetrazines and finally tetrazines by oxidation (Fig. 9a).[74] Another well-established, and probably, the most widely used method for the synthesis of tetrazines is the condensation of two aromatic or alkyl nitriles with hydrazine (Fig. 9b(i)). Hydrazine, depending on the type of starting materials, is often used as the hydrate or anhydrous forms with THF or ethanol as co-solvents. Although useful, this nitrile-based route is however limited if the aim is to prepare disubstituted asymmetric tetrazines since a statistical mixture of products of difficult purification is obtained (Fig. 9b(ii)). By using a large excess of one of the components, asymmetric tetrazines could be afforded, however, still with poor yields (<22%) and on relatively small scales.[40] Of note, the condensation reaction of one nitrile and formamidine acetate results in the formation of monosubstituted tetrazines (Fig. 9b(iii)). The addition of sulphur as catalyst is also being extensively explored for the synthesis of both symmetric and asymmetric tetrazines and leads to improved reaction yields (60–70%, Fig. 9b(iv)).[75,76] Sulphur is described to react first with hydrazine to give NH_2NHSH, which serves as an active nucleophile towards nitriles, generating a reactive intermediate that eliminates H_2S to form the dihydrotetrazine core.[43,75,77] Importantly, although these conditions have been successfully used for the synthesis of aromatic tetrazines, very low yields are reported in the case of alkyl tetrazines. Alternatively, *N*-acetylcysteine was successfully tested as catalyst for the synthesis of tetrazines possibly through the formation of amidrazone intermediates.[78]

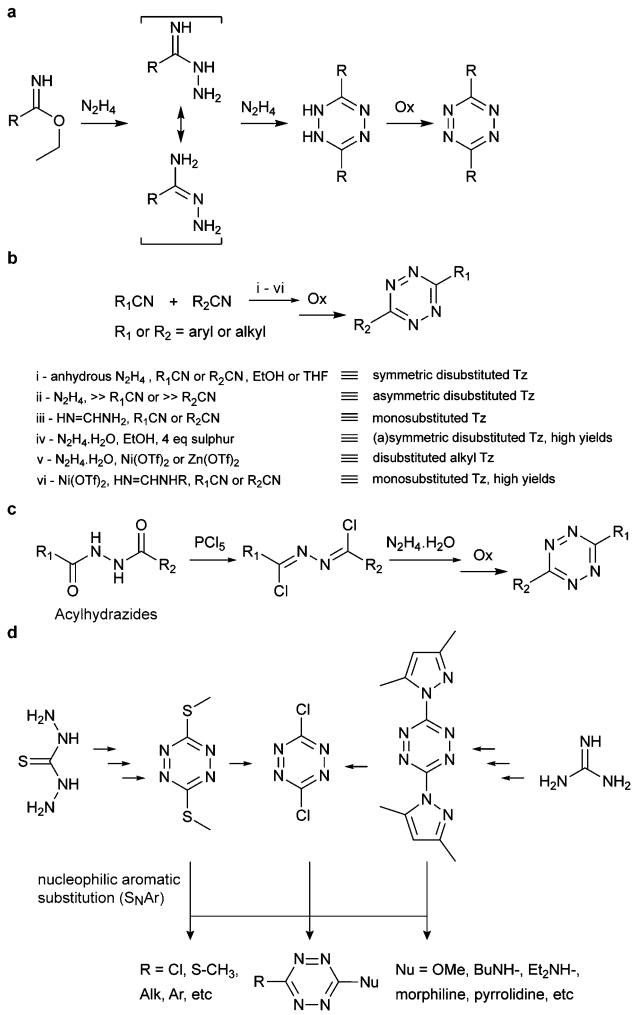

Fig. 9 Classic synthesis routes for tetrazines using (a) imidoesters, (b) nitriles, (c) acylhydrazides and (d) nucleophilic aromatic substitution.

Recently, new synthetic routes have been explored for the synthesis of tetrazines. Devaraj *et al.* reported the use of Lewis acids as catalysts for the activation of nitriles, including unreactive alkyl nitriles, by coordinating to the nitrile and promoting the nucleophilic addition of hydrazine. It was shown that nickel and zinc triflates allowed the one-pot synthesis of both symmetric and asymmetric dialkyl tetrazines in good yields (Fig. 9b(v)).[79] $Ni(OTf)_2$ catalyst was later used for the preparation of asymmetric monosubstituted tetrazines in high yield (~75%) on gram-scale synthesis (Fig. 9b(vi)), whereas sulphur-promoted reaction only resulted in yields lower than 20%.[80] Importantly, this method was applied in the synthesis of coumarin-tetrazine and BODIPY–tetrazine fluorescent probes.[81,82] Although high yields were achieved, this one-step synthesis method has limitations of substrate scope. The hydrazine and heating conditions are not compatible with several functional groups that are susceptible to either nucleophilic addition or reduction, such as carbonyls and alkyl halides. To overcome these limitations acylhydrazides have been used for the synthesis of (a) symmetric substituted tetrazines, in a stepwise reaction first reported by Stolle *et al.*, involving the synthesis of 1,2-dichloromethylene hydrazines by treatment with PCl_5 and subsequent condensation with hydrazine and oxidation (Fig. 9c).[83,84] With this general methodology, both symmetric and asymmetric tetrazines with EWGs and aliphatic substituents were synthesized with modest yields.[85] Microwave irradiation has also been proved to assist the formation of tetrazine.[86] A further optimization on the condensation of 1,2-dichloromethylene hydrazine with hydrazine monohydrate by the same group showed that microwave irradiation could reduce the reaction time from 5–16 h to 30 mins with an extra 10–20% yield increase, compared to refluxing conditions.[42] Another alternative method commonly used for tetrazine synthesis is the nucleophilic aromatic substitution (S_NAr) starting from the relevant precursors (*e.g.* methylthio-1,2,4,5-tetrazine, 3,6-dichloro-1,2,4,5-tetrazine, 3,6-(3,5-dimethylpyrazolyl)-1,2,4,5-tetrazine, Fig. 9d).[87]

2.3.2 Modern methods for tetrazine synthesis by C–C bond formation. As mentioned, a relatively small number of asymmetric substituted-tetrazines have been reported due to the difficulty of their preparation and purification. To overcome these limitations transition metal-catalysed coupling reactions have been used to prepare tetrazines by C–C bond formation directly onto the tetrazine core or onto a number of different substituents attached to tetrazines (see next section for further details). Both approaches have been particularly useful for introducing multi-functionality on tetrazines such as fluorescent probes or functional groups (*e.g.* amino groups) for further coupling reactions, which is desirable for biological and material chemistry. The first reported cross-coupling reaction on tetrazines was *via* the Sonogashira coupling reaction of various chlorotetrazines with acetylene derivatives in the presence of $Pd(PPh_3)_2Cl_2$ and CuI (Fig. 10a).[88] The starting materials were prepared in moderate to good yields by selective displacement of one chlorine atom from the commercial available 3,6-dichlorotetrazine by different nucleophiles. The Sonogashira coupling products were obtained in low, moderate or good yields (30–65%) depending on the conjugated substituents. Indeed, success of the reaction depends on the electron-donating properties of the ring substituent. More electron-deficient chlorotetrazines tend to result in tetrazine decomposition.

Negishi coupling of chlorotetrazines with hexynylzinc chloride also affords coupling products with 30% yield (Fig. 10b).[88] Under Suzuki-like and Stille-like conditions Guillaumet *et al.* reported the reaction of 3-methylthio-1,2,4,5-tetrazine derivatives with boronic acids and organostannane precursors (Fig. 10c and d).[89] Yields of 30–70% were achieved under microwave conditions for both reactions. This Pd-catalysed cross-coupling reaction represents the first of few methods to construct asymmetrical tetrazines using vinyl, aryl and heteroaryl substituents.[89] Recently, Pd-catalysed Stille cross coupling reactions were developed for the derivatization of tetrazines at positions C3 and C6 with fluorescent probes (Fig. 10e). Wombacher *et al.* identified 3-bromo-6-methyl-1,2,4,5-tetrazine as a suitable building block for coupling with protected fluorophore-organotin derivatives, giving yields around 20%. Interestingly, this method is applicable for fluorescein and Oregon green derivatives but not for rhodamine or Si-rhodamine dyes.[90] The replacement of the chlorine on tetrazines by nucleophilic aromatic substitution using alkyllithium is another alternative method developed by Tang *et al.* (Fig. 10f).[91] A number of tetrazine derivatives have been also prepared by Audebert *et al.* by nucleophilic substitution of chlorotetrazines with ethynyl compounds in the presence of n-BuLi, although in low yields (~12%).[92]

2.3.3 Coupling reaction on tetrazine substituents. Considering the high need for the preparation of fluorescent-tetrazine conjugates, various cross coupling reactions have been tested for the direct conjugation of 1,2,4,5-tetrazines to fluorescent dyes. Recently, Devaraj *et al.* introduced an elimination-Heck cascade reaction (Fig. 11a) for such purposes. In the presence of $Pd_2(dba)_3$ and a co-ligand (iron complex) alkenyl highly fluorogenic tetrazines were afforded in good to excellent yields bearing popular dyes such as xanthene and BODIPY fluorophores.[93] At the same time, Wombacher *et al.* also managed to synthesize tetrazine fluorophores by Sonogashira cross-coupling reactions (Fig. 11b). With $PdCl_2(PPh_3)_2$, and Cu(I) as catalysts, tetrazine ethynyl fluorophores were synthesized in good yield (64% and 69%) and on a relatively large scale.[94] Suzuki- or Heck-type cross-coupling reactions were also used for synthesizing tetrazine-phenoxazine derivatives with reasonable yields (Fig. 11c and d).[95] Recently, Friedel–Crafts alkylation was also developed

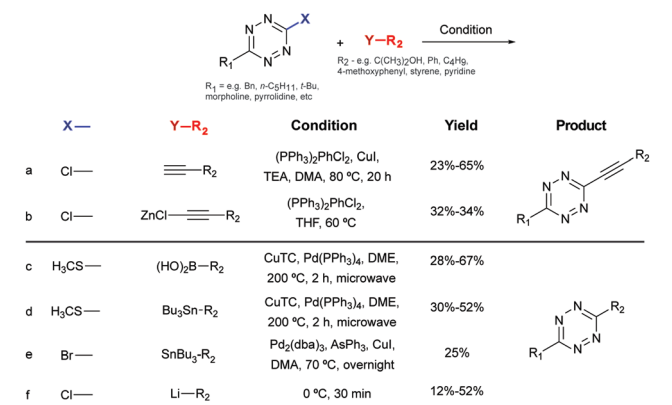

Fig. 10 Tetrazine crosslinking reactions based on C–C bond formation.

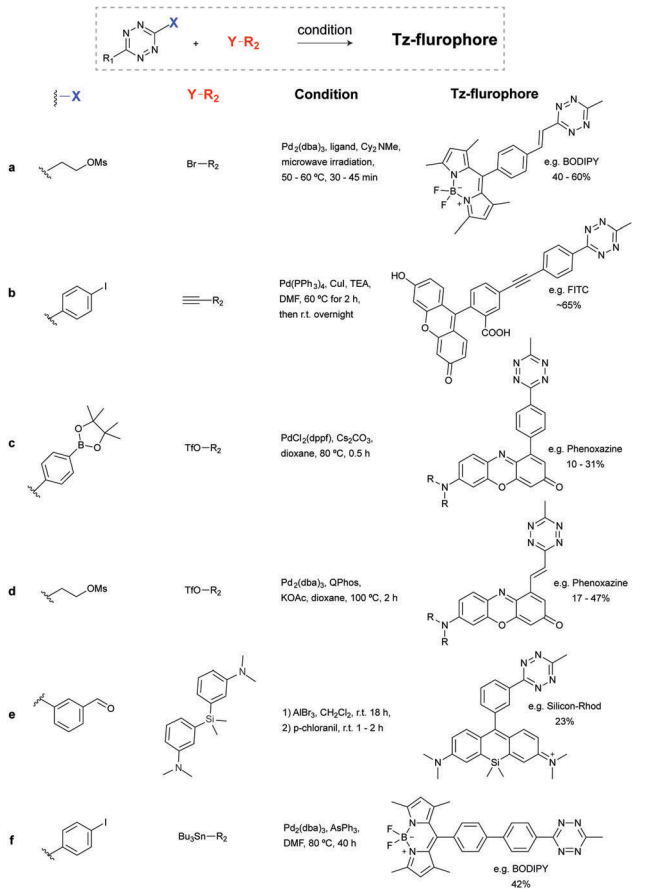

Fig. 11 Synthesis of tetrazine conjugates by functionalization of tetrazine substituents.

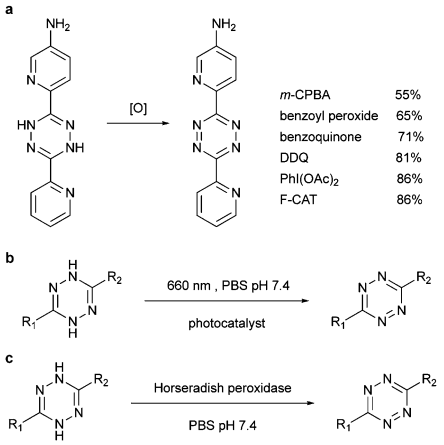

Fig. 12 Methods to oxidize dihydrotetrazine by (a) organic oxidants, (b) photocatalyst and (c) enzyme.

for the preparation of red-shifted tetrazine fluorophores using aldehydes and diarylether or diarylsilane compounds (Fig. 11e).[90] Stille coupling has also been widely explored in several reports of tetrazine synthesis. Different conditions have been examined with reasonable yields (Fig. 11f).[94]

2.3.4 Oxidation of dihydrotetrazine. Nitrous gas, generated from sodium nitrate with acid, is the most commonly used oxidant for converting dihydrotetrazine into the corresponding tetrazine (Fig. 12a). A typical protocol involves addition of $NaNO_2$ solution together with 1 M HCl or glacial acetic acid at 0 °C until the oxidation is completed. However low yields might occur when dealing with intolerant functional groups, such as amino groups. Metal oxides MnO_2[96] and CrO_3[97] have also been explored for oxidation of dihydrotetrazines but the moderate yields and toxic chromium waste limit their applications. Other oxidants like peroxy acid, *m*-CPBA[98] and benzoyl peroxide[99] are being used for oxidation of dihydrotetrazines. DDQ (dichlorodicyanobenzoquinone) has recently been reported to oxidize amino dipyridine–dihydrotetrazines where $NaNO_2$ fails. However, the product was difficult to separate from the hydroquinone byproducts.[100] A recent systematic study by Fox *et al.* identified $PhI(OAc)_2$ as an efficient oxidant and the product could easily be separated from the byproduct iodobenzene (Fig. 12b). The oxidant is amine-tolerant and robust for synthesizing dialkyl- and diaryl-tetrazine bearing and heteroaromatic rings.[99] During this study iodogen and a fluorous analogue of chloramine-T (F-CAT), were found to oxidize the dihydrotetrazine along with the halodemetalation reaction. Similarly, F-CAT could oxidize the amino substituted dipyridine-tetrazine with 86% yield and the product could be easily separated through fluorous solid-phase extraction.[101,102]

Alternatively, by using photocatalysts, the dihydrotetrazine could be oxidized to tetrazine in quantitative yields with 660 nm LED in the presence of methylene blue within 200 s. Even under ambient light, the photoredox reaction could be afforded in 47% conversion in 2 h (Fig. 12b). Similarly, horseradish peroxidase could also oxidize dihydrotetrazine with fast reaction rates (K_m = 1.0 × 10^{-4} M, k_{cat} = 27 s^{-1}, and k_{cat}/K_m = 2.7 × 10^5 M^{-1} s^{-1}, Fig. 12c).[103]

2.4 Synthesis of dienophiles

For metabolic oligosaccharide engineering and genetic encoding applications, the synthesis of dienophile-bearing sugars and amino acids is usually performed by using commercially available NHS- and *p*-nitrophenyl-activated dienophiles. Otherwise, multistep synthesis is required where unstrained dienophiles, such as terminal alkenes, are of advantage. Cyclopropenes are usually accessed from TMS-protected propynes *via* rhodium-catalysed cyclopropenation with diazo compounds (Fig. 13a).

For the preparation of cyclopropene amide-linked derivatives, the TMS-protected ester subsequently undergoes base-catalysed hydrolysis (*e.g.* potassium hydroxide) to give the TMS-free acid, which is then subjected to the corresponding amine to afford the desired amide (Fig. 13a). For the synthesis of cyclopropenes containing a carbamate scaffold, DIBAL reduction agent is typically used to produce the appropriate alcohol, followed by carbamate formation and TMS removal.[104–106] Importantly, methylcyclopropenyl methanol cannot be isolated as it is prone to rapid polymerization upon concentration, where a one-pot synthesis is required.[106,107]

The fast grow of IEDDA reaction in the bioorthogonal chemistry field is closely boosted with the advanced TCO synthesis methodology. A robust synthesis of this IEDDA partner was reported by Fox *et al.* in 2008 using a one-step reaction *via* flow photo isomerisation. Recently, in order to improve the *trans*/*cis* ratios and reduce the photo degradation of the active *trans*-cyclooctene, a new synthetic route was proposed in a closed-loop

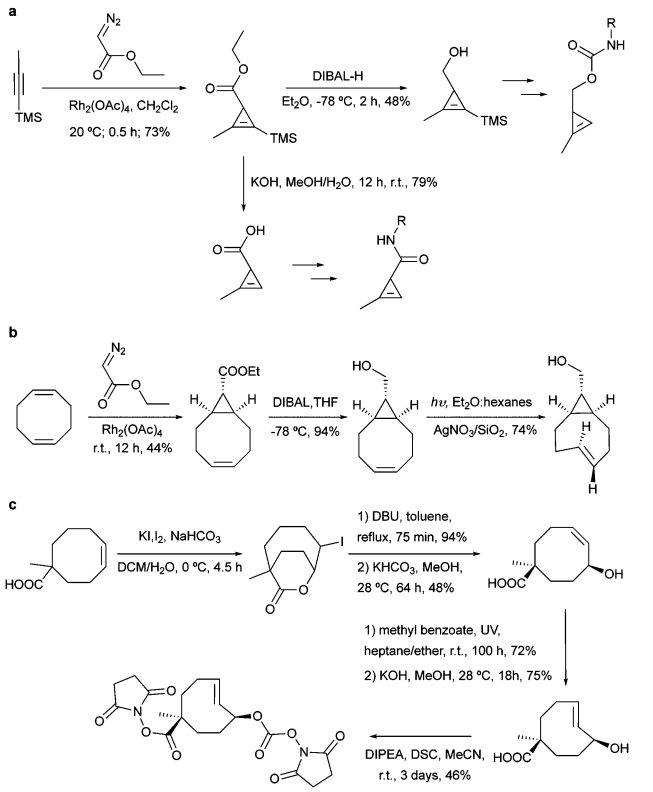

Fig. 13 Common synthetic routes for the preparation of most common dienophiles.

flow apparatus.[108,109] In this synthesis, the reaction mixture is continuously photo irradiated at 254 nm and pumped through $AgNO_3$ impregnated silica, which binds strongly with the desired *trans*-isomer, eluting the *cis*-isomer to be isomerised again until completely consumed. This direct method was further applied in the synthesis of most TCO derivatives published so far since then.[108]

Despite the extensively use of TCO in bioorthogonal chemistry, the commercial availability of TCO is still limited. All typical syntheses for TCO derivatives involve the construction of the corresponding *cis*-derivatives and then *trans*-isomerisation. Efforts have been made to introduce extra ring strain and functionality at defined positions. For example, rhodium-catalysed cyclopropenation on bicyclo[6.1.0]non-4-yne was also used to annihilate the cyclopropane ring to maintain the half chair conformation of bicyclo[6.1.0]non-4-ene (Fig. 13b).[59] Robillard *et al.* designed an elegant synthesis route to construct a bis-NHS-activated TCO-bearing linker for antibody-targeted therapy. A methyl group near the carboxylic acid was introduced to prevent epimerization and to control regioselectivity[15] (Fig. 13c).

3. The toolbox of bioorthogonal partners for IEDDA reactions

3.1 Dienophiles as IEDDA precursors

As abovementioned, the IEDDA reaction can be tuned to reach rate constants from 1 up to 10^6 M^{-1} s^{-1} by changing the electron deficiency of the 1,2,4,5-tetrazine precursors, or by manipulating the ring strain and electronic effects on the dienophiles. Significant efforts have focused on accelerating the reaction rate by expanding the scope of dienophiles. The first reported dienophile for protein bioconjugation *via* IEDDA reaction was the strained TCO introduced by Fox *et al.* that revealed an unusually fast second-order rate constant towards a dipyridyl-tetrazine precursor (Tz **8**) of k_2 1140 M^{-1} s^{-1} in MeOH and 2000 M^{-1} s^{-1} in 9 : 1 MeOH/water (Fig. 14a).[100] In pure water at 25 °C, the equatorial-diastereomer of TCO reacts with a water-soluble dipyridyl-tetrazine derivative (Tz **9**) with an increased rate constant of 22 600 M^{-1} s^{-1} while the axial-diastereomer reacts faster with a k_2 of 80 200 M^{-1} s^{-1} (Fig. 14a).[60] Robillard *et al.* also reported that the axial diastereomer of 5-hydroxy-TCO is more reactive than the equatorial diastereomer due to instability of the axially substituted ring induced by transannular interactions.[110] Fox *et al.* subsequently optimized TCO in terms of reactivity by fusing a *cis*-cyclopropane onto the cyclooctene moiety to increase the ring strain (s-TCO, Fig. 14b).[59] When Tz **8** is reacted in MeOH at 25 °C, this strained derivative is 19 times more reactive than the parent TCO (k_2 = 22 000 M^{-1} s^{-1}).[59] Later, it was demonstrated that a water soluble s-TCO derivative bearing a PEG linker reacts with Tz **9** in pure water at a rate constant of 3 300 000 M^{-1} s^{-1} (s-TCO, Fig. 14b), which makes this dienophile the fastest to date.[60] There are some limitations, however, that emerge from the high reactivity of the "TCO dienophiles". One is the deactivation of TCO by isomerisation in the presence of high thiol concentrations. As an example,

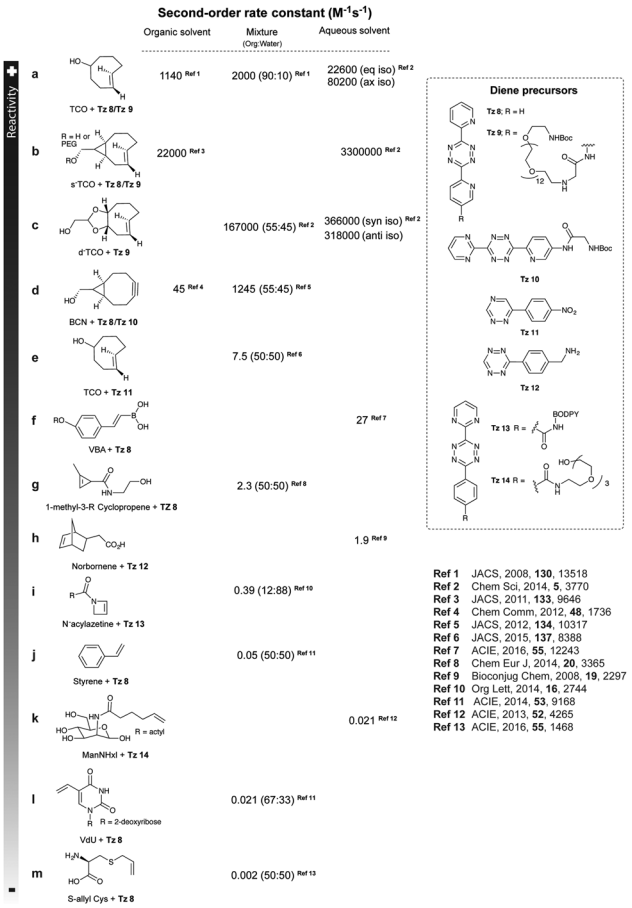

Fig. 14 Examples of strained and unstrained dienophiles for IEDDA reactions and their corresponding reaction rates.

Robillard *et al.* showed that in fresh mouse serum at 37 °C the TCO isomer converts into *cis*-cyclooctene with a half-life of 3.26 h.[110] Secondly, the "TCO dienophiles" TCO/s-TCO are not stable enough for prolonged storage. Recently, Johnson *et al.* introduced a new variant of s-TCO complexed with $AgNO_3$, which has improved stability and can be used directly in cells for rapid bioorthogonal reactions with tetrazines.[111] Alternatively, to address the stability limitations of s-TCO Fox *et al.* designed a new conformationally-strained dioxolane-fused *trans*-cyclooctene (d-TCO), which maintains high reactivity towards tetrazines (k_2 366 000 M^{-1} s^{-1} for *syn* isomer and 318 000 M^{-1} s^{-1} for anti-isomer at 25 °C in pure water with Tz **9**) but displays enhanced stability and is more easily prepared (Fig. 14c).[60] Stability studies of the syn isomer in human serum at room temperature showed no isomerisation or decomposition after 24 h neither after 4 days (>97% *trans* isomer).

Bicyclooctynes (bicyclo[6.1.0]nonyne, BCN) were found also to undergo fast IEDDA reactions with tetrazines (k_2 = 45 M^{-1} s^{-1} in MeOH at 24 °C with Tz **8**; k_2 = 1245 M^{-1} s^{-1} in 55% MeOH/H_2O at 25 °C with Tz **10**; Fig. 14d).[61,112] Recently, Prescher *et al.* showed that 1,2,4-triazines participate in IEDDA reactions with strained alkenes (Fig. 14e).[45] In particular, it was found that 1,2,4-triazines react with TCO, but not with norbornene or cyclopropene.[45] Considering the latter two undergo efficient

cycloadditions with 1,2,4,5-tetrazines, this suggests an opportunity for sequential dual-labelling. However, this methodology remains unexplored most likely because the relatively slow kinetics of the 1,2,4-triazine: TCO reaction (k_2 = 7.5 M^{-1} s^{-1} in 50% ACN/PBS at 25 °C with Tz **11**, Fig. 14e). Importantly, this new class of IEDDA reagents showed enhanced stability enabling its direct use in recombinant protein production (fully stable in PBS and in excess of cysteine for 1 week at 37 °C).[45] A contemporaneous study showed that 1,2,4-triazines also react with strained alkynes (BCN), however, with even with more sluggish kinetics (k_2 = 0.38 × 10^{-3} M^{-1} s^{-1} with BCN in acetonitrile).[46]

Recently, vinylboronic acids (VBA) appeared as a new interesting class of compounds for fast and water-soluble reactions with tetrazines (27 M^{-1} s^{-1} with Tz **8**; Fig. 14f).[113] The use of cyclopropenes as tetrazine reactive partners was also proposed as an alternative to TCO dienophiles (Fig. 14g). The Devaraj group demonstrated that modulating the substituents of cyclopropenes has a dramatic effect on their stability and on the kinetics towards tetrazines. Indeed, it is well described that unsubstituted cyclopropenes are susceptible to both nucleophilic attack and polymerization reactions. To overcome these limitations, Devaraj *et al.* "protected" the double bond with a methyl group, and the resulting 1-methyl-3-substituted cyclopropene derivatives appeared as fast and *in vivo* stable dienophiles with one of these analogues having a second-order rate constant of 2.3 M^{-1} s^{-1} (in 50% aqueous solutions with Tz **8**; Fig. 14g).[69,104,106] Faster reaction rates for this dienophile are expected if measured under purely aqueous conditions. Norbornenes, another class of cyclic dienophiles, offer an excellent balance between facile strain-promoted reactivity with tetrazines and overall chemical stability (Fig. 14h). Tetrazine Tz **12** reacts rapidly with norbornene in aqueous buffer with a second-order rate constant of 1.9 M^{-1} s^{-1} (Fig. 14h).[114] Recently, a new bioorthogonal *N*-acylazetine small tag showed equal efficiency as the norbornene for protein modification *via* IEDDA reaction with a rate constant of 0.39 M^{-1} s^{-1} against Tz **12** (Fig. 14i). Vinylbenzyl groups (styrene) also react efficiently in IEDDA reactions (0.05 M^{-1} s^{-1} against Tz **8** in 50% MeOH/water, Fig. 14j)[115,116] Other minimal-tags include terminal unstrained alkene-decorated sugars[117] (0.021 M^{-1} s^{-1} against Tz **14**) and nucleosides (5-vinyl-2′-deoxyuridine, VdU, 0.021 M^{-1} s^{-1} against Tz **8**, Fig. 14k).[115] Recently, our group explored chemical installed *S*-allyl handles for "IEDDA labelling" with tetrazines (Fig. 14l). Although, this handle reacts significantly slower (0.002 M^{-1} s^{-1} against Tz **8** in 50% MeOH/PBS) compared to *trans*-cyclooctenes, it was suitable for pretargeting live cell imaging.[118]

While most studies of reaction kinetics are performed on small molecule models, it is important to study what is the actual kinetics of these reactions in the protein context. In one example, Chin *et al.* showed that the second-order rate constant for the labelling of sfGFP bearing a 1,3 disubstituted cyclopropene with a fluorescent analogue of Tz **8** was 27 ± 1.8 M^{-1} s^{-1} (Fig. 15). Importantly, it was shown that the rate constant for this reaction in the test tube and in cells is approximately 10-fold faster when compared to the cyclopropene model (2.3 M^{-1} s^{-1}, Fig. 15). The differences in the reaction rates should be related with the reaction solvent (water for protein and 50% water/org for small molecule). Similarly, Lemke *et al.* demonstrated that the tetrazine ligation (Tz **12**-TAMRA) with a BCN-GFP bearing protein occurs with a reaction rate constant of k_2 = 29 000 ± 7500 M^{-1} s^{-1} (Fig. 15**a**).[119] Progress of the labelling reaction was determined using Förster resonance energy transfer (FRET) to follow the decrease in GFP fluorescence and the increase of the TAMRA fluorescence upon GFP excitation. Just recently, the Lemke group developed a new hydrophilic TCO analogue (DOTCO; dioxo-TCO) for genetic encoding which showed fast reactions with a Cy5 (cyanine dye) tetrazine when incorporated into GFP (6370 M^{-1} s^{-1} in pure water with Tz **12**-Cy5; Fig. 15a).[120]

An ideal bioorthogonal reaction requires a rate of $>10^4$ M^{-1} s^{-1} inside cells to reach completion in seconds to min at biological concentrations (μM to nM) of the bioorthogonal target.[121]

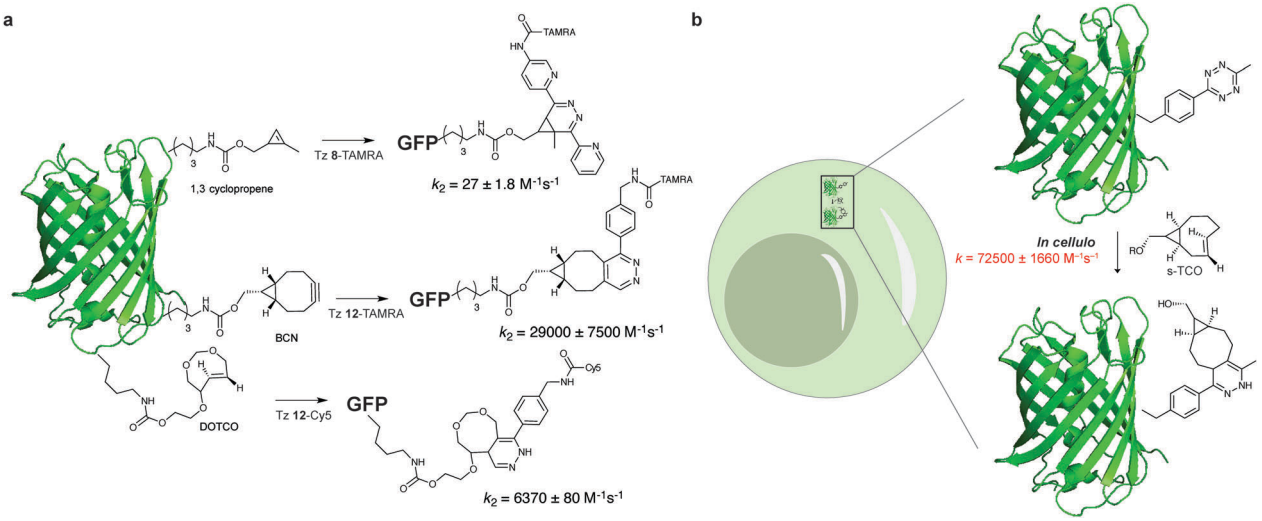

Fig. 15 On protein and in cellular rate constant determination for reaction of GFP bearing dienophiles and tetrazine.

To meet these rates, Mehl *et al.* developed a tetrazine-modified GFP (GFP-Tet-v2.0) that reacts in cells with s-TCO with a rate constant of 72 500 ± 1660 M^{-1} s^{-1} (Fig. 15).[121] The authors predict that this reaction rate allows 95% labelling in <1 min at 1 μM concentrations of Tet-v2.0-protein and s-TCO, meeting the needs of the ideal bioorthogonal ligation. Compared to the "cuvette second-order rate" (87 000 ± 1440 M^{-1} s^{-1}) the rate constant reduction is justified by the *in vivo* cellular environment or hampered uptake of s-TCO.[121]

3.2 Dienes as IEDDA precursors – fast kinetics *versus* stability

Tetrazine partners are also a key factor in the IEDDA reaction rates. Hilderbrand *et al.* have shown that electron-withdrawing substituents enhanced IEDDA reactivity of tetrazines, however, these substituents may also induced their degradation.[40] An optimal balance between reactivity and stability must be achieved for effective labelling in *in vivo* systems. The disubstituted tetrazines Tz **15**–Tz **16** comprising electron-donating substituents show the highest stability (~90% stable), but also suffer from slow kinetics (200–2000 M^{-1} s^{-1}) (Fig. 16). Hydrogen substituted tetrazines Tz **22** and Tz **23** demonstrate a good balance of stability (~70% stable for Tz **23**) and fast reaction kinetics (30 000 M^{-1} s^{-1}). These compounds are not the most electronically favourable (no electron-withdrawing substituents) but the fastest suggesting these tetrazines may react faster due to less steric interference. The least stable tetrazine, but also one of the fastest, comprises electron-withdrawing groups (R_2 = pyrimidine; Tz **21**).

3.3 Fluorogenic tetrazines for IEDDA ligations

In bioorthogonal labelling approaches a large amount of the bioorthogonal fluorescent dye is often required to increase reaction efficiency. In these examples the excess of the fluorescent probe has to be removed using several washing steps in order to reduce background fluorescence of the unreacted probes. One alternative approach to minimize background fluorescence is based on the use of fluorogenic probes, which become fluorescent only upon transformation. Such fluorogenic dyes are extremely advantageous for *in vivo* labelling applications, since they usually result in highly conspicuous images without requiring washing steps.

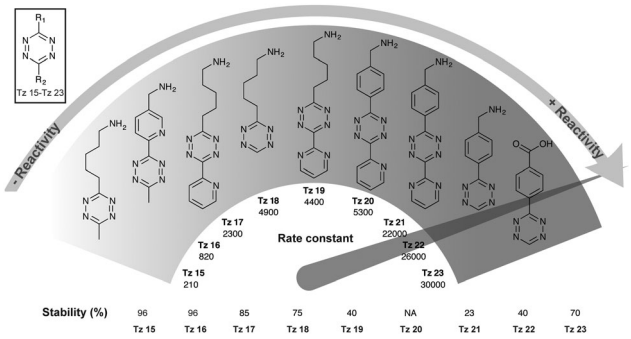

Fig. 16 Second order rate constants of selected tetrazines with TCO in PBS at 37 °C and corresponding stability assessed in PBS at 37 °C for 10 h. NA, not assessed.[40]

3.3.1 Principles behind fluorogenicity in bioorthogonal reactions. In general, there are 4 main strategies to develop fluorogenic probes and these are based on (1) protonation–deprotonation species (pH sensitive probes), (2) complexation (including direct complexation and competitive displacement), (3) cleavage and formation of covalent bonds, and (4) redox reaction. These strategies have recently been reviewed in detail.[122] In bioorthogonal chemistry, fluorogenic probes are designed to have a functional group that quenches the fluorescence emitted from the fluorophore. Upon reaction, the quencher is transformed/modified, enabling the fluorescence to be restored. Other approaches use the bioorthogonal reaction to trigger the release of either photocaging or quencher moieties. One of the very first examples of fluorogenic dyes activated by click chemistry used azido groups to quench coumarins, which after reaction with terminal alkynes afforded intense fluorescent 1,2,3-triazole products.[123] In another example, Wong *et al.* developed azido-BODIPY probes, which showed strong fluorescence upon triazole formation (Fig. 17a).[124] The most important feature of fluorogenic system is the enhancement factor (or "turn on" effect) that is conferred by the ratio of the fluorescent intensity or quantum yield of the product and the starting material at a given wavelength. The azido-BODIPY probes were found to have a 52-fold increase in fluorescence quantum yield after CuAAC reaction (Fig. 17a).

There are three major photophysical quenching mechanisms, which involve Förster resonance energy transfer (FRET), through-bond energy transfer (TBET), and photoinduced electron transfer (PET).[125] In the CuAAC reaction the increase in fluorescence quantum yield (52×) upon triazole formation is due to the lowering of the HOMO energy level of the aryl moiety that reduce the PET to the BODIPY acceptor (Fig. 17a).[124] The presence of an alkyne motif can also function as a quencher, although not so frequently. After the pioneering work on terminal alkynes by Farhni *et al.*[126] and on cyclooctyne-fused coumarins by Bertozzi *et al.*,[127] Boons *et al.* reported a dibenzocyclooctyne, which exhibited a ~59-fold fluorescent increase after SPAAC reaction with alkynes (Fig. 17b).[128] Fluorescence increase is due to large differences in oscillator strengths of the $S_0 \leftrightarrow S_1$ transitions in the planar C_{2v}-symmetry of the starting material compared to the nonplanar cycloaddition product.[128] Staudinger ligation has also been exploited for the development of fluorogenic probes (Fig. 17c). In one example, a phosphane-modified coumarin showed a 59-fold increase in fluorescence quantum yield after click reaction (λ_{exc} 443, λ_{em} 495 nm).[129] Prior to the Staudinger reaction the original phosphine is responsible for the quenching *via* internal charge transfer (ICT). Upon oxidation to the phosphine oxide, the ICT originating from the phosphorous' lone pair is no longer possible, therefore the fluorescence is restored.[129] For more information about the applications of click fluorogenic probes the reader is directed to a recent review by Kele *et al.*[130]

3.3.2 Photophysical quenched fluorogenic probes for IEDDA. Tetrazines have become important for bioconjugation strategies also due to their high fluorogenicity. Since tetrazines are chromophores absorbing light at around 500–530 nm they can act as

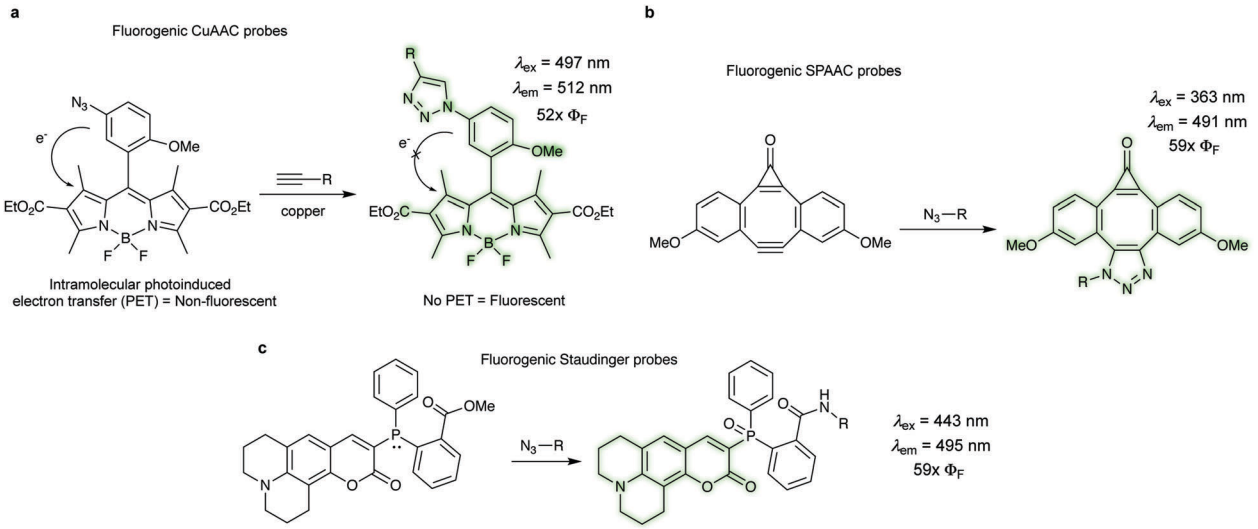

Fig. 17 Bioorthogonal fluorogenic probes. (a) Fluorogenic CuAAC reaction of azido-BODIPY with alkynes. (b) Fluorogenic dyes activated by SPAAC. (c) Coumarin-phosphine fluorogenic dye activated by the Staudinger ligation. Φ_F = fluorescent quantum yield.

quenchers towards a series of fluorophores. Interestingly, depending on the substituent, tetrazines themselves can also exhibit intrinsic fluorescence. However, due to the low extinction coefficient of the associated absorption band their fluorescence suffers from low intensity.[131,132] In 2010 Weissleder *et al.* showed that a series of tetrazine–fluorophore conjugates (coumarin, BODIPY FL, Oregon Green 488, BODIPY TMR-X, VT680) are efficiently quenched by tetrazines, resulting in a ''turn-on'' effect up to a 20-fold after destruction of the tetrazine core upon IEDDA cycloaddition.[133] The authors propose that the fluorescence quenching is due to resonant energy transfer between the fluorescent chromophore and the tetrazine (benzylamino-1,2,4,5-tetrazine, Tz **12**), which has a visible absorbance maximum at 515 nm (Fig. 18a). This explains the wavelength dependence of the quenching; green- and red-emitting tetrazine dyes (BODIPY FL, λ_{ex} = 505 nm, λ_{em} = 512 nm, 15-fold increase; Oregon Green 488, λ_{ex} = 495 nm, λ_{em} = 523 nm, 18.5-fold increase; BODIPY TMR-X, λ_{ex} = 543 nm, λ_{em} = 573 nm, 20.6-fold increase) showed higher

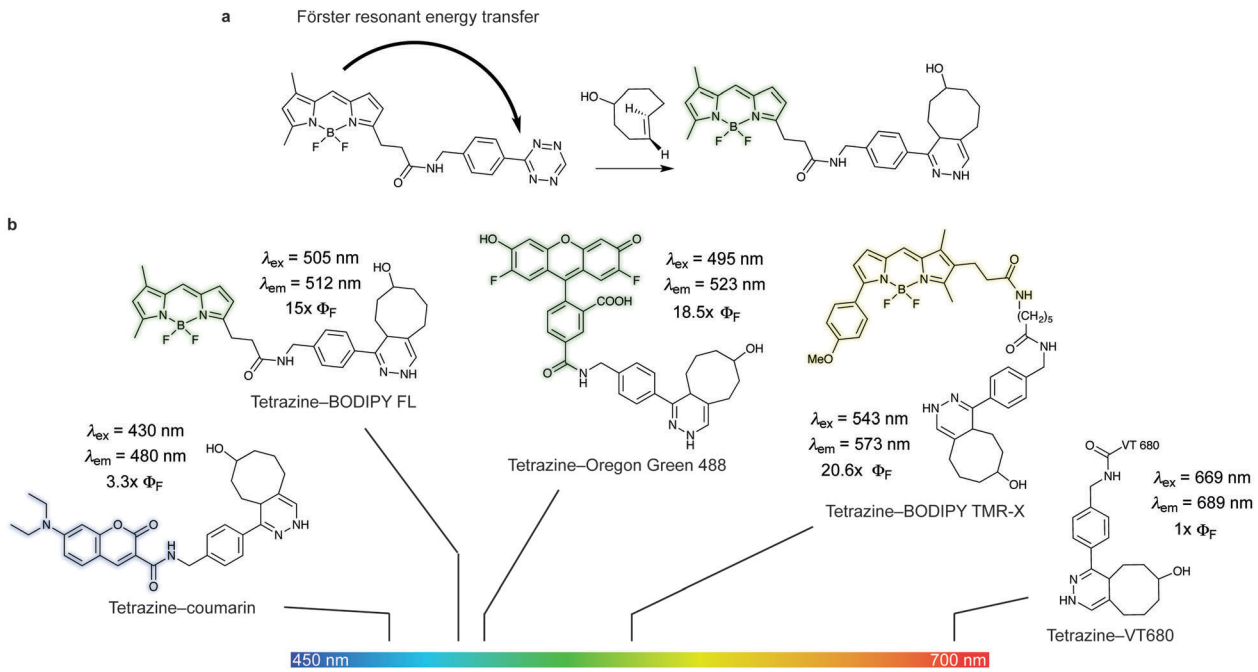

Fig. 18 (a) Example of the mechanism of quenching of fluorophore–tetrazine conjugates by Förster Resonance Energy Transfer. As the tetrazine is consumed by cycloaddition the FRET quenching is forbidden and fluorescence is restored. (b) Photophysical properties of the depicted dyes before and after reaction with TCO.[133] The extent of fluorescence quenching depends on the wavelength emission of the fluorophores and the absorption spectra of the tetrazine. Φ_F = fluorescent quantum yield.

fluorescence enhancements upon cycloaddition, while near-IR-emitting dyes (tetrazine-VT680; λ_{ex} = 669 nm, λ_{em} = 687 nm) were not quenched (Fig. 18b).[133]

Fluorogenic BODIPY probes. We and the Chin group also showed that tetrazines can quench tetramethylrhodamine (yellow-emitting, λ_{ex} = 550 nm, λ_{em} = ~585 nm, 4–5-fold increase) but the fluorescence enhancement is less pronounced.[72,118] In a following work the group of Weissleder proposed an alternative way for designing more efficient turn-on probes, which consisted in the design of conformationally restricted tetrazine–BODIPY conjugates for fluorescence quenching through bond energy transfer (TBET).[82] TBET systems require the energy donor and acceptor moieties to be connected through twisted, but otherwise conjugated, π-electron systems. In addition, unlike traditional FRET, TBET quenching does not require overlapping emission and absorption bands of fluorophores and tetrazines, respectively.[134] This approach resulted in new fluorogenic probes with a turn-on up to 1600 times (Fig. 19a). It was shown that structures with enhanced spatial donor–acceptor proximity resulted in higher magnitudes of fluorescence turn-on. The exceptional fluorogenic turn-on ratios of the new probes compared to the flexible linked tetrazine–fluorophore conjugates (*e.g.* 80-fold greater than tetrazine–BODIPY TMR-X) suggest that TBET is the most likely quenching mechanism for these compounds. The suitability of this fluorophore for biological applications was demonstrated by imaging EGFR expression with TCO-functionalized antibodies on both fixed and live cells.[82] Later in 2014 Wombacher *et al.* reported other rigid tetrazine–BODIPY conjugates, which showed less fluorogenicity upon reaction with TCO (Fig. 19b). This work further demonstrated that the close proximity between the tetrazine and the fluorophore as well as fixation of transition dipoles is crucial to obtain strong quenching.[94] Indeed, the new probes Tz–BODIPY **4** and Tz–BODIPY **5** show little structural flexibility and identical geometrical layouts concerning their donor and acceptor transition dipoles. However, the BODIPY derivative with a shorter interchromophore (Tz–BODIPY **5**) exhibits twice of the fluorescence of the one with a longer linker (Tz–BODIPY **4**).[94]

Fluorogenic coumarin probes. A series of coumarin–tetrazine probes were also prepared and their design included aligned transition dipoles of the coumarin fluorophore and the tetrazine in order to maximize contributions from FRET in addition to TBET (Fig. 20a). These probes, named HELIOS probes (HELIOS = hyperemissive ligation-initiated orthogonal sensing), exhibit the highest brightness enhancements reported for any bioorthogonal fluorogenic dyes with fluorescence enhancements up to 11 000-fold. The fluorescence quenching of the coumarin cores by tetrazines occurs mainly *via* a TBET mechanism.[81] Imaging of epidermal growth factor receptor (EGFR) on the surface of cancer cells using a TCO labelled anti-EGFR antibody (Cetuximab) and HELIOS 370H was performed within seconds of dye addition and exhibited no nonspecific signal according to the control experiments (Fig. 20b).

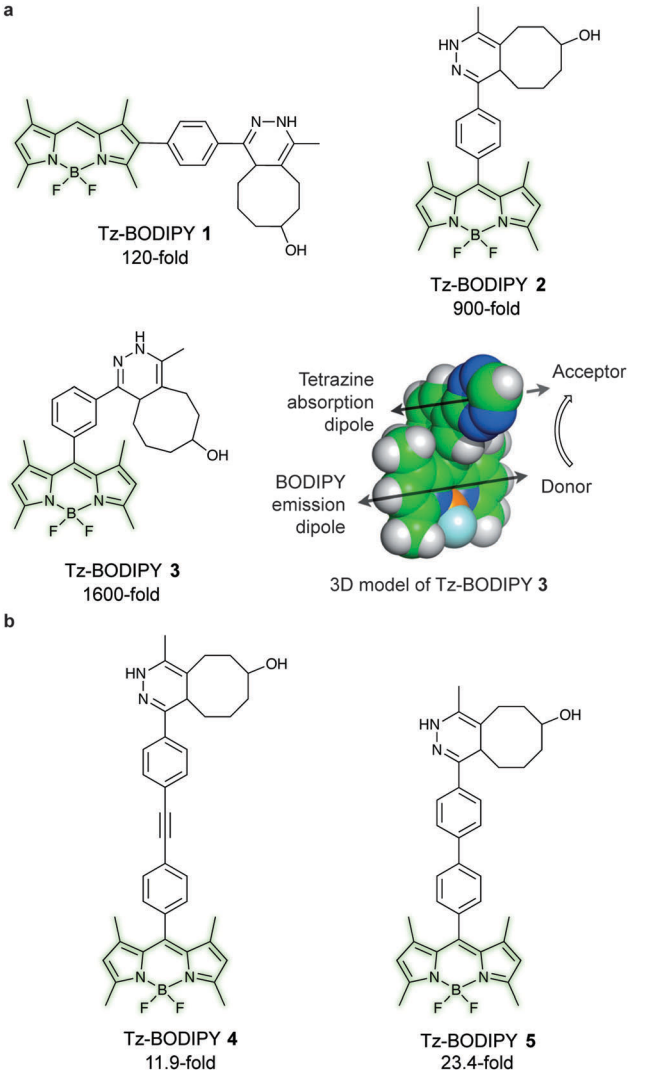

Fig. 19 TBET-based tetrazine quenched fluorogenic probes. (a) Superbright fluorogenic tetrazine–BODIPY derivatives where the tetrazine was directly attached off the BODIPY core with a rigid phenyl linker for TBET quenching. 3D model of Tz–BODIPY **3** is depicted, illustrating a twisted phenyl linker between the BODIPY and the tetrazine chromophore and the orientation of the donor and acceptor transition dipoles.[82] (b) New BODIPY derivatives with longer interchromophore linkers.[94] Turn-on effect (*e.g.* 1600-fold for Tz–BODIPY **3**) denotes the relative fluorescence quantum yield of the fluorophores before and after reaction with TCO. From ref. 82, Copyright © 2013 by John Wiley & Sons, Inc. Reprinted in part by permission of John Wiley & Sons, Inc.

Fluorogenic xanthene probes. Xanthene dyes, such as fluorescein and rhodamine derivatives, are arguably the most popular class of fluorescent probes for cellular imaging and are typically highly soluble in aqueous solutions.[93] In this regard, Devaraj *et al.* synthesized tetrazine-conjugated xanthene dyes such as Oregon-Green and tetramethylrhodamine (TAMRA) conjugated to tetrazines *via* a rigid styrenyl linker.[93] The Oregon Green probe (Tz–OG **1**) underwent a 400-fold fluorescence enhancement upon TCO reaction while the red-emitting TAMRA (Tz–Rh **1**) showed a 75-fold enhancement in fluorescence (Fig. 21a).[93]

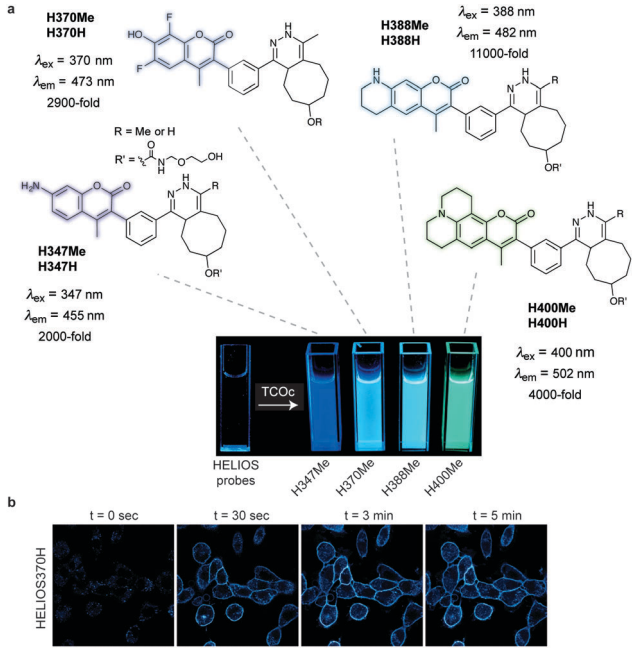

Fig. 20 Ultra-bright fluorogenic coumarin–tetrazine probes. (a) Turn-on response of HELIOS probes using a handheld UV lamp. Fluorescence enhancement (*e.g.* 11 000-fold for H388H) represents the relative fluorescence quantum yield of the fluorophores before and after reaction with TCO. (b) No-wash fluorogenic imaging of EGFR expression on A431 cells. Cells were incubated with an α-EGFR–TCO antibody, washed briefly, and then imaged sequentially after addition of HELIOS 370H. From ref. 81, Copyright © 2014 by John Wiley & Sons, Inc. Reprinted in part by permission of John Wiley & Sons, Inc.

Recently, Kele *et al.* reported new tetrazine-phenoxazine fluorogenic probes. The red excitability and emission properties of these probes ensure minimal autofluorescence, while TBET fluorogenicity reduces nonspecific background fluorescence. Indeed, due to its high lipophilicity phenoxazine is often compromised by high background fluorescence, however, the high fluorogenicity of the new tetrazine-phenoxazine probes (up to 275× turn-on) allowed efficient labelling of live cells (Fig. 21b).[95] To expand on this approach in the context of multicolor imaging, Wombacher *et al.* synthesized a panel of rigidly-linked green- to far-red-emitting fluorogenic tetrazine probes (Fig. 21c).[90] Once again the authors found that the distance between the tetrazine and the fluorophore, and the fluorophore itself, are crucial for efficient quenching and for the resulting fluorescence turn-on upon conversion by IEDDA reaction.

3.3.3 IEDDA fluorogenicity induced by fluorophore generation. All previously mentioned strategies to design IEDDA fluorogenic bioorthogonal reactions are based on the destruction of the tetrazine moiety that suppresses fluorescence of a fluorophore. Another strategy is based on the simultaneous generation of a fluorophore through a bioorthogonal chemical transformation. In this regard, Guo *et al.* developed a new approach for fluorogenic bioorthogonal labelling *via* IEDDA reaction.[135] This unprecedented approach is based on the intrinsic fluorescence of 4-phenyl-3,6-di(pyridin-2-yl)-1,4-dihydropyridazine (PDHP), the product from the reaction of styrene and Tz **1** (k_2 = 0.078 M^{-1} s^{-1}) (Fig. 22a). Comparing to some commonly used fluorophores (*e.g.* fluorescein pH 9, Φ = 0.95, ε = 93 000 M^{-1} cm^{-1}, Stokes shift = 24), PDHP (ex = 360 nm, em = 465 nm) has relatively low quantum yield (0.011 in MeOH and 0.251 in ACN) and extinction coefficient (4329 M^{-1} cm^{-1} in MeOH and 3769 M^{-1} cm^{-1} in ACN).[135] On the other hand, PDHP has a large Stokes shift (~100 nm), which could be beneficial (*e.g.* less self-quenching and/or auto-fluorescence background) in certain imaging applications. Finally, a lysine-derived non-canonical amino acid containing styrene moiety (KStyr) was genetically encoded into an intracellular stress response protein, HdeA, and labelled in living cells after tetrazine reaction. Recently, Vrabel *et al.* reported a fluorogenic reaction between axial-TCO with tetrazine (Fig. 22b). By screening a series of tetrazines, the photochemical properties of the resulting 1,4-dihydropyridazines could be tuned towards 91-fold fluorescence intensity increase and emissions ranging from 480 to 605 nm. By modifying tetrazines with peptides on resin, the addition of axial-TCO resulted in rapid fluorescent product within 1.5 min. Furthermore, taxol- and triphenylphosphonium-tetrazine derivatives were also synthesized for targeting subcellular compartments and efficient and fast fluorogenic labelling was observed on microtubules and mitochondria.[136]

4. Methods for installing IEDDA chemical reports on biomolecules

Selective and site-specific labelling of proteins is essential for studying protein structure, activity, localization and trafficking. During the last decade, a wide variety of IEDDA bioorthogonal reporters have been incorporated into biomolecules through genetic encoding of non-canonical amino acids (ncAAs) during protein synthesis, or through enzymatic and chemical modification of native residues on post-expressed proteins. These methods will be presented and discussed in the following sections.

4.1 Genetic code expansion

The development of strategies to genetically encode ncAAs into proteins has had arguably the greatest impact upon the progress of bioorthogonal chemistry in recent years. In this approach, an aminoacyl-tRNA synthetase (aaRS)/transfer RNA (tRNA) pair is used to insert an ncAA into the growing protein chain in response to an amber stop codon (UAG) on the mRNA.[137–139] A plethora of ncAAs bearing ketones, aldehydes, azides, alkynes, alkenes, tetrazines, or aryl halides reactive groups have been developed in recent years using this strategy and incorporated into *E. coli*, yeast, mammalian cells[140] and even animals.[141,142]

The vast majority of studies on the incorporation of ncAAs in IEDDA applications so far have used the pyrrolysine synthetase/tRNA pair (PylRS/$tRNA_{CUA}$) from *methanosarcinia* for three reasons. Firstly, this synthetase, in its native form, incorporates none of the 20 canonical amino acids. Secondly, the high promiscuity of PylRS and the evolutionary mutants allowed

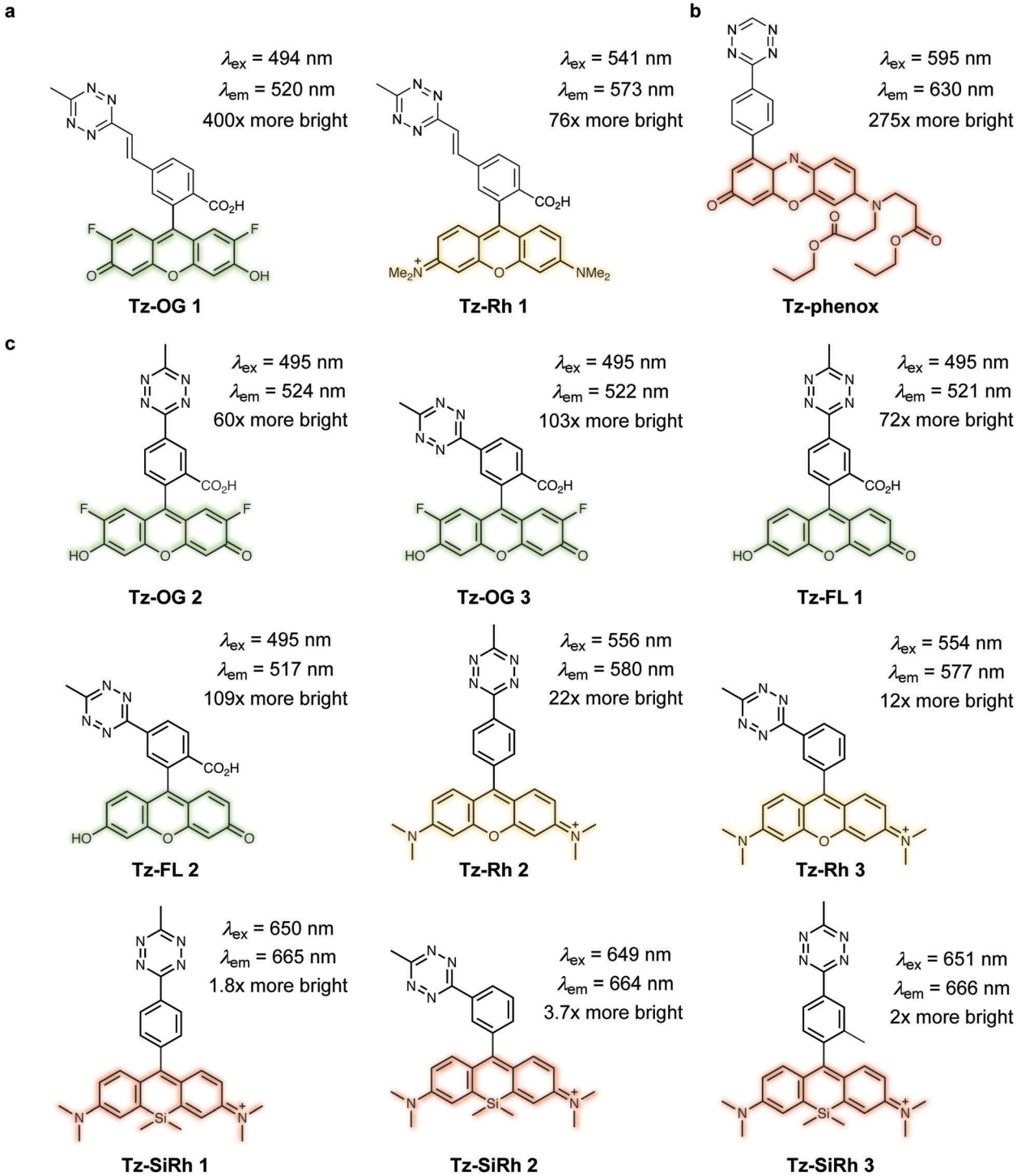

Fig. 21 TBET-based tetrazine quenched fluorophores. (a) OG and Rh fluorophores conjugated to tetrazines *via* a rigid styrenyl linker.[93] (b) Red-emitting fluorogenic phenoxazine probe.[95] (c) Green- to far-red-emitting fluorogenic tetrazines-fluorophore conjugates.[90] Turn-on effect values represent the relative fluorescence quantum yield of the fluorophores before and after IEDDA reaction. FL = fluorescein; OG = oregon Green; Phenox = phenoxazine; Rh = rhodamine; SiRh = silicon-rhodamine.

the incorporation of more than 300 hundreds kind of ncAAs.[143] Finally, while the use of other synthetase–tRNA pairs for incorporating ncAAs is limited to cells from a particular organisms, orthogonal PylRS variants can be selected for *E. coli* and then used to incorporate ncAAs into yeast, mammalian cells and animals.[143,144] The enormous progresses made in the field of genetic code expansion over the recent years has resulted in up to 26 ncAAs incorporated into proteins for IEDDA applications (Fig. 23). A summary of the most significant examples is described in the following sections.

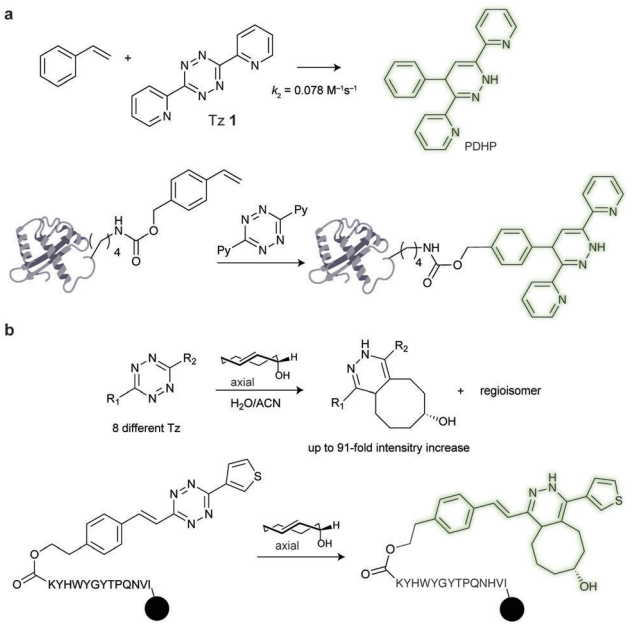

Fig. 22 (a) Fluorogenic reaction between styrene and tetrazine, and selective labelling of HdeA. A Plasmid pHdeA was constructed to encode an HdeA mutant containing the lysine-styrene non-canonical amino acid (KStyr) at position 28 (HdeA-F28KStyr). *E. coli* cells expressing HdeA-F28KStyr were successfully labelled after tetrazine reaction. (b) Fluorogenic reaction between a-TCO and tetrazines, and fluorogenicity with a peptide-linked beads.

4.1.1 Norbornene. As the first published example of a genetically encoded dienophile, encoded carbamate-norbornene derivatives were reported simultaneously in 2012 by the groups of Chin (ncAA 1)[72] and Carell (ncAA 2)[145] (Fig. 23). Using the wild type *Mm*PylRS/$tRNA_{CUA}$ pair (*Mm* = *Methanosarcina mazei*) a norbornene-containing Lys ncAA (ncAA 1) was incorporated into an epidermal growth factor receptor-green fluorescent fused protein (EGFR-GFP) in HEK293 and efficiently labelled with minimal background using a fluorogenic tetrazine-based fluorophore.[72] Later, the *Mm*PylRS/$tRNA_{CUA}$ pair was found to be orthogonal to the translation system of Drosophila melanogaster.[141] In order to optimize the genetic introduction and labelling efficiency of various norbornene-Lys derivatives (*endo*-, *exo*- and strained-norbornene, ncAA **2–4**), a *Mm*PylRS triple mutant (Y306G, Y384F, I405R) was successfully tested for the incorporation of ncAA **2–4** into human carbonic anhydrase II (HCA) in *E. coli*, indicating the promiscuity of this triple mutant synthetase with norbornene derivatives.[146] Recently, Bertozzi *et al.* established a robust method for cell surface display of mucins. This has been accomplished by genetically encoding a norbornene chemical handle into the extracellular portion of EGFR membrane proteins using the MmPylRS/$tRNA_{CUA}$ pair. The next step involved the modification of the encoded protein by reaction with tetrazine end-modified glycopolypeptides.[147] Norbornene-containing Tyr ncAAs (ncAA **5–7**) were also incorporated into proteins using an evolved *Mm* PylRS mutant (Y306A/N346A/C348A/Y384F).[148]

4.1.2 *trans*-Cyclooctene (TCO). A TCO-Lys (ncAA **8**) was first incorporated site-specifically into proteins in 2012 using a double-mutant synthetase *Mm*PylRS (Y306A, Y384F).[149] Similarly, a *Methanosarcina barkeri* PylRS triple mutant (*Mb*PylRS, Y271M, L274G, and C313A) was later used to incorporate TCO into an EGFR-GFP fusion protein in HEK293 cells, allowing rapid and specific labelling with a tetrazine fluorophore in <2 min. In contrast, under identical conditions, a reaction period of 2 h was required for labelling the corresponding norbornene-modified protein.[112] The fast labelling of TCO-tagged EGFR–GFP with tetrazines was recently explored for studying the trafficking of EGFR.[150] Importantly, the same mutant was used to incorporate s-TCO into the same fusion protein. However, in this case no reaction was observed upon addition of the tetrazine probe, suggesting the *in vivo trans*-to-*cis* isomerisation of the dienophile.[112] Other ring isomers of TCO, namely $TCO^{\#}$ (ncAA **9**) and TCO* (ncAA **10**), are also tolerated by the promiscuous double-mutant *Mm*PylRS. Importantly, TCO*, but not TCO or $TCO^{\#}$, showed a high stability against isomerisation to the non-reactive *cis* form due to a carbamate bond shielding effect.[8] In a recent study, the superior stability and reactivity of TCO* was explored for cross-linking proteins in living cells by reaction of TCO*-proteins with peptides bearing tetra-cysteine motifs through a ''tetrazine FlAsH linker'' (Fig. 24a), in a method called T-CrAsH (Fig. 24b).[151]

Although TCO has been successfully used for labelling genetically encoded proteins, several reports have described that the ncAA TCO-Lys is relatively sticky resulting in high non-specific fluorescence background upon addition of the tetrazine dyes, even if extra washing steps are applied to remove excess of non-incorporated ncAA.[8,112,152] With this in mind, an hydrophilic TCO-Lys derivative containing *exo*- and *endo*-cyclic heteroatoms introduced in the TCO ring was developed in order to increase hydrophilicity. The new hydrophilic ncAA DOTCO-Lys (ncAA **11**) showed high incorporation efficiency in both prokaryotic and mammalian cells using a double-mutant pyrrolysyl-tRNA synthetase.[120] Importantly, comparative washout studies revealed that only 5 min are required to remove DOTCO-Lys from cells whereas more than 6 h are needed to remove excess of BCN-Lys and TCO*Lys (Fig. 25). Thus, this hydrophilic DOTCO-Lys could be used to label and track intracellular proteins with rapid turn-over and expressed in low concentrations.[120] Apart from Lys derivatives, TCO-Tyr ncAAs (ncAA **12**, ncAA **13**) have been also incorporated into proteins in *E. coli*.[148,153]

4.1.3 Cyclopropene. Cyclopropene functionalisation has the drawback of slower kinetics in IEDDA reactions in comparison to other stained alkenes, but its relatively small size endows it a suitable candidate for certain biological applications where large ncAAs may interfere with structure and function of the target proteins. Lin *et al.* first genetically encoded a 3,3-disubstituted cyclopropene handle on proteins for photoclick chemistry with tetrazoles.[154] Later, the Chin group explored 1,3-disubstituted cyclopropene ncAA (ncAA **14**) for IEDDA protein labelling, in particular, for proteome tagging and labelling (more details in Section 5.4).[155] In general, the cyclopropene handle has the advantage of being efficiently incorporated into proteins without suffering from isomerisation and presenting a relatively small size and fast kinetics (labelling reaction on proteins completed within 30 min).[155,156]

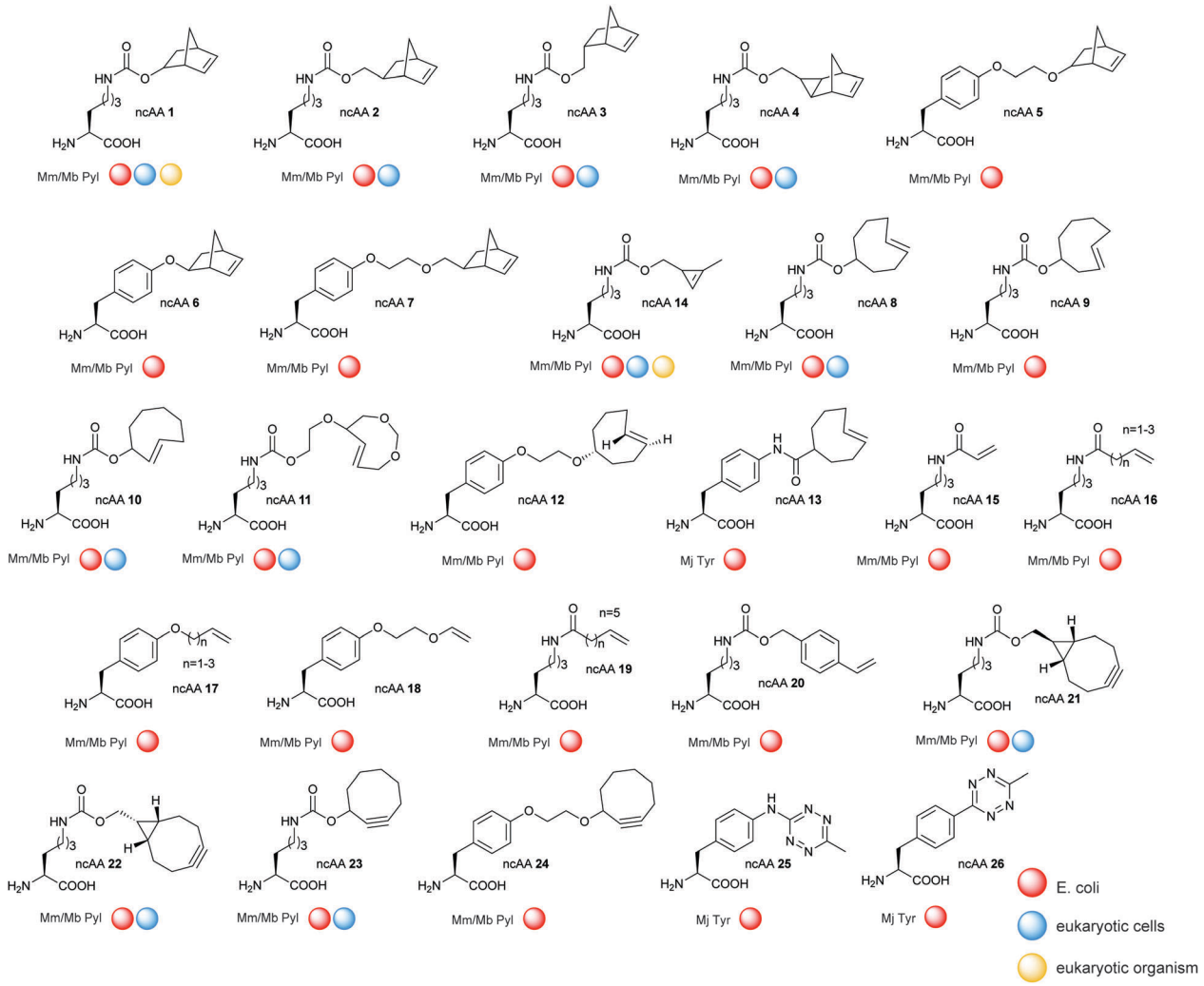

Fig. 23 Summary of ncAAs that have been genetically encoded into proteins for IEDDA application.

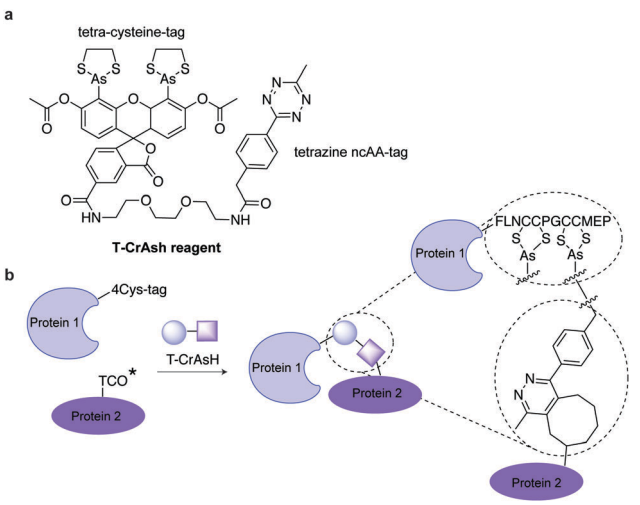

Fig. 24 (a) Chemical structure of T-CrAsH reagent and the products of the two covalent reactions. (b) General scheme of the T-CrAsH method.

4.1.4 Unstrained alkenes. Unstrained alkenes react with tetrazine with second-order rate constants of more than 0.001 M^{-1} s^{-1}, rates comparable to those of the Staudinger ligation and the

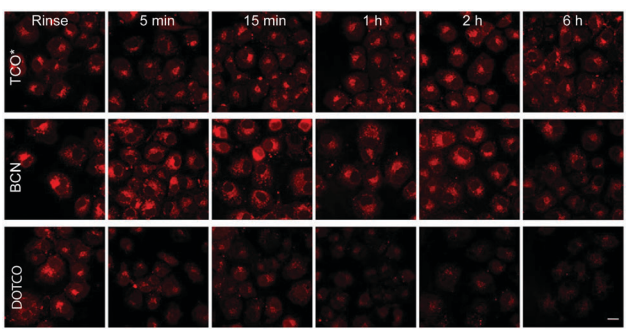

Fig. 25 Comparative washout studies with DOTCO, BCN and TCO ncAAs. Confocal microscopy imaging of non-transfected cells washed for different times before labelling with a tetrazine dye. With DOTCO intracellular nonspecific background is easily removed from the cytoplasm after washing for 5 min. From ref. 120, Copyright © 2016 by John Wiley & Sons, Inc. Reprinted in part by permission of John Wiley & Sons, Inc.

copper-free dibenzocyclooctyne–azide cycloaddition. In comparison to strained alkenes, unstrained alkenes provide some advantages such as their small size, easy synthesis and enhanced stability towards cellular nucleophiles. Even though unstrained alkenes have already been successfully incorporated into proteins *via* genetic code expansion, it was not until 2015 that these terminal alkene-encoded proteins were successfully used for IEDDA applications. Liu group successfully incorporated 9 different terminal alkene-bearing amino acids (ncAA **15–18**) into *E. coli* using mutant PylRS/$tRNA_{CUA}$ pairs. Four of these ncAAs (with highest reaction rates and stability) enabled the selective labelling of proteins on the surface of live bacterial cells (outer membrane protein X-3 and 8, OmpX-3 and OmpX-8) by reaction with tetrazine dyes, although with poor reaction rates (over 8 h incubation).[157] In a following paper, a terminal alkene-containing fatty acyl lysine (ncAA **19**) was genetically encoded into ubiquitin and histone H3 and selectively labelled by reaction with tetrazine dyes.[158] Apart from aliphatic alkenes, a styrene-bearing lysine (ncAA **20**) was also recently incorporated into super folded GFP in *E. coli* using a PylRS/$tRNA_{CUA}$ triple mutant (L274A, C313S, Y349F).[135]

4.1.5 Cyclooctyne. Contrasting with alkenes that form various isomers upon tetrazine ligation, cyclooctynes such as strained cyclooctynes (SCO) or bicyclo6.1.0nonyne (BCN) have the advantage of yielding single products after IEDDA ligation, which allows the construction of homogeneous protein conjugates.

Bicyclo6.1.0nonyne (BCN). BCN-Lys (ncAA **21**) was first encoded into sfGFP in *E. coli* and live mammalian cells by Chin *et al.* using a *Mb*PylRS triple mutant (Y271M, L274G, and C313A).[112] Contemporaneous with this work Lemke *et al.* reported the incorporation of BCN (ncAA **22**) into several other proteins (EGFR, hepatitis D virus, actin, vimentin and FK506-binding protein), *via Mb*PylRS and *Mm*PylRS mutants.[151,152,159,160] Recently Chin *et al.* developed a genetically directed bioorthogonal ligand tethering (BOLT) method and used it for selective inhibition (iBOLT) of protein function. Specifically, BCN-MEK variants (MEK = mitogen-activated protein kinase) and specific MEK inhibitors conjugated to a tetrazine through different linkers were used for rapid and covalent inhibition of MEK isozymes. By introducing an azobenzene linker between the tetrazine and the inhibitor (photo-BOLT), reversible and optical regulation of MEK kinase activity was achieved in live cells by *cis*/*trans* isomerisation of the azobenzene. This technique was shown useful for spatiotemporal control of protein function.[161] In another example, BCN encoded sfGFP has been found to undergo IEDDA ligations with tetrazine glycan conjugates both *in vitro* and *in vivo*, providing another method for rapidly and homogenous engineering of glycoproteins.[162]

Strained cyclooctyne (SCO). First developed for site-specific protein labelling through SPAAC with fluorogenic azides,[163] genetically encoded SCO handles were later used for IEDDA applications. SCO (ncAA **23**) was incorporated into GFP *via* a double mutant synthetase from *Mm* and labelled with a Cy5 tetrazine dye. Detectable fluorescence was observed only after 2 h with excess of dye that led to significant background staining.[119,149] Apart from Lys derivatives, SCO-Tyr ncAA (ncAA **24**) has been also incorporated into proteins in *E. coli* and modified through IEDDA.[148]

4.1.6 Tetrazine. Despite the excellent kinetics displayed by TCO ncAAs, their isomerisation and consequent reduced reactivity limits their utility for *in vivo* approaches (half-life 3.26 h for TCO in fresh plasma and ~3 h for s-TCO in MeOH with excess of thiol).[59,110] A stable and reactive tetrazine-bearing amino acid could be an alternative for site-specific labelling through IEDDA. The first genetic encoded tetrazine amino acid (tet-v1.0, ncAA **25**), a derivative of *p*-aminophenylalanine derivative conjugated to a tetrazine, was incorporated in *E. coli via* an evolved orthogonal *Mj*TysRS/$tRNA_{CUA}$ pair. A tet-v1.0-GFP conjugate was shown to react with s-TCO, however, only with modest kinetics (k_2 ~880 M^{-1} s^{-1} and ~330 M^{-1} s^{-1} under *in vitro* and *in vivo* conditions, respectively).[164] In line with these results the same tet-v1.0-GFP construct was later labelled with d-TCO with an *in vitro* rate constant around 100 M^{-1} s^{-1}.[60] Due to the synthetically inaccessibility and moderate reaction rates of tet-v1.0, a new version of this ncAA, a phenylalanine-tetrazine (ncAA **26**), was developed for ideal bioorthogonal labelling. Tet-v2.0 showed high stability (several days) in the presence of thiols in PBS buffer and could be successfully incorporated into GFP with the help of an evolved *Mj*TysRS/$tRNA_{CUA}$ pair. The resulting Tet-v2.0-GFP undergoes IEDDA several orders of magnitude faster than Tet-v1.0 with a rate constant of ~72 500 M^{-1} s^{-1} and a half reaction time of 12–14 seconds against s-TCO. This new ncAA enabled the efficient sub-stoichiometric labelling of proteins in live cells, eliminating the need for washing out excess labelling agents.[121]

4.1.7 Dual genetic encoding. Substituting two native amino acids in a protein with two ncAAs of interest can be useful for example for dual labelling with distinct probes to study folding and conformational changes of proteins. For this purpose, evolved aaRS/tRNA pairs were used to incorporate two ncAAs into a protein in response to an amber and quadruplet codon.[165] Specifically, ncAAs bearing alkyne and cyclopropene reactive handles were incorporated together into a single protein using the orthogonal PrpRS/$tRNA_{CUA}$ and PrpRS/$tRNA_{UACU}$ pairs. The latter decodes the quadruplet codon with the help of the evolved orthogonal ribosome ribo-Q1. Because CuAAC and IEDDA reactions are orthogonal, quantitative dual labelling of proteins was rapidly achieved by reaction with the corresponding tagged-fluorophores (within 30 min).[166] In another example, due to the slow kinetics between deactivated tetrazines and norbornene, aminophenylalanine-tetrazine and norbornene amino acids were shown not to cross-react with each other even when placed in close proximity within the same protein. Thus, these two amino acids were site-specifically incorporated into calmodulin using the optimized orthogonal translation system. Orthogonal reaction with a BCN fluorophore (for labelling the tetrazine ncAA) and a fluorescent activated tetrazine (for labelling the norbornene ncAA), respectively, led to dual labelling. The orthogonal installation of fluorophores at defined sites enabled monitoring local conformational change of CaM towards calcium ions binding using FRET.[167]

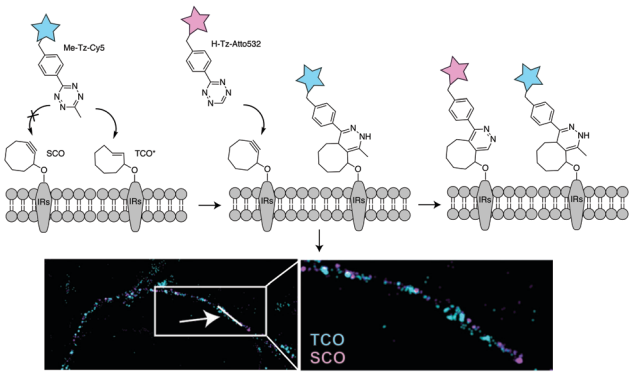

Fig. 26 Dual protein labelling on live cell surface for super-resolution microscopy. TCO-bearing and SCO-bearing amino acids were incorporated into insulin receptors. The labelled proteins were visualized *via* treatment with a fluorescent Me-Tz (cyan, Me-Tz-Cy5, to tag TCO), followed by a fluorescent mono-substituted tetrazine probe (magenta, H-Tz-Atto532 to tag SCO). From ref. 8, Copyright © 2014 by John Wiley & Sons, Inc. Reprinted in part by permission of John Wiley & Sons, Inc.

Dual genetic encoding has been also described using the promiscuity of tRNA synthetases. Indeed, Lemke *et al.* showed that a PylRS/$tRNA_{CUA}$ double mutant from *Mm* could accept both SCO and TCO*. As a result, simultaneous incorporation of two different ncAAs into proteins was possible *via* a pulse-chase labelling strategy.[8] By fine-tuning the diene partners, selective labelling of these ncAAs allowed dual colour labelling of biological relevant proteins (Fig. 26). Specifically, Lemke's lab found that, under certain reaction conditions and timescale of the experiment, TCO* reacts with both mono-substituted (H-Tz) and di-substituted (Me-Tz) tetrazines, while SCO reacts only with mono-substituted variants (Fig. 26). Of note, the reactivity of H-Tz and Me-Tz with other dienophiles was recently studied in detail and to proceed as follows: H-Tz:*endo*BCN > or ≈ *exo*BCN > TCO*mix isomers ≫ SCO ≫ norbornene; Me-Tz: TCO*mix isomers ⋙ *endo*BCN > or ≈ *exo*BCN ⋙ SCO > norbornene. This provides guidance for constructing orthogonal reactions and dual labelling systems.[67]

4.2 Alternative enzymatic methods or enzyme tags for protein modification by IEDDA

An alternative to genetic encoding methods for protein bioconjugation uses engineered enzymes that covalently attach a labelled substrate to a tagged protein of interest by recognizing a peptide sequence or a small fused protein (*e.g.* trypsiligase, lipoic acid ligase, PFTase, sortase). Another approach involves the use of self-labelling enzymes that have been engineered to attach a fluorescent molecule to one of its own amino acid residues (SNAP/Clip tag, HaloTag).[1,3]

4.2.1 Trypsiligase. The introduction of the tripeptide recognition sequence YRH at the N- or C-terminal region of a protein of interest (POI) *via* standard mutagenesis enables site-specific enzymatic conjugation of click handles. Trypsiligase, an engineered trypsin variant, is both able to cleave the YRH peptide bond and to attach diverse moieties to the ensuing terminal amino acid. The N-terminal cleavage of the tag is followed by the introduction of the click handles provided in the form of acyl-4-guanidinophenyl ester derivatives (OGp), whose ester leaving groups mimic trypsin-specific arginyl substrate side chains (Fig. 27a). Addition of the click counterpart leads to the final modified protein. Cleavage of the tag at the N-terminal results in a transient acyl–enzyme intermediate that reacts with Arg-His-containing peptides bearing a tetrazine that could be used for further conjugation (Fig. 27a). Using trypsiligase-catalysed reaction, Bordusa *et al.* managed to modify peptides proteins and antibodies with norbornene and Tz-moieties at N- and C-terminus respectively. Most reactions are completed in one hour with nearly quantitative product yield, suggesting the high efficiency of the trypsiligase reaction. Subsequent IEDDA enables fluorescence labelling, PEGylation and drug conjugation.[168]

4.2.2 Lipoic acid ligase. Site-specific protein labelling using PRIME (probe incorporation mediated by enzymes), is based on a mutant lipoic acid ligase from *E. coli* that covalently conjugates chemical handles to a LplA acceptor peptide (LAP) fused proteins (Fig. 27b). Ting *et al.* have shown that an engineered LplA with a single mutation at Trp37 (LplA W37V) can efficiently ligate TCO into target proteins (*e.g.* lipoproteins, neuroligin, actin, and vimentin). The TCO-ligated LAP reacts with tetrazine–fluorophores with high second-order rate constants ($\sim 5000 \pm 700\ M^{-1}\ S^{-1}$). The use of fluorogenic tetrazine probes (~13-fold increase in fluorescence intensity upon reaction) allowed, for example, the labelling of LAP-tagged low-density lipoprotein receptors in HEK 293T cells (15 min for TCO ligation and 3 min for tetrazine labelling).[83] Similarly, by using LplA W37V, Wombacher *et al.* successfully ligated a norbornene derivative with a transmembrane protein with an extracellular LAP-tag in HEK293T cells.[169]

4.2.3 Protein farnesyltransferase. Protein farnesyltransferase (PFTase) has been used to covalently attach farnesyl diphosphate site-specifically at the cysteine residue of the recognizing sequence CAAX (Fig. 27c). Using the promiscuity of PFTase, Distefano *et al.* synthesized a TCO geranyl diphosphate for PFTase mediated chemoenzymatic bioconjugation. CAAX-box containing peptides and proteins proved to be attached to TCO moieties by the catalysis of PFTase. Despite the bulkiness of TCO, the hydrophobic tag fits the active site of PFTase with only 2-fold difference k_m compared with its physiological substrate. Interestingly, further optimized by site-directed mutagenesis, Y205A mutant of PFTase was proved to enhance k_{cat} by 5-fold when compared to the wildtype, reaching a sub-micromolar k_m.[170]

4.2.4 Sortase. Another method uses sortase (SrtA) to mediate site-specific protein labelling. The enzyme recognizes a 5 amino acid peptide sequence near the C-terminus of its target site, cleaves a specific peptide bond within this sequence, and forms an amide bond between the new C-terminal amino acid and an N-terminal glycine of a polyglycine species (Fig. 27d). By using an optimized penta-mutant sortase A, a single domain antibody VHH bearing LPXTG sequence at its C-terminal was site-specifically modified by $(Gly)_3$-TCO. TCO-modified VHH was then ligated with radioactive aminooxy-tetrazine derivative for PET imaging of pancreatic cancer.[171] A Tz-modified VHH

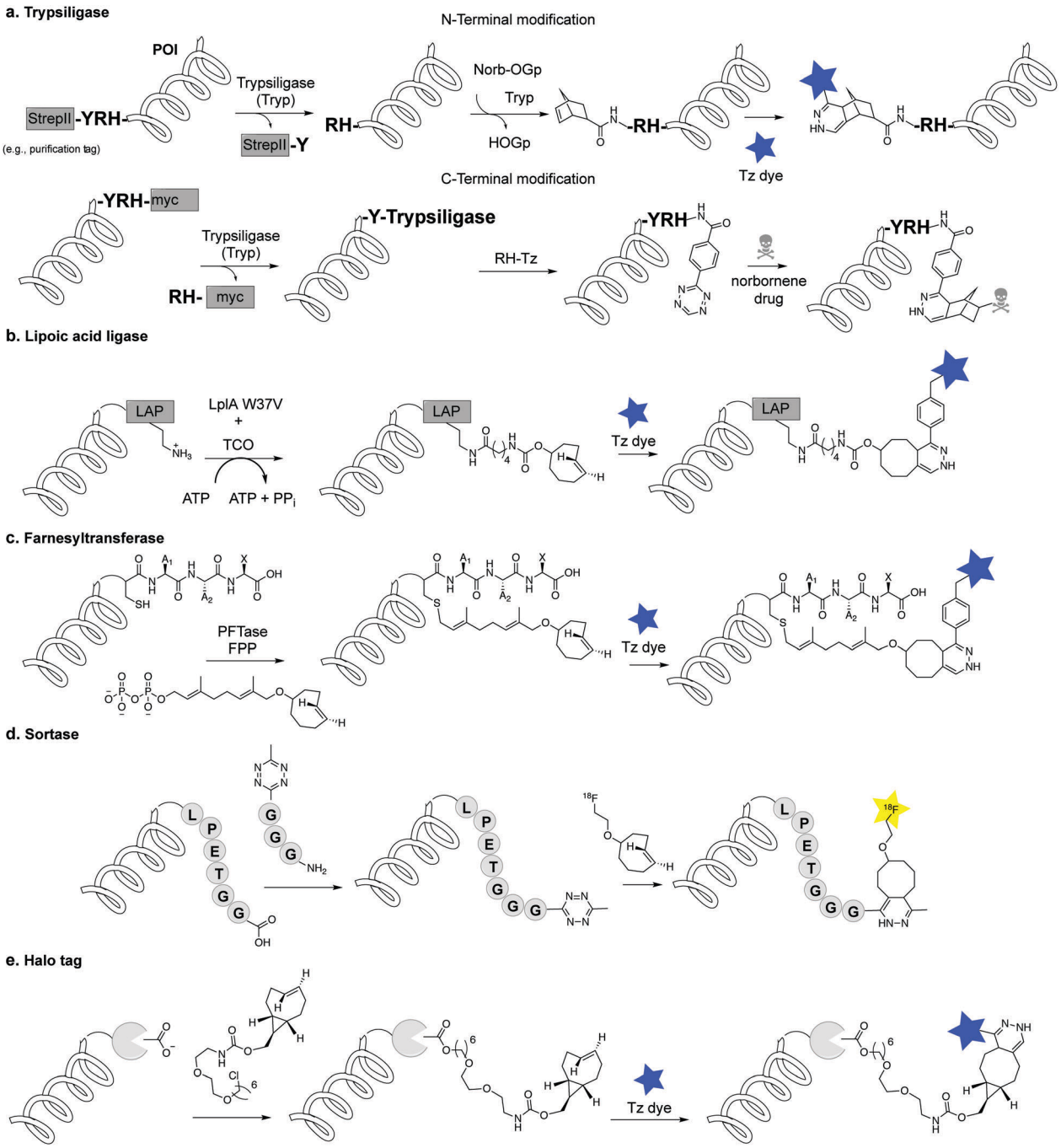

Fig. 27 Enzymatic methods for protein labelling through IEDDA. (a) Protein modification *via* trypsiligase. (b) Site-specific fluorescence labelling of proteins using LplA and tetrazine reactions. (c) Labelling of CaaX peptide motif at the C-terminus with farnesyl isoprenoid analogs catalysed by PFTase. (d) Sortase bioconjugation. (e) HaloTag-based bioconjugation.

followed by labelling with a ^{18}F-TCO derivative has also been used for tumour imaging.[172] Just recently, Cochran *et al.* engineered a sortase variant 7M (SrtA7M), which could use various small amines instead of polyglycine as substrates.[173]

4.2.5 Halo tag. The bacterial enzyme haloalkane dehalogenase has been engineered as a self-labelling protein tag (Halo Tag). Indeed, an engineered variant of this enzyme catalyses the formation of a covalent ester bond between an aspartate in the enzyme and the alkyl group of the alkyl halide, enabling the covalent attachment of synthetic labelled substrates (Fig. 27e). By using this Halo Tag protein labelling technology, both dienophiles and tetrazines were incorporated into proteins, followed by IEDDA with a suitable dye-conjugated partner. Intracellular labelling of different Halo tagged histone proteins (Halo-H_2B-GFP and Halo-H_2B-mCherry) was validated and evaluated in HeLa cells using in-gel fluorescence and fluorescence microscopy.[111] This two-step strategy was recently applied for visualization of compartmentalized cations.[174]

4.3 Direct incorporation of unnatural nucleotides into RNA/DNA for IEDDA modification

4.3.1 Solid-phase synthesis of oligonucleotides containing IEDDA bioorthogonal handles. Solid phase synthesis has been used as an efficient approach to incorporate reactive handles into DNA/RNA. Due to the sequential and flexible nature of solid phase approaches, alterations may be introduced on different regions of an oligonucleotide, namely, on the sugar, nucleobases or even backbone.[175,176] For instance, site-specific chemical incorporation of Nor,[68,177–179] TCO,[180] and Tz[68] at internal or terminal positions within DNA or RNA has been accomplished for subsequent IEDDA reactions (Fig. 28a). Importantly, Schorr *et al.* showed that synthetic RNA oligonucleotides tagged with a norbornene dienophile could be labelled in mammalian cells by reaction with a tetrazine probe.[179] The stability of IEDDA reactants under the conditions required for solid-phase synthesis has, however, been a concern. For instance, the synthesis of a TCO-modified oligonucleotide required the use of *t*-butyl hydroperoxide as an oxidant due to the quantitative degradation of the TCO moieties using standard aqueous iodine oxidation.[180] Additionally, due to the general instability of tetrazines during oligonucleotide cleavage from the solid support, post synthetic labelling was only achieved on beads.[68] Alternatively, enzymatic approaches have been developed for site-specific incorporation of unnatural nucleotides on RNA/DNA.[175] Current methods used for incorporation of bioorthogonal handles directly into oligonucleotides for click chemistry are represented in Fig. 28.[175,176,181]

4.3.2 Enzyme-mediated modification of RNA. Functionalisation of nucleotides with small bioorthogonal handles is a versatile approach for transcriptional labelling, however, this approach leads to random incorporation of the clickable moieties into RNA (Fig. 28a). Alternatively, incorporation of modified nucleosides into the RNA strands is possible *in vitro* during transcription using the well-known 5′-initiation method employing the T7 RNA polymerase (Fig. 28b). This enzyme efficiently initiates transcription using the T7 promoter and a guanosine nucleotide as the +1 base. Jäschke *et al.* showed that this polymerase could terminally modify RNA, using norbornene- and BCN-modified guanosine monophosphate (GMP) as the initiator nucleotides.[178,182] A related approach by Royzen *et al.* showed that a cytidine triphosphate (CTP) analogue with a TCO group at the 5-position of the nucleobase is recognized by the T7 RNA polymerase, and therefore is internally and site-specifically incorporated in a RNA strand.[183] Another alternative method for RNA modification uses an engineered methyltransferase that recognises *S*-adenosyl-L-methionine analogues containing reactive handles and transfers these handles to a RNA of interest (Fig. 28c).[116] The advantage of selectively targeting a particular RNA class (*e.g.* tRNA, snoRNA or mRNA) or sequence of interest makes this method a valuable approach for chemoenzymatic labelling of RNA.

Recently, Rentmeister *et al.* showed that a variant of trimethylguanosine synthase 2 from Giardia lamblia (GlaTgs2-Var1) recognises a novel AdoMet-analog bearing a vinylbenzyl group, allowing the modification of capped RNA structures at the N2 position of the 5′ cap (30% yield in 3 h with 10% of GlaTgs2-Var1).[116] Similarly, an allyl modified RNA was prepared in 90% yield. The differences in yields were attributed to steric constraints in the substrate-binding pocket of the methyltransferase. Subsequent IEDDA labelling with a tetrazine-TAMRA

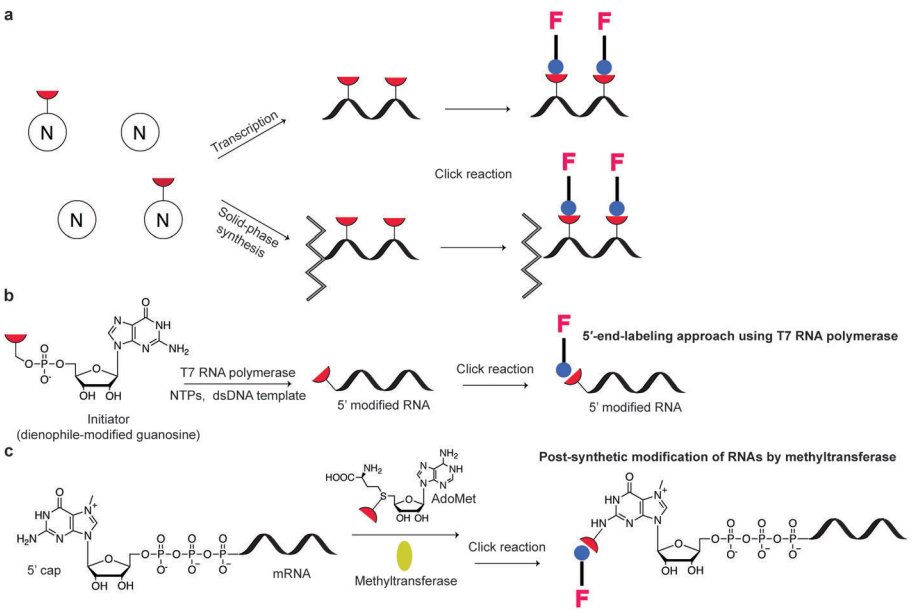

Fig. 28 Methods used for incorporation of IEDDA bioorthogonal handles into RNA for subsequent labelling by click chemistry. (a) The promiscuity of various RNA polymerases tolerates the incorporation of unnatural nucleotides, producing modified RNAs. (b) Labelling of RNAs using the 5′-end-labelling approach employing the T7 RNA polymerase. (c) Post-synthetic modification of RNA by chemo-enzymatic labelling of 5′-capped RNAs. A methyltransferase (MTase) variant can be used to modify the mRNA cap with the reactive handle if the respective *S*-adenosylmethionine (AdoMet) analog is provided. NTP = Nucleoside triphosphate.

derivative showed quantitative conversion of the vinylbenzyl modified 5′-capped RNA, but not on the allyl-modified RNA, possibly due to the relatively low reactivity of the allyl handle. This approach was proven to be efficient for a 106-long capped RNA.[116] It has also been shown that a cap (guanine N7) methyltransferase from the microsporidian parasite *Encephalitozoon cuniculi* (Ecm1) could transfer bulky side chains from AdoMet analogues to 5′-capped mRNAs at position N7 with almost quantitative conversion, which allowed efficient labelling with a tetrazine dye.[184] By using the above-mentioned methyltransferases and exploring their regioselectivity, dual 5′ Cap labelling of mRNAs was also achieved.[185]

4.3.3 Enzyme-mediated modification of DNA. DNA IEDDA labelling has also been achieved using DNA polymerase, reverse transcriptase *via* primer extension (PEX) or reverse transcription. A number of nucleotides bearing vinyl,[186] cyclopropene,[187] Nor,[188] TCO[189,190] and tetrazine[187] handles have been successfully incorporated in DNA and labelled (Fig. 29). Work by Jäschke *et al.* used norbornene-bearing primers to synthesise modified DNA through PCR without concerns over polymerase tolerance.[191] Another approach to incorporate functional groups into DNA uses terminal deoxynucleotidyl transferase (TdT) that catalyses the addition of modified nucleoside triphosphate (NTP) to DNA 3′-termini.[192]

4.3.4 Site-specific DNA functionalisation with alkenes. While PEX, PCR and *in vitro* transcription can modify DNA with multiple dienophiles, these modifications are usually not selective. Applying the above-mentioned nucleoside derivatives to complex cellular environments results in labelling of all nascent transcripts. Since selectivity is highly desirable, approaches for site-specific introduction of non-native nucleotides are required.

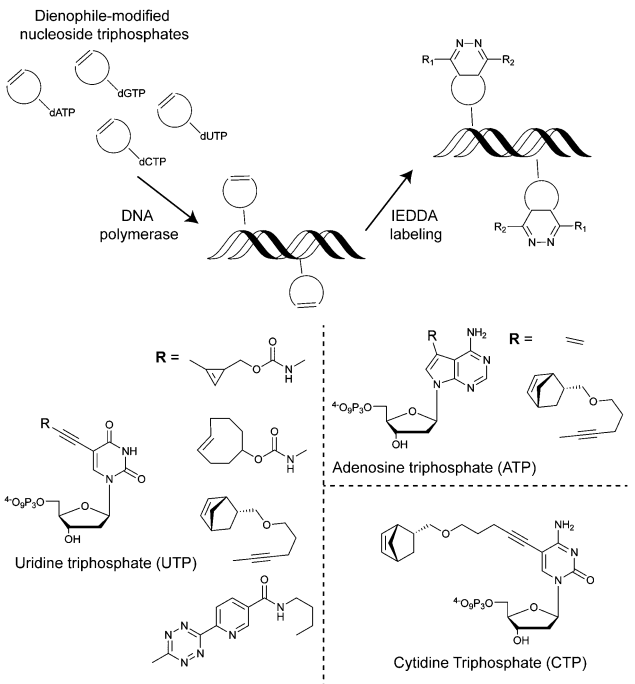

Fig. 29 Examples of IEDDA nucleotides incorporated into DNA.

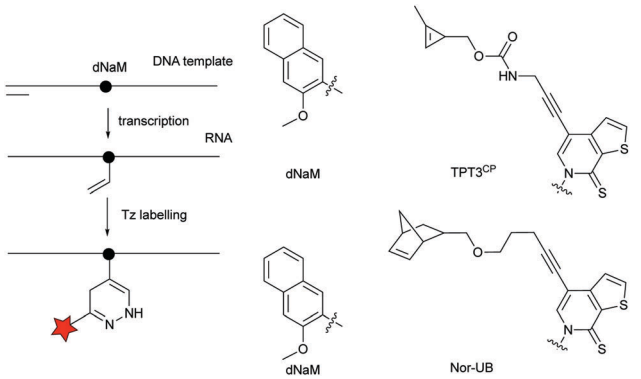

Fig. 30 Unnatural nucleobase 2-methoxy-3-methylnaphthalene (dNaM) is placed in the DNA template to site-specifically incorporate the complementary cyclopropene ($TPT3^{CP}$) or norbornene-bearing unnatural base (Nor-UB) during T7 *in vitro* transcription.

Recently, two artificial base pairing systems have been developed for incorporation of functionalities at defined positions. Instead of H-bonding interactions, these unnatural bases form hydrophobic interactions efficiently and selectively even during PCR amplification. Using an dTPT3-dNaM artificial base pair, a ribonucleoside triphosphate containing either norbonene[193] or cyclopropane,[194] was introduced into RNA *via* T7 *in vitro* transcription using DNA templates with the complementary unnatural nucleobase (Fig. 30).

4.3.5 Unnatural nucleotide. Recently, nucleotides bearing alkene handles were shown to be accepted by cellular machineries, providing an alternative strategy for DNA labelling. A vinyl bearing nucleotide (5-vinyl-2′-deoxyuridine, VdU) was synthesized by Luedtke *et al.* and selectively incorporated into cellular DNA in Hela cells *via* endogenous enzymes. VdU treated cells were stained with TAMRA-Tz rapidly in 30 min and dual labelling of cellular DNA was achieved on VdU and EdU (5-ethynyl-2′-deoxyuridine) on cells *via* tetrazine and CuAAC ligation.[115]

4.4 Metabolically incorporation for glycan modification

The simplest method for chemically labelling relevant biomolecules in living systems is metabolic labelling, in which the endogenous machinery of living cells is used to incorporate reactive handles into the biomolecules. In general, this is accomplished by growing cells or organisms in media in which a specific natural substrate (*e.g.* amino acid, nucleotide and carbohydrate) is replaced with a close analogue bearing a chemical reporter for subsequent modification with affinity or biophysical tags. Consequently, cells use the chemical analogue instead of the natural substrate to synthesize or modify glycans, nucleic acids or proteins. Numerous bioorthogonal probes have been developed for metabolic labelling including azidohomoanaline for labelling newly synthesized proteins by replacement of natural Met residues, azido sugars for labelling glycoproteins and 5-ethynyl-2′-deoxyuridine (EdU) for labelling nucleic acids.[195] To the best of our knowledge, IEDDA reactions have thus far been successfully applied for metabolic labelling of glycans, and nucleic acids, but the possibility of using the tetrazine click reaction to label proteins tagged with a dienophile-bearing

ncAA (or *vice versa*), incorporated using the natural translational machinery, is still to be explored.

Glycans participate in diverse biological processes such as extracellular matrix formation, protein folding, protein stability and function, regulation of the interaction of proteins with one another, *etc.*[196] In addition, disordered glycosylation is associated with a number of diseases.[197] The ability to monitor glycans could provide fundamental insights into their roles in cell biology. While azide and alkyne reactive handles have been the most popular for labelling tagged glycans using bioorthogonal chemistry,[198] IEDDA-based approaches are now advancing.

4.4.1 Cyclopropene-modified sugars. The possibility of using alkene-functionalised sugars for metabolic oligosaccharide engineering was first demonstrated in 2012 by Prescher *et al.*[106] In this work the authors showed that a methylcyclopropene handle, incorporated as part of methylcyclopropene-linked sialic acid analogue (Neu **1**, Fig. 31), could meet the stringent steric demands required for metabolic incorporation, allowing the visualization of sialylated glycoproteins on live cell surfaces. Following this work, in 2013 Devaraj *et al.* demonstrated that methylcyclopropene bioorthogonal handles could be used for metabolic imaging of unnatural mannosamine derivatives (Man **1**) on live-cell surfaces.[199] Later, Wittmann *et al.* investigated the effect of having either an amide or carbamate linker between the glycan and cyclopropene moiety. This work showed that *N*-acyl-mannosamine derivatives bearing a methylcyclopropene tag attached to the sugar *via* a carbamate moiety (Man **2**) reacts faster with tetrazines (second-order rate constant of $0.99 \pm 0.1\ M^{-1}\ s^{-1}$) and could be efficiently accepted by the cell's metabolism. In this case rapid membrane staining was achieved with a fluorogenic tetrazine in only 5 min.[107] In a similar approach, Prescher *et al.* synthesised probes based on glucosamine, galactosamine, and mannosamine (Man **2**, Gal **1**, Glc **1**) with different linkers (carbamates *versus* amides).

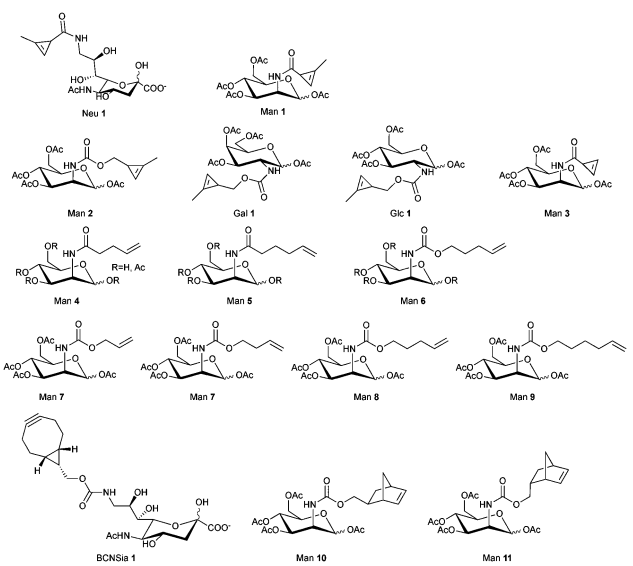

Fig. 31 Carbohydrate derivatives used in glycan engineering to date for IEDDA labelling.

As previously observed carbamate-functionalized cyclopropenes showed improved utility for glycan imaging and profiling.[200] It has also been shown that cyclopropenes outfitted with carbamates (*versus* amides) at C-3 react about 100 times faster with electron-poor tetrazines.[17,18,21,26] In order to fulfil enhanced kinetics for *in vivo* dynamic glycan labelling, Ye *et al.* compared the stability and reactivity between methyl (Ac_4ManNMCp, Man **1**) and unsubstituted (Ac_4ManNCp, Man **3**) cyclopropene *N*-acetylmannosamine derivatives. The metabolic incorporation efficiency of Ac_4ManNCp was found to be superior to Ac_4ManNMCp in all cell lines leading to a significant increase in fluorescence intensity after Tz labelling. With almost 10-fold faster kinetics and high stability against excess of thiols when compared to Ac_4ManNMCp, Ac_4ManNCp could rapidly probe *in vivo* sialylated glycoproteins from splenocytes as well as other tissues.[201] Wittmann *et al.* showed that methylcyclopropene-tagged *N*-acetylgalactosamine (Ac_4GalNCyoc, Gal **1**) and *N*-acetylglucosamine (Ac_4GlcNCyoc, Glc **1**) were successfully incorporated into HEK 293T, Jurkat and HeLa cells and could be used to monitor glycosylation of intracellular glycoproteins.[202] Recently, the same group explored Ac4GlcNCyoc (Glc **1**) for probing glycosylation of intracellular proteins (*e.g.* OGT, Foxo1 or p53) fused with GFP by detecting FRET between the tetrazine labelled glycans and the fused protein.[203]

4.4.2 Terminal alkene-modified sugars. Unstrained terminal alkenes handles, due to their relatively small size, stability and easy synthesis are also being explored as chemical reporters for metabolic oligosaccharide engineering. Wittmann *et al.* developed and metabolically incorporated mannosamine and glucosamine derivatives bearing terminal double bonds with carbamate and amide linkage into live cells. Most sugar derivatives (Man **4–9**) show kinetics between 0.01–0.1 $M^{-1}\ s^{-1}$, which are comparable to Staudinger and SPAAC ligations. By varying the length of the alkene side chain, it is possible to fine-tune the balance between kinetics and incorporation efficiency. Specifically, kinetic studies showed that the reactivity of alkene-sugar derivatives increase with growing chain length (from C3 to C6). When applied to metabolic oligosaccharide engineering, all sugar derivatives could be employed to label cell-surface carbohydrates on living HEK 293T cells, however, a mannosamine derivative with a median alkene side chain (ManNBeoc, Beoc = butenyloxycarbony) had the optimal balance between metabolic incorporation efficiency and reactivity for cell-surface labelling.[117,204]

4.4.3 Norbonene-modified sugars. Aside from these small IEDDA handles, bulkier, but more reactive groups have also been engineered for imaging glycosylation. Two norbornene bearing mannosamine derivatives (Man **10** and **11**) were incorporated in HEK 293T cells with a 1% incorporation rate. Importantly, *exo*-norbornene-modified mannosamine derivative showed more distinctive cell staining in line with its faster (2×) kinetics ($k_2 = 4.6 \pm 0.5\ M^{-1}\ s^{-1}$) compared to the *endo* derivative. Although with comparable kinetics to cyclopropene-modified sugars, the norbornene–mannosamine derivatives required 3 hours of reaction, instead of 15 minutes, to obtain significant staining. This was attributed to low incorporation of the bulky norbornene structure.[205]

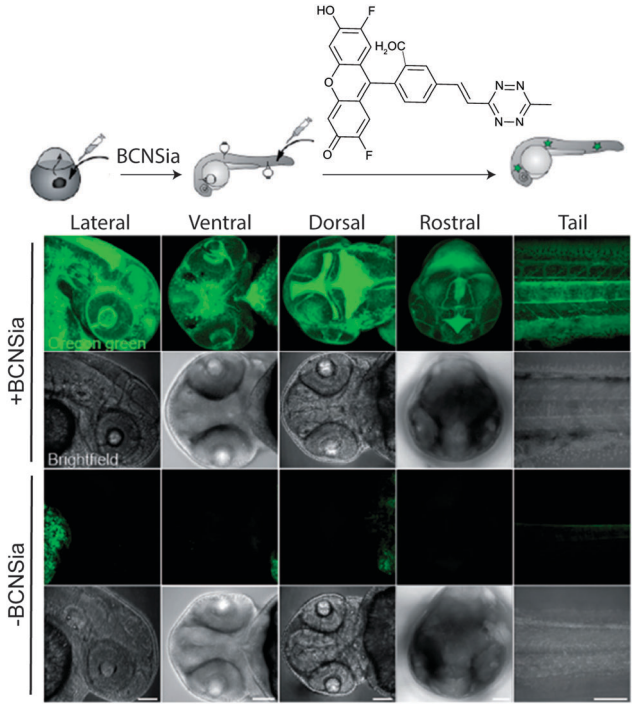

Fig. 32 Zebrafish embryos treated with or without BCNSia and subsequently injected with a fluorescent tetrazine. From ref. 207, Copyright © 2014 by John Wiley & Sons, Inc. Reprinted in part by permission of John Wiley & Sons, Inc.

4.4.4 BCN-modified sugars. Examples of probing glycosylation *in vivo* have also been reported in mouse[206] and zebrafish[207] using bioorthogonal sugar derivatives. In one example, Bertozzi *et al.* developed a bioorthogonal approach for systemic imaging of glycans by metabolically incorporating a BCN-functionalized sialic acid (BCNSia **1**) at various development stages of Zebrafish, following by IEDDA labelling.[207] Despite its relatively large size, BCNSia could be adopted and tolerated by relevant enzymes. First, the authors successfully incorporated BCNSia into cultured HEK293, Jurkat and CHO cells, and verified that BCNSia is processed through the sialic acid metabolic pathway. Additionally, BCNSia was metabolically incorporated into zebrafish embryos by systemic microinjection of BCNSia followed by reaction with a fluorogenic tetrazine probe, resulting in a robust BCNSia-dependent fluorescence of interior cells with minimal background (Fig. 32). Notably, with this robust system, several novel sialylated structures were observed (*e.g.* sialylation of the optic nerve and hindbrain). Furthermore, by incorporating BCNSia and SiaNAl (*N*-4-pentynoyl neuraminic acid), orthogonal labelling was observed, with BCNSia labelling internally and SiaNAl labelling the envelope layer. It should be noted that the embryo's yolk showed BCNSia independent fluorescence labelling, possibly due to reaction between the fluorogenic tetrazine and unsaturated fatty acids or sterols. This highlights the importance of bioorthogonality, as unexpected targets in cells may be labelled.[207]

4.4.5 Dual glycan labelling. Due to the orthogonality between IEDDA and azide–alkyne cycloaddition, most IEDDA-sugars may be used for dual labelling with Ac4GlcNAz.[106,107,117,199,200,205] In one example, Wittmann *et al.* simultaneous incorporated cyclopropene and azide handles in cell surfaces and performed orthogonal dual labelling with a Tz dye and DIBO-488.[107] Despite the fast kinetics of IEDDA compared to SPAAC, longer incubation of Tz probes (3 hours for the norbornene sugar and 6 hours for terminal alkenes) was necessary for efficient staining due to low incorporation efficiency.[107,117,205] In addition, it should be noted that DIBO-dye always leads to some non-specfic labelling due intracellular staining of thiols.[20,107,117]

4.5 Unnatural D-amino acids IEDDA reporters

Exogenous unnatural D-amino acids have been incorporated in place of the terminal D-alanine of bacterial peptidoglycans and are being used for remodelling and imaging of bacterial surfaces. Thanks to the promiscuity of transpeptidase, various alkene-displaying D amino acids (from terminal alkenes to norbornene) were incorporated onto the cell surface and labelled by reaction with fluorescent tetrazines.[208] A D-Dap-norbornene (Dap = D-diaminopropionic acid) showed the best labelling efficiency with a balance between incorporation efficiency and IEDDA reactivity. A tetrazine bearing D-amino acid (D-Dap-Tet-NH_2) was also tested for metabolic remodelling and subsequent TCO imaging. Despite the expected fast kinetics, labelling efficiency with D-Dap-Tet-NH_2 was lower than with D-Dap-NB-NH_2, presumably due to limited incorporation levels.[208]

4.6 Bioorthogonal IEDDA lipid chemical reporters

Bioorthogonal chemical reporters for lipid labelling and imaging have also attracted widespread interest in recent years.[209] In one example, a cyclopropene tagged phospholipid was used for visualizing phospholipid uptake and distribution in human cells (SKBR3 breast cancer cells). Upon treatment with a fluorogenic tetrazine, rapid membrane staining was observed.[104] Following these studies, a TCO-tagged ceramide lipid and a reactive tetrazine were used for imaging Golgi structures and dynamics in live cells by 3D confocal and stimulated emission depletion (STED) microscopy.[210]

4.7 Chemical introduction of IEDDA bioorthogonal handles

In addition to genetic encoding, the development of reactions that enable the selective installation of reactive handles on relevant biomolecules for subsequent modification/imaging would facilitate the study of the biological function of these targets. Within the last few years few examples were reported for the chemical installation of IEDDA reporters on proteins. Functionalization of proteins with IEDDA partners using NHS-chemistry has been widely developed for conjugation; however, this method is not site-selective resulting in heterogeneous mixtures of conjugates. As example, Weissleder *et al.* converted TCO into the reactive succinimidyl carbonate for conjugation to amine-containing biomolecules, including antibodies. Cetuximab–TCO conjugate was used for pre-targeted imaging of A549 cancer cells that overexpress EGFR (Fig. 33a). Recently, we demonstrated that *S*-allyl Cys could be easily chemically installed into apoptotic protein markers through a [2,3]-sigmatropic

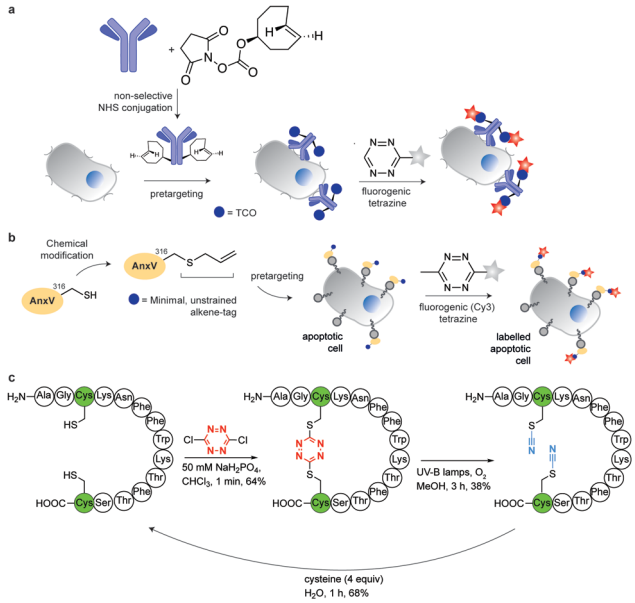

Fig. 33 Chemical installation of IEDDA reporters for pretargeting imaging approaches. (a) TCO-antibody prepared by NHS-chemistry for pre-targeted antibody labelling. (b) Chemical installation of terminal alkene handles for imaging apoptotic cells. (c) *S*,*S*-tetrazine crosslinking mechanism that regenerates the starting disulfide by a UV-catalysed tetrazine decomposition release process.

rearrangement with allyl selenocyanate. We further demonstrate the utility of this minimal handle for the efficient pre-targeted labelling of apoptosis in cells using fluorogenic tetrazine dyes (Fig. 33b).[118] Recently, Smith *et al.* developed a protocol for the direct labelling of peptides/proteins using a crosslinking dichlorotetrazine reagent that reacts with two proximate cysteine sulfhydryl groups by nucleophilic displacement. Importantly, the authors could extend the strategy to label a protein (thioredoxin), which contains a single, solvent-exposed disulfide bond necessary for its activity. An attractive feature of the *S*,*S*-tetrazine crosslinking is the possibility to regenerate the starting disulfide by a UV-catalysed tetrazine decomposition release process and thus, in the case of thioredoxin, restore original activity (Fig. 33c).[211] Another method for chemical modification uses a bifunctional linker that contains a "IEDDA clickable" handle and a maleimide to tag cysteine/selenocysteine residues on protein surfaces.[212]

5. Selected applications of IEDDA reaction in biological systems: examples where tetrazine ligation is needed

IEDDA ligations have enormous potential for bioorthogonal approaches and thus have been used to get insights into the behaviour and function of a variety of biomolecules such as proteins, antibodies, nucleic acids, glycans, lipids or bioactive small molecules. As an example, the very fast kinetics in biological media at low concentrations make the tetrazine–TCO ligation particularly useful for tracking and imaging fast biological processes.[167,213] Other applications of the "tetrazine ligation" include fluorescent labelling of low-abundance proteins within living cells for super-resolution imaging,[152] identification of the targets of bioactive small molecules and proteins in living cells,[214] protein profiling in living systems,[155] and sequence-specific detection of DNA and mRNA.[215] The most exciting and recent examples on these topics are summarized in the next sections.

5.1 Super-resolution imaging of site-specifically labelled proteins

Until today, fluorescent proteins (*e.g.* green fluorescent protein (GFP)) have been widely used to image and track recombinant proteins in live cells. Although powerful, fluorescent protein tags are limited since their relatively large sizes may potentially interfere with protein function.[216] In contrast, methods to site-specifically label proteins in their cellular context with small, bright and photostable fluorophores by means of bioorthogonal approaches would substantially advance super-resolution imaging.[3,216] In fact, coupling fluorophores directly to a protein of interest has, comparing with fused fluorescent proteins, the tremendous advantage of minimizing the distance between probe and target, increasing spatial resolution. This becomes apparent when comparing the resolution achieved in live-cell stimulated emission depletion (STED) imaging experiments of microtubules labelled with SiRh fluorophore coupled *via* a SNAP-tag to a microtubule-binding protein[217] or directly using a docetaxel-SiR derivative[218,219] (SiR-tubulin).[3] In addition, synthetic fluorophores can have more favourable spectroscopic properties (*e.g.* brightness and photostability) than fluorescent proteins.[220] Recent advances in genetic code expansion and bioorthogonal chemistry have enabled the efficient labelling of proteins. However, super-resolution imaging has been accomplished only just recently.[8,152] Two challenges have limited progress in this area: (i) the low efficiency of non-canonical amino acid incorporation that limits labelling density and therefore spatial resolution and (ii) the uncharacterized specificity of intracellular labelling that will define signal-to-noise, and ultimately resolution, in imaging.[152,221] Optimization of incorporation efficiency, coupling chemistry, and labelling protocols recently opened the way to the application of IEDDA chemistry in super-resolution microscopy. In one example, Chin *et al.* reported the efficient production of cytoskeletal proteins (β-actin and vimentin) containing a bicyclo[6.1.0]nonyne-Lys at a specific site. These functionalized proteins could be efficiently labelled with SiRh tetrazines creating densely labelled cytoskeletal ultrastructures. Super-resolution imaging by stochastic optical reconstruction microscopy (STORM) revealed sub-diffraction features, including nuclear actin filaments (Fig. 34).[152] Furthermore, actin with distinct morphologies at different cellular locations could be observed with nanometre-scale refined features (Fig. 34).[152] Even though the super-resolution imaging was performed on fixed samples, which usually show much less background signal than live samples because it is easier to wash out unreacted probe, the experiments underline the potential of

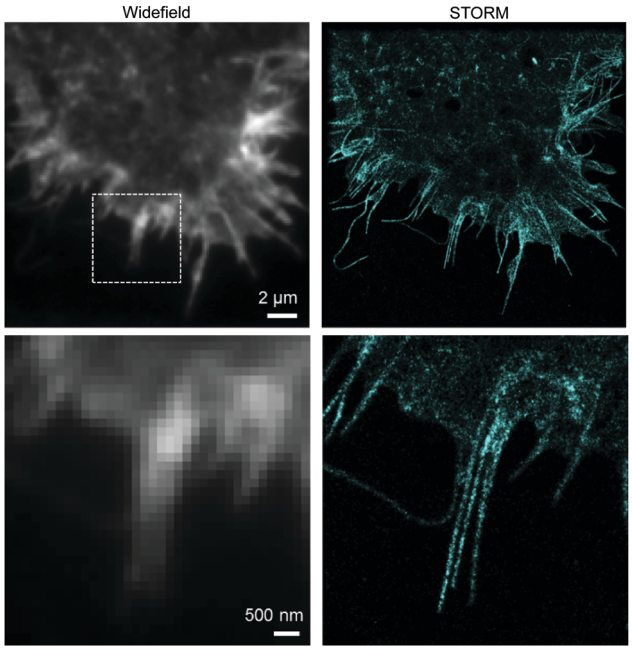

Fig. 34 STORM imaging of actin in COS-7 cells. Upper images: wide field image of actin and corresponding STORM image. Bottom images are zoom-in images of the boxed region in the upper wide field image. Adapted in part with permission from ref. 152. Copyright 2015 American Chemical Society.

the combination of genetic encoding and bioorthogonal chemistry for super-resolution microscopy.

Even though ncAA encoding technology and IEDDA reactions have been used for super-resolution imaging of highly abundant cytoskeletal proteins and surface proteins as in the previous example, applications to less abundant proteins are largely obscured by the limited efficiency of incorporation that requests the use of excess of the ncAA. This fact, results in high concentrations of non-incorporated ncAA that can also react with the dyes leading to nonspecific binding (sticking) of the fluorescent dyes. For intracellular labelling, new hydrophilic tetrazine dyes with higher "turn-on" fluorescence upon reaction, which may be washed out easily, would help to achieve higher signal to noise.[120,221,222] Alternatively, Lemke's group developed a site-specific click-PAINT super-resolution microscopy method for imaging of low-abundant proteins inside mammalian cells, namely, the protein nucleoporin Nup153, a component of the nuclear pore complex (NPC) (Fig. 35).[222] A schematic representation of this approach is outlined and the respective imaging data is presented in Fig. 35.

5.2 Study of fast dynamic process in living cells: where speed makes the difference

Although the strategy of combining site-specific incorporation of ncAAs with IEDDA bioorthogonal reactions may be advantageous for the labelling of intracellular proteins, there are several criteria that must be satisfied. One of these criteria is the careful selection of the tetrazine-conjugated fluorophores, as their cellular properties, such as membrane permeability, intracellular distribution, and retention, can affect protein labelling efficiency and specificity.

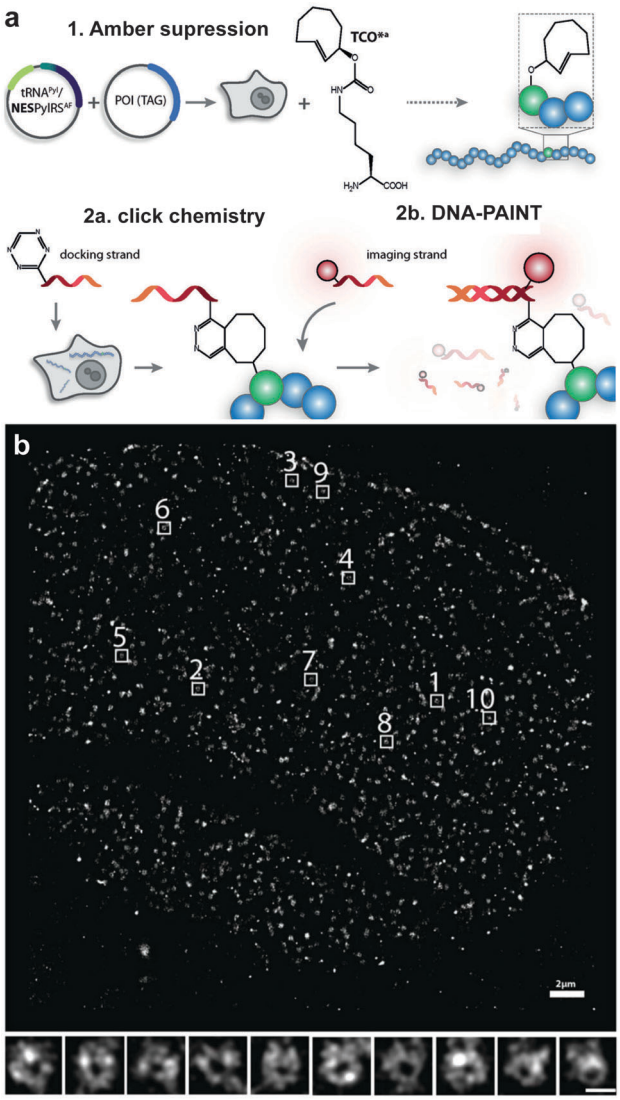

Fig. 35 Super-resolution imaging of NPC. (a) Schematic representation of the Click-PAINT method. A protein of interest and a PyltRNA/NESPylRS pair (NES = nuclear export signal coupled to PylRS to reinforce cytoplasmic localization) are expressed in mammalian cells in the presence of TCO*. The expressed TCO*-tagged protein is first reacted with a tetrazine-functionalized DNA strand and then with a complementary imaging DNA strand conjugated to a dye. (b) Super-resolved images showing the typical circular appearance of NPCs. From ref. 222, Copyright © 2016 by John Wiley & Sons, Inc. Reprinted by permission of John Wiley & Sons, Inc.

Recently, Hang *et al.* performed a systematic evaluation of bioorthogonal IEDDA reactions between site-specifically incorporated ncAAs and various tetrazine fluorogenic probes for fluorescence labelling and imaging of low-abundance intracellular proteins in live cells. In particular, it was reported that the bioorthogonal fluorescence imaging of the intracellular protein interferon (IFN)-inducible transmembrane protein 3 (IFITM3), a small vesicle-associated membrane protein that is involved in host restriction of influenza virus and many other pathogenic viruses. Fluorescent labelling of the TCO-tagged HA-IFITM3 (HA, Human influenza hemagglutinin) with various tetrazine fluorophores resulted in fluorescence puncta that are characteristic to IFITM3-containing vesicles (Fig. 36a).[213]

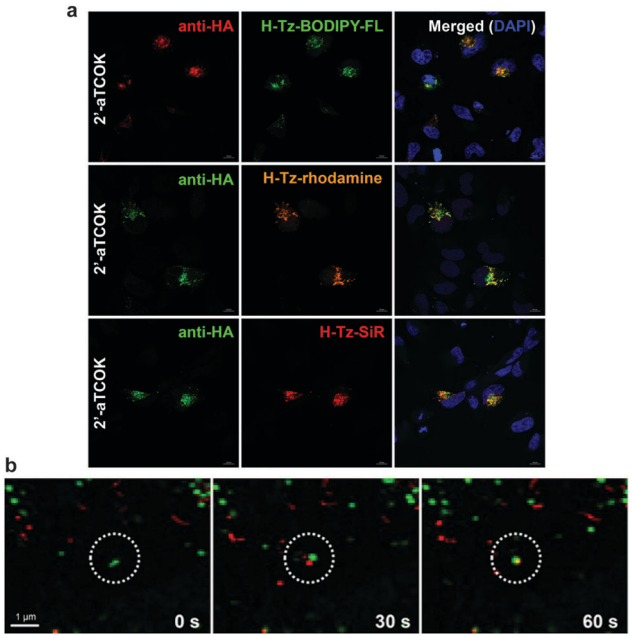

Fig. 36 Bioorthogonal fluorescence imaging of HA-IFITM3-TCOK. (a) HeLa cells expressing HA-IFITM3-TCOK were labelled with H-Tz–BODIPY–FL, H-Tz–rhodamine, or H-Tz–SiR and then subjected to anti-HA immunofluorescence staining. DAPI (blue) was used to stain nuclei. (b) Time-lapse imaging of the fusion process of IFITM-containing vesicles with dextran particles. IFITM3-TCOK was labelled with H-Tz–BODIPY–FL and dextran particles were labelled with pHrodo Red. Images were acquired every 30 seconds. Reprinted in part with permission from ref. 213. Copyright 2016 American Chemical Society.

Importantly, immunofluorescence microscopy performed in parallel with tetrazine labelling showed that tetrazine fluorophore signals overlapped with anti-HA fluorescence signals confirming labelling efficiency and specificity (Fig. 36a). Notably, when the imaging of IFITM3 in live cells was performed using N- or C-terminal fusions with fluorescent proteins (*e.g.* GFP or mCherry), both cellular localization and antiviral activity of IFITM3 were disrupted.[213] To explore the trafficking of IFITM3 in live cells, the authors evaluated the dynamics of IFITM3 with exogenously added fluorescent cargoes that are internalized into endocytic vesicles. Interestingly, it was shown that red dextran particles were internalized into cells and then fused with BODIPY-labelled green IFITM3-residing puncta to yield yellow vesicular structures, demonstrating that IFITM3 traffics to the same location as exogenously acquired cargoes after their internalization in the endocytic pathway (Fig. 36b). Moreover, the time-lapse imaging showed that this fusion process is completed within min. These studies significantly expand the scope of site-specific bioorthogonal imaging of intracellular proteins in live cells, and demonstrated the utility of fast and fluorogenic IEDDA reactions for the localization and real-time dynamic trafficking of fast biological events.[213]

5.3 Identification of bioactive targets of small molecules and proteins in living cells

Monitoring how, when, and where small molecules engage their targets intracellularly is a major challenge in chemical

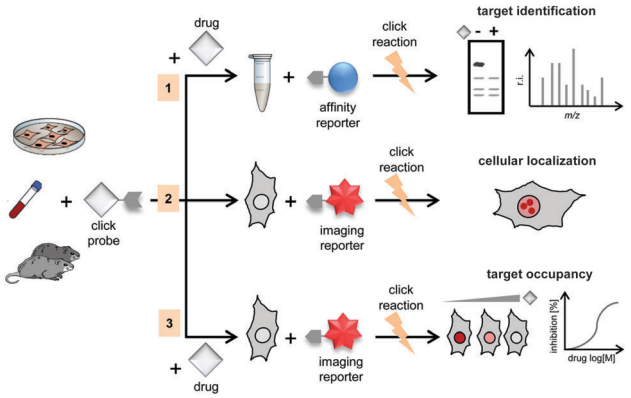

Fig. 37 A single functionalized probe containing a bioorthogonal moiety (click-probe) for (1) target/off-target identification, (2) compound colocalization with the target protein, and (3) measurement of target occupancy of unmodified compounds. Reprinted with permission from ref. 224. Copyright 2016 American Chemical Society.

biology and pharmacological research, because it provides insights that can assist the design or more efficient binders and to understand their mode(s) of action.[223] For this purpose, Bantscheff *et al.* developed a modular strategy that enabled small molecule localization, target identification and target occupancy measurements of unmodified drugs in cells using bioorthogonal ligation reactions.[224] Generally, the strategy uses a click-probe derived from a drug of interest that can be functionalized either with tags for affinity purification of potential target proteins or with fluorophores for high-resolution imaging. The feasibility of the modular probe strategy was demonstrated with noncovalent PARP inhibitors. Using a proteomic assay, the authors showed that dose-dependent competitive titration with the unmodified drug (Olaparib) allowed the determination of target and off-target affinity by quantitative mass spectrometry of the click-probe targets that are also bound to the free drug (Fig. 37(1)). In addition, attachment of a fluorophore to the click-probe allows localization of the probe inside cells by confocal microscopy (Fig. 37(2)).

This approach also allowed the determination of target occupancy by measuring the reduction of the localized fluorescence signal in the presence of unmodified drug (Fig. 37(3)).[224] Of note, the authors systematically evaluated the compatibility and efficiency of a number of bioorthogonal reactions (IEDDA, SPAAC and CuAAC) and identified TCO labelled probes and tetrazine-tagged reporters to be the most efficient bioorthogonal coupling partners.[224] Similarly, a dienophile-modified paclitaxel derivative with identical activity to the parent drug was used for imaging microtubular networks in cells upon IEDDA labelling with tetrazine fluorophore probes.[133] Similarly, TCO-modified kinase inhibitors labelled with tetrazine-tagged fluorescent reporters could be used to track and image kinase activities in live cells.[225]

The detection of protein–protein interactions (PPI) within native cellular environments could provide key insights for drug design. To address this challenging question, minimalist linkers cyclopropene and diazirine were synthetically introduced

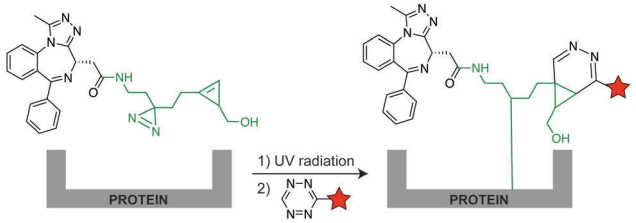

Fig. 38 Minimalist linkers for proteome profiling. The diazirine moiety generates reactive species upon ultraviolet (UV) irradiation creating covalent bonds with targeted proteins. Covalent ligation allows for affinity pull-down assays of the target for further proteome profiling using the cyclopropene handle as chemically tractable tags.

within a small molecule bromodomain inhibitor. In this approach, the inhibitor is used for target identification, while the diazirine photo-cross-linker enables covalent linking. Lastly, the cyclopropene handle is used either for bioimaging or affinity-based protein labelling using biotin-tetrazine derivatives. The resulting probes were used for proteomic analysis and resulted in the identification of several hundreds of protein candidates targeted by the bromodomain BRD-4 inhibitor (+)-JQ1 (Fig. 38).

5.4 Protein profiling in organisms

The ability to identify newly synthesised proteins at specific times in cells of interest will facilitate the study of dynamic cellular processes. In this regard, several protein tagging strategies through genetic code expansion have been employed to interrogate several complex cellular processes.[226] In one example, an azide-containing analogue (L-azidohomoalaine, AHA) of methionine (Met) was introduced at Met codons and subsequently labelled through cycloaddition with alkyne-bearing probes.[227] Based on auxotrophic strains, incorporation of the amino acid analogues is often achieved in minimal media under starvation conditions for the amino acid to be replaced. This limits the availability of the natural amino acid and decreases labelling efficiency.

A novel technology that addresses some of the above-mentioned issues was developed – stochastic orthogonal recoding of translation with chemoselective modification (SORT-M) (Fig. 39).[155] SORT-M uses a set of reengineered orthogonal pyrrolysyl-tRNA synthetase/tRNA pairs that enable codon-selective incorporation of a cyclopropene Lys derivative, which can be chemoselectively modified with various tetrazine probes for fluorescence imaging and proteome profiling of engineered bacteria, mammalian cells and in specific cell types or tissues in animals (Fig. 39).[155] Importantly, the method could be performed directly in flies for developmental stage-specific proteomic studies.[155] More specifically, by confining PylRS expression to the ovaries of *Drosophila* melanogaster using a specific promoter, selective incorporation of a cyclopropene-bearing amino acid into proteins derived from these organs was achieved. This was confirmed by fluorescent labelling of proteins specifically synthesised in the ovary. Protein identification could be also performed combining 2-D in-gel fluorescence electrophoresis and MS analysis.[155] More recently, an improved version of SORT-M called SORT-E (SORT with enrichment) was developed.

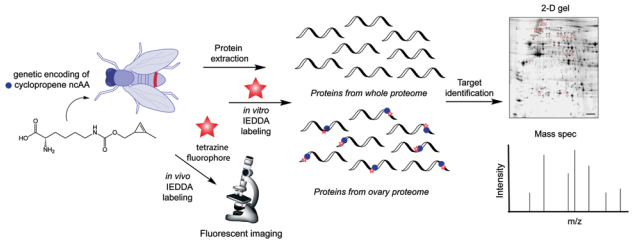

Fig. 39 "SORT-M" allows the incorporation of diverse chemical groups into the proteome, at diverse codons by PylRS aminoacylation of the corresponding $tRNA_{XXX}$ ($PyltRNA_{XXX}$, XXX indicates choice of anticodon). This system results in stochastic incorporation of the ncAA (yellow star, and yellow triangle) in the resulting protein. A GAL4 fly lines expressing $PyltRNA_{XXX}$, PylRS (under GAL-4 control) is fed with an ncAA (red star, cyclopropene-Lys derivative). The ncAA is incorporated into the proteome of specific tissues where the GAL-4 reporter is active (red ovary). Combining fluorescent 2D-gel electrophoresis and mass spectrometry is possible to identify these proteins. Direct visualization of synthesized proteins by tetrazine labelling in tissue has been also by demonstrated fluorescent microscopy.

In this version, SORT-tagged cellular proteins are reacted with a tetrazine diazobenzene biotin compound and then captured on streptavidin beads. The beads can be washed and enriched proteins may be detected using MS after reductive cleavage of the diazobenzene linker.[156]

5.5 Sequence-specific detection of DNA and mRNA in living systems

As mentioned a beneficial characteristic concerning the use of tetrazines during IEDDA is the "turn-on" effect in case a tetrazine–fluorophore conjugate is used. By using these probes, fluorescence is only observed when the bioorthogonal partners meet and, thus, where exactly the bioorthogonal reaction occurs. This feature has been used in the development of tetrazine smart probes for the sequence-specific detection of DNA and mRNA in living systems. Devaraj *et al.* first applied template-driven reactions with fluorogenic tetrazines for nucleic acid detection.[215] Specifically, a quenched fluorophore-tetrazine and a methyl-cyclopropene group were conjugated to two different oligonucleotides and showed to react by IEDDA ligation only in the presence of the DNA template that can hybridize with both oligonucleotides. The use of the template increases the effective molarity (52–123 mM) by confining the tetrazine and cyclopropene partners in close proximity, and the bioorthogonal reaction rapidly takes place, leading to strongly fluorescent products. This approach allowed detection of template DNA inside living mammalian cells (Fig. 40a).[215]

One limitation of this approach is that the resulting product reacts with a similar affinity for the template as the reactive starting oligonucleotides, impeding reaction turnover and signal amplification. To address these issues, the same research group reported an optimized system using oligonucleotide templates derivatised with a norbornadiene and a highly fluorogenic tetrazine–BODIPY probe. The use of a highly quenched tetrazine probe enables a >100-fold increase in fluorescence in response to hybridization and subsequent proximity-driven reaction. In addition, the new antisense probes undergo dynamic strand

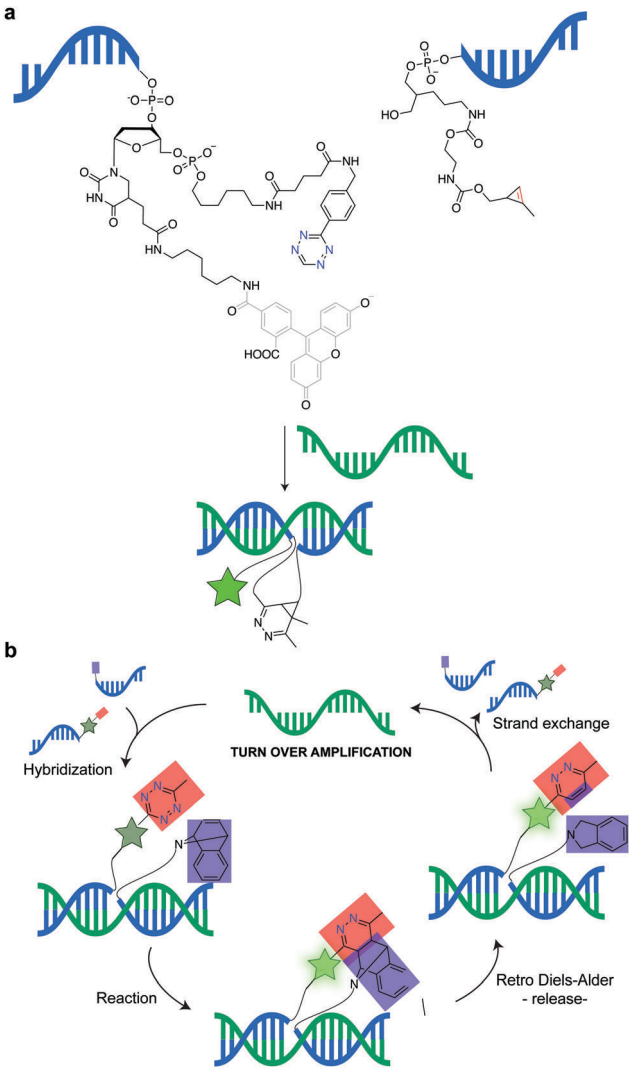

Fig. 40 (a) Schematic of DNA-template fluorogenic tetrazine ligations. (b) Schematic of DNA-template tetrazine-mediated transfer reaction for live cell miRNA detection.

exchange, which resulted in high turnover amplification allowing the detection of endogenous oncogenic miRNA target mir-21 (*in vitro* and cells) down to low-picomolar levels (Fig. 40b). Importantly, this system was able to distinguish single-base mismatches in miRNA templates.[228]

6. IEDDA applications in nuclear medicine

6.1 Overview of click radiochemistry

Nuclear imaging techniques are based on the radiolabelling of specific molecular probes using radioisotopes that are used as contrast agents for imaging of pathologic processes or cellular functions either by single-photon computed tomography (SPECT) or positron emission tomography (PET). A major advantage of SPECT and PET over other imaging techniques (*e.g.* optical and magnetic resonance imaging) is the high sensitivity that allows the detection of radiotracers in concentrations as low as 10^{-10} to 10^{-12} M.[229,230] For SPECT, more than 80% of radiotracers used in nuclear medicine centers are with Technetium-99m,[231,232] while for PET imaging the most clinically useful isotope is Fluorine-18.[233] Other attractive isotopes for medical applications are Indium-111, Iodine-123, and Thalium-201 for SPECT and Carbon-11, Copper-64, Gallium-68 and Zirconium-89 for PET.[234,235] Usually, radioisotopes are linked to targeting vectors (*i.e.*, small bioactive molecules, peptides, proteins or antibodies) *via* a (i) bifunctional chelating agent for labelling radiometals or by (ii) direct or (iii) indirect methods for labelling with non-metallic isotopes (*e.g.* ^{11}C, ^{18}F or ^{131}I).[233–239]

Over the past decade, bioorthogonal chemistry has gained momentum and has been increasingly applied in the field of radiopharmaceutical chemistry.[240,241] The chemoselectivity and fast kinetics of such reactions in aqueous media makes them ideal for the radiosynthesis of molecular imaging agents. Marik and Sutcliffe *et al.* reported the first application of click chemistry for ^{18}F-labelling of peptides through a CuAAC reaction between azido-decorated peptides and various [^{18}F]fluoroalkynes groups or *vice versa* (Fig. 41a(i)).[242,243] Since these initial studies a variety of ^{18}F-prosthetic groups for CuAAC labelling have been prepared in radiochemical yields (RCY) ranging from 25% to 71% and reaction times of 5–10 min. Some examples of these ^{18}F-building blocks are depicted in Fig. 41a(i) ([^{18}F]PEG-alkyne,[243] [^{18}F]FDG-β-N_3,[244] [^{18}F]Fluorobenzyl-N_3[245]). The CuAAC click reaction has found applications in the development of PET probes for *in vivo* imaging, with one example (^{18}F-RGD-K5)[246] entering clinical trials in the US for diagnosis of integrin $\alpha_v\beta_3$ expressing tumours. The same click reaction was applied for the design and synthesis of radiometal-based radiotracers; Schibli *et al.* introduced the click-to-chelate concept to form novel ligand scaffolds containing a triazole group known to efficiently chelate the "^{99m}Tc(CO)$_3$" core (Fig. 41a(ii)).[247] Although a large number of radiotracers have been developed using this reaction some limitations have been reported. One obvious disadvantage is the use of a large excess of potential cytotoxic copper, which should be avoided for *in vivo* applications. For such applications, the SPAAC reaction was expanded for quick radiolabelling under physiological conditions in the absence of catalyst and widely used for the incorporation of radioisotopes into biomolecules for PET and SPECT imaging in animals (Fig. 41b(i)).[248–255] Typical conditions for SPAAC labelling involves reaction times within 15–30 min, with isolated RCY of 19–98% and specific activities of ~60 GBq μmol^{-1} (Fig. 41b(ii)).[248–253] Another example of the click reaction in radiochemistry is the traceless Staudinger reaction.[27,256] The first ^{18}F variants for Staudinger radioligation were described by Steinbacha *et al.* and Gouverneur *et al.* (Fig. 41c).[257–259] The Staudinger ligation has, however, one major limitation whereby the phosphine precursor is subject to oxidation, abolishing its reactivity. In addition to the classical click chemistry ligations, the reaction of unprotected aminooxy- or hydrazine-modified peptides with ^{18}F-labelled aldehydes or ketones have also been explored for radiolabelling, resulting in the corresponding oxime or hydrazone conjugates (Fig. 41d(i)).[260–262] These reactions are

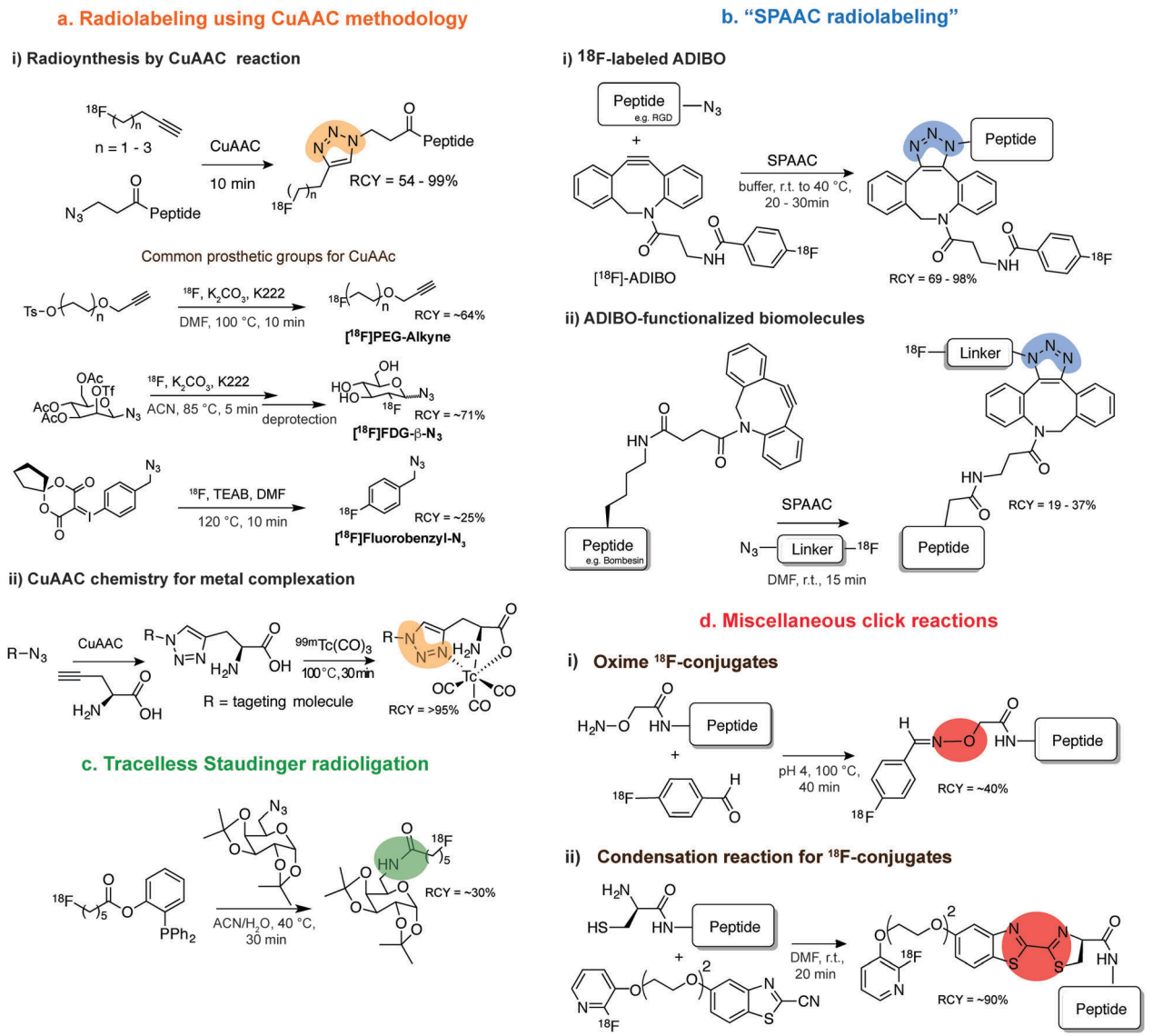

Fig. 41 (a) Click methods for radiosynthesis. (i) CuAAC click reaction for preparation of radiotracers including the synthesis of the most common prosthetic groups. (ii) $^{99m}Tc(CO)_3(H_2O)^{3+}$ radiolabelling through complexation by triazole moieties formed by CuAAC cycloaddition. (b) Copper-free click radiolabelling by SPAAC reaction. (i) ^{18}F introduced into the cyclooctyne prosthetic group (^{18}F-labelled aza-dibenzocyclooctyne derivative, [^{18}F]-ADIBO) and then subjected to strain-promoted cyclization with azide-functionalized biomolecules.[248] (ii) Labelling of ADIBO-functionalized biomolecules with ^{18}F-azides.[249] (c) Staudinger radiolabelling.[257] (d) Other examples of click radiolabelling. (i) Radiolabelling by oxime formation between an aminooxy-functionalized peptide and a ^{18}F-fluorobenzaldehyde ([^{18}F]FBA). (ii) Cyanobenzothiazole–cysteine (CBT–Cys) condensation reaction for ^{18}F-radiolabelling.

however limited due to the large excess of the components required, which results in very low specific activities. In addition, oximes and hydrazones are known to be prone to hydrolysis. The cyanobenzothiazole–cysteine (CBT-Cys) condensation reaction has also been recently established as an efficient, aqueous-compatible, and generally applicable method for labelling with ^{18}F (Fig. 41d(ii)).[263–265]

Although the mild conditions of the abovementioned click reactions are compatible with radiochemical approaches, they often require large amounts of purified peptide/protein precursor to obtain usable reaction rates for radiosynthesis. This leads to low specific activities (*i.e.*, the ratio of labelled-to-unlabelled molecule), which is an important issue since the *in vivo* targets of PET/SPECT tracers are often receptors or enzymes that are present in low copy number. The slower reaction rates also exclude the use of these click reactions for *in vivo* pretargeting applications. These limitations have led to the search of alternative fast and catalyst-free methods applicable to radiochemistry, *i.e.*, fast and high (radiochemical) yielding reactions that proceed under mild aqueous conditions using low concentrations of precursors. Notably, the IEDDA ligation has shown promising features, which make this click reaction suitable for both radiolabelling and "*in vivo* labelling", *i.e.* pretargeting labelling. As mentioned, this reaction achieves unusually fast rates with no need for

excess amount of reactants, or catalyst, resulting in radioactive preparations with high specific activities. The reaction is also not dependent on the solvent (tolerates water, organic solvents, cell media and blood plasma without reducing the reaction yields) and is highly selective in the presence of a broad range of functional groups. A pioneering work in this field was first reported by Robillard *et al.*[266] In this work an ^{111}In-DOTA-tetrazine derivative was used to label *in vivo* an antibody bearing TCO groups. Although first applied for radiolabelling with metals, over the past ~8 years the tetrazine–TCO ligation (Tz/TCO ligation) has instead attracted attention for the construction of ^{18}F- and ^{11}C-based imaging probes, primarily due to the short half-life of these isotopes that required fast labelling reactions.

6.2 IEDDA applications with ^{18}F

The application of Tz/TCO ligation for ^{18}F labelling was first published by Fox *et al.* in 2010, where it was demonstrated that Tz **8** reacts with [^{18}F]TCO in an excellent RCY of 98% at room temperature within seconds, using micromolar concentrations of the precursors (Fig. 42a).[267] The synthesis of the [^{18}F]TCO precursor was accomplished also in good yields (RCY of 71% within 15 min) by reacting the corresponding nosylate derivative with [^{18}F]-fluoride/tetrabutylammonium bicarbonate (TBAB) in acetonitrile (Fig. 42a). Further studies on the stability of this precursor have found that it is quickly metabolized *in vivo* (plasma metabolites observed within 5 min). At later time points (240 min post-injection, p.i.) PET imaging and *ex vivo* biodistribution studies showed a significant bone uptake indicating defluorination.[268] The first *in vivo* imaging approach using a ^{18}F-labelled peptide prepared *via* IEDDA chemistry consisted of the labelling of a tetrazine-RGD derivative with the [^{18}F]TCO precursor (Fig. 42b). The resulting ^{18}F-labelled tracer was prepared with a RCY of 90% within 5 min at room temperature showing a high tumour accumulation, but also a high liver uptake associated to the hydrophobicity of this first-generation system (Fig. 42c).[269]

In the previous example the tetrazine functionality is introduced through Lys acylation, which results in non-specific labelling of Lys residues that may be important for biologic activity. In this context, Conti *et al.* developed a bifunctional tetrazine–maleimide partner for efficient ^{18}F-labelling of free Cys residues on peptides (cRGDyC) and proteins (VEGF-SH).[270] As an example, labelling of Tz-^{18}F-cRGDyC peptide was obtained in >95% RCY with a specific activity of 111–222 GBq μmol^{-1}.[270] More recently exendin-4, a glucagon like peptide-1 receptor (GLP-1R), was also modified *via* tetrazine–maleimide conjugation, and labelled with ^{18}F-TCO for PET imaging of intraportally transplanted islet cells.[271] Importantly, the ^{18}F-labelled prosthetic groups *N*-[2-(4-^{18}F-fluorobenzamido)ethyl]maleimide (^{18}F-FBEM) and [^{18}F]fluorobenzaldehyde (^{18}F-FBA) have also been used for radiolabelling exendin. In this case the ^{18}F-labelled exendin tracers were obtained in low specific activity, which resulted in low binding to the GLP-1R in tissues in comparison with the tetrazine-labelled exendin.[271,272] The disadvantage of the tetrazine–maleimide approach relates with the occurrence

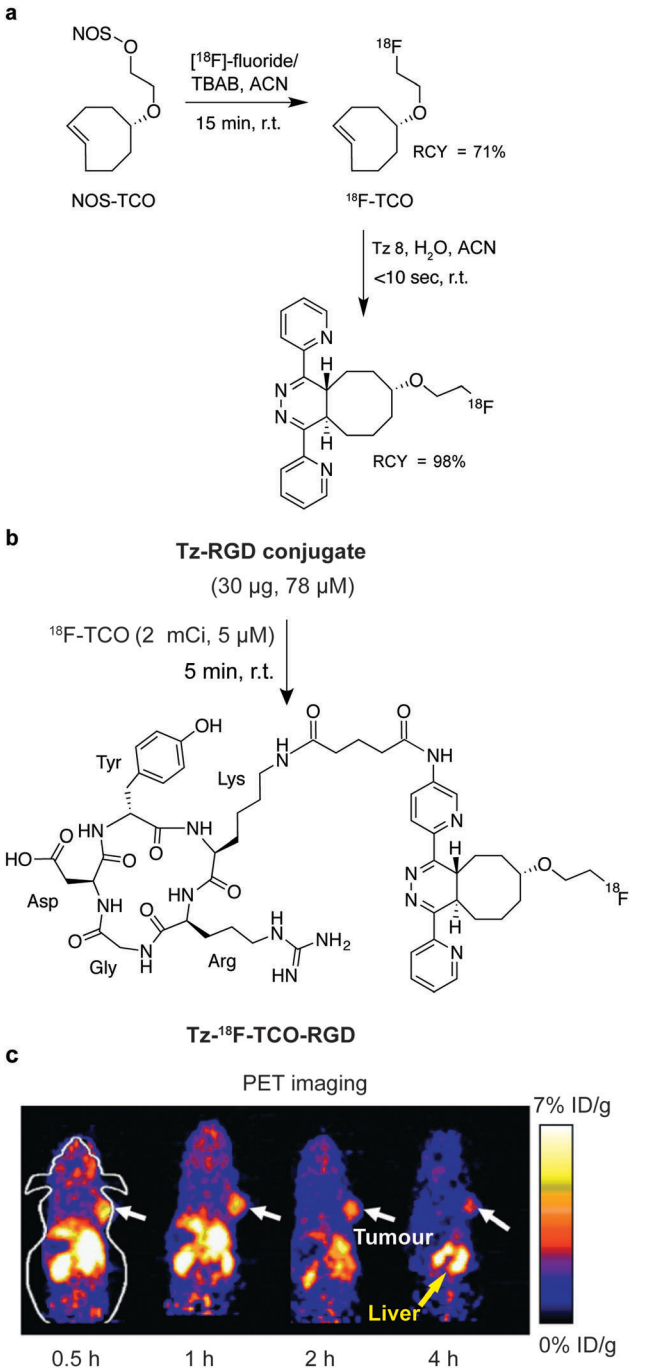

Fig. 42 (a) IEDDA conjugation between ^{18}F-TCO and Tz **8**. (b) Synthesis of [^{18}F]TCO. (c) PET imaging and *ex vivo* biodistribution of Tz-^{18}F-TCO-RGD. Reprinted in part (panel c) with permission from ref. 269. Copyright (2011) Elsevier B.V.

of known thiol-exchange reactions that the maleimide products undergo in plasma.[273,274]

[^{18}F]TCO has also been used for labelling poly(ADP-ribose) polymerase 1 (PARP1) inhibitors. *In vivo* studies have shown that ^{18}F-AZD2281, one of the labelled molecules, accumulates in tumours overexpressing PARP1. Interestingly, the authors have used magnetic TCO-decorated beads to "pull out" the excess of unlabelled tetrazine-conjugated AZD2281 from the reaction

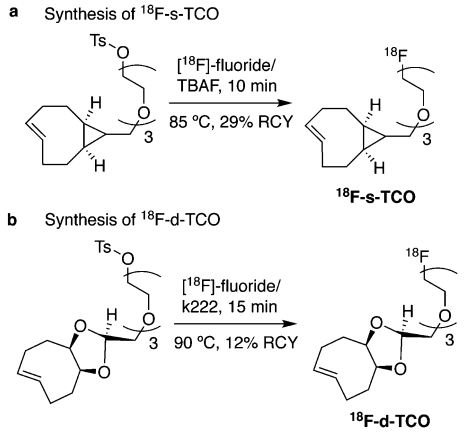

Fig. 43 Synthesis of (a) ^{18}F-s-TCO and (b) ^{18}F-d-TCO.

mixture resulting in high specific activities without lengthy HPLC purifications.[275]

Toward the development of faster IEDDA ^{18}F-labelling reactions Fox *et al.* developed a new radiotracer based on s-TCO by treating the corresponding tosylate precursor with ^{18}F-tetrabutylammonium fluoride (^{18}F-TBAF) in acetonitrile at 85 °C for 10 min (~29% isolated yield) (Fig. 43a).[276] ^{18}F-sTCO is stable in PBS pH 7.4 up to 2 h at 37 °C. In fetal bovine serum ^{18}F-sTCO retains 74% of radiochemical purity, after 1 h. This degree of degradation is not an issue, as the IEDDA reaction takes place within few minutes. In fact, it was shown that ^{18}F-sTCO completely reacts with a RGD-tetrazine in less than 5 min (26–40 GBq μmol^{-1}) and can be used to rapidly assemble probes for PET imaging in human U87MG tumour-bearing mice.[277] More recently, a ^{18}F version of d-TCO was prepared by nucleophilic substitution of the corresponding tosyl analogue with 12% radiochemical yield (^{18}F-d-TCO, Fig. 43b).[278] In PBS pH 7.4, ^{18}F-d-TCO is stable, with 94% of the compound being intact after 2 h incubation at 37 °C. In rat plasma, ^{18}F-d-TCO slowly isomerises into the corresponding *cis*-derivative, with 52% and 34% of the intact *trans*-compound being present after 1 and 2 hours incubation at 37 °C, respectively.

"Hot IEDDA" ligations are not only restricted to the ^{18}F-TCO moiety. For example, Knight *et al.* used a ^{18}F-norbornene derivative (^{18}F-Norb) for labelling of a tetrazine-bombesin peptide. The authors demonstrated that ^{18}F-Norb is capable of undergoing IEDDA click reactions with tetrazine species with promising reaction rates and high specific activities.[279]

6.2.1 Tetrazine prosthetic groups for ^{18}F-IEDDA labelling. Generally, ^{18}F can be introduced either into the tetrazine or the dienophile. However, because of the insufficient stability of tetrazines most reports have focused on using an ^{18}F-labelled dienophile. A disadvantage of this strategy is that it requires the attachment of a tetrazine to the targeting biomolecules, which involves complex and cumbersome reaction steps. In contrast, the efficient and straightforward methods available for modification of TCO and norbornene facilitate their bioconjugation to targeting biomolecules. As a result, significant efforts have been made for the direct radiolabelling of tetrazine precursors with ^{18}F, providing higher versatility for the application of IEDDA ligations in *radiochemistry*. The first attempts to label a 1,2,4,5-tetrazine variant with ^{18}F were described by Fox *et al.* but the instability of the tetrazine precursors during radiofluorination resulted in residual labelling yields (<1%, Table 1, entry 1).[267] After these initials efforts, Mikula *et al.* reported the successful preparation of a [^{18}F]-3-(3-fluoropropyl)-6-methyl-1,2,4,5-tetrazine (^{18}F-Tz **2**) by direct fluorination of the tosylated intermediate with a RCY of up to 18% (SA = 9.8 GBq μmol^{-1}, Table 1, entry 2).[280] A three-methylene spacer was considered between the fluorine and the tetrazine moiety to avoid the undesired high reactivity of benzyl-type precursors. *In vivo* studies with ^{18}F-Tz **2** revealed

Table 1 Summary of ^{18}F-tetrazine derivatives

	Radiolabelled tetrazine	Yield conditions
1	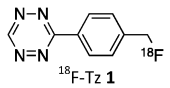 ^{18}F-Tz **1**	<1% MeCN, 85 °C, 15 min
2	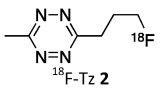 ^{18}F-Tz **2**	<18% MeCN, 90 °C, 5 min
3	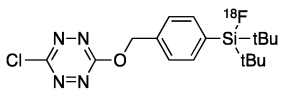 ^{18}F-Tz **3**	~78% MeCN/DCM, r.t., 20–25 min
4	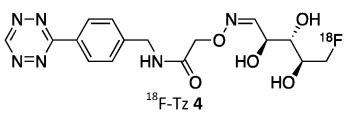 ^{18}F-Tz **4**	96% anilinium acetate buffer pH 4.6, r.t., 10 min
5	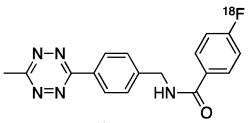 ^{18}F-Tz **5**	10% DMF, Et_3N, 60 °C, 7 min

a low degree of metabolic degradation and a highly favourable pharmacokinetic profile indicating the suitability of this radiolabelled tetrazine *in vivo* applications.[280]

Despite this progress, the radiolabelling of small tetrazine derivatives was still limited by low RCYs due to the instability of the tetrazine moiety under conditions typically used in direct ^{18}F-fluorination. A more efficient synthesis of a ^{18}F-labelled tetrazine derivative used a [^{18}F]SiFA–OH building block (RCY = ~78%) that effectively reacts with 1,4-dichlorotetrazine to generate [^{18}F]SiFA-OTz (^{18}F-Tz **3**). Using a specific activity of 7.0–8.5 GBq μmol^{-1} ^{18}F-Tz **3** reacts quantitatively with TCO in 1 minute (Table 1, entry 3).[281] Recently, a new ^{18}F-labelled tetrazine derivative was developed also in high yields and with specific activities of 12–16 GBq μmol^{-1} under mild reaction conditions *via* conjugation of 5-[^{18}F]fluoro-5-deoxyribose with an aminooxy functionalized tetrazine to give ^{18}F-Tz **4** (Table 1, entry 4). The ^{18}F-tetrazine exhibited sufficient blood circulation time and favourable elimination characteristics.[282] More recently Liang *et al.* labelled a tetrazine with [^{18}F]SFB (RCY = 10%) to give ^{18}F-Tz **5** and successfully constructed PET probes with TCO tagged antibody fragments for tumour imaging (Table 1, entry 5).[283]

6.3 "Tetrazine radiolabelling" with other relevant isotopes

Few examples of the application of the IEDDA reaction for direct labelling of bioactive molecules with other relevant isotopes have been described. In one example, a modular strategy for antibody labelling was developed. Specifically, norbornene was conjugated to trastuzumab – an anti-HER2 targeting antibody – and reacted with a tetrazine bearing different chelators (DOTA and desferrioxamine, DFO) for labelling with radiometals (^{64}Cu and ^{89}Zr) (Fig. 44a). *In vivo* PET imaging and *ex vivo* biodistribution experiments revealed significant and specific uptake of the ^{64}Cu-DOTA and ^{89}Zr–DFO–trastuzumab bioconjugates in HER2-positive BT-474 xenografts (Fig. 44a). The authors showed that a dienophile modified antibody can be reacted selectively with various radiometal chelators facilitating cross-comparisons in the development of antibody-based radiopharmaceuticals since the modified antibodies are synthesized using identical ligation conditions.[284] Additionally the use of mild IEDDA conditions avoids the use of high temperatures that are usually required for labelling antibodies bearing coordinating agents. Recently, Weissleder *et al.* developed a tetrazine conjugate that incorporated the DFO ligand for installation of ^{89}Zr and a BODIPY fluorophore for multimodal imaging. ^{89}Zr–DFO–BODIPY–trastuzumab was prepared within minutes by Tz/TCO ligation and PET imaging showed high tumour conspicuity. In addition, biodistribution studies confirmed high specific probe uptake in BT474 xenografts (HER2+) (237.3 ± 14.5% ID per g in BT474) compared to low, nonspecific probe uptake in BT20 xenografts (HER2−) (16.4 ± 5.6% ID per g) 96 h p.i. (Fig. 44b). *Ex vivo* fluorescence of selected tissues confirmed target localization and persistence of the fluorescence of ^{89}Zr–DFO–BODIPY–trastuzumab. Similar systems may find utility to identify targets intraoperatively through fluorescence.[285] Similarly, Spivey *et al.* used a tetrazine modified ^{68}Ga-DOTA to construct probes for labelling norbornene-containing biomolecules.[286] In another example, Reiner *et al.* used tetrazine bearing amino acids as building blocks for the synthesis of peptides and performed labelling studies with these peptides applying a ^{89}Zr–DFO TCO derivative.[287]

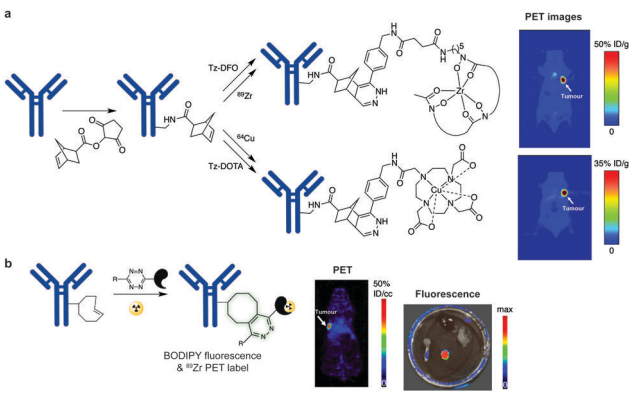

Fig. 44 (a) Schematic of the modular radiolabelling strategy based on the ligation of norbornene-modified antibody and radiometal-labelled tetrazines. (b) Tz/TCO chemistry for multimodal imaging by using trastuzumab–TCO and a tetrazine incorporating ^{89}Zr–DFO for PET imaging and BODIPY for fluorescence. Reprinted in part with permission from ref. 284 (panel a) and ref. 285 (panel b). Copyright (2011 and 2016) American Chemical Society.

6.4 Pretargeting based on IEDDA

The IEDDA reaction between tetrazines and TCOs has been employed in a variety of settings from fluorescence imaging of targeted biomolecules to magnetic resonance imaging with nanoparticles,[72,133,288,289] however, the most significant impact of this ligation may lie in *in vivo* pretargeting imaging applications. For such challenging approaches the bioorthogonal reactant pairs should have high stability towards the amino and thiol nucleophiles (among others) present in biological systems as well as high selectivity to ensure that only the target biomolecules are labelled *in vivo*. In addition, the bioorthogonal reaction should proceed with fast kinetics even in the case of low concentration of the target protein, as is the case with *in vivo* pretargeting, where the reacting partners are diluted in the blood pool.[290] Among all the existing bioorthogonal reactions the IEDDA ligation is the one with most potential for pretargeting applications.[291] In these systems, the radionuclide is administered separately from the targeting protein, most often a tumour-targeting antibody. In the first step, the targeting antibody bearing a strained alkene (or tetrazine) is administered and allowed to accumulate in the specific tissue. Lastly, when the excess antibody has cleared from the circulation, a radiolabelled tetrazine (or dienophile) is administered (Fig. 45). In a general way pretargeting can be regarded as *in vivo* labelling, since the antibody is radiolabelled at the target tissue after *in vivo* administration.

Until recently, most pretargeting approaches for radioimmunoimaging and radioimmunotherapy were based on the ligation of an antibody and a radionuclide using the avidin–biotin system, exploiting the high specificity and strong affinity

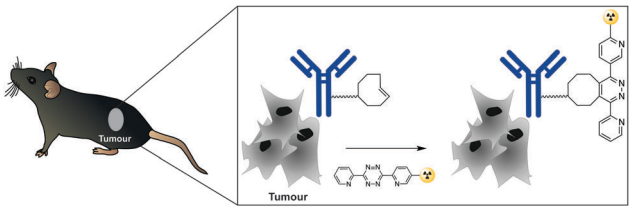

Fig. 45 Schematic representation of tumour pretargeting with IEDDA reaction in mice.

($k_d = 10^{-15}$ M) of avidin (or streptavidin) for biotin. Indeed, this pretargeting approach has been shown to be unaffected by extremes of pH, high temperatures, organic solvents and biological systems.[292] Despite these features, the avidin–biotin system does have limitations, in particular, the high immunogenicity of the (strept)avidin, which cannot be humanized precluding its repeated use. The antibody-based pretargeting systems based on bioorthogonal click chemistry address such limitations. The use of IEDDA in pretargeting was pioneered largely by Robillard *et al*. In this work TCO was conjugated to anti-TAG72 monoclonal antibody [CC49] *via* an oligoethyleneglycol linker and used as a tagging compound while a DOTA modified tetrazine moiety was used for labelling with ^{111}In. The ^{111}In–DOTA–tetrazine conjugate was injected one day after administration of the TCO–antibody conjugate (CC49–TCO) in mice bearing colon cancer xenografts. Impressively, the chemically tagged tumours reacted rapidly with ^{111}In–DOTA–tetrazine using only a small excess (3.4 equivalents) of the tetrazine radioactive tracer, resulting in pronounced accumulation in the tumour, as demonstrated by SPECT (Fig. 46).[266] *Ex vivo* biodistribution studies confirmed a high tumour uptake (~3.0 ID per g) but a lower tumour-to-blood (T/B) ratio, which was assigned to the reaction of ^{111}In–tetrazine with freely circulating CC49–TCO. In addition, although this pretargeting approach enabled straightforward antibody modification the highly strained antibody-conjugated TCO tag was prone to slow *in vivo* deactivation (25% in 24 h).[266]

In a follow up study, the same researchers showed that the TCO tag is potentially deactivated *in vivo* through isomerisation to the unreactive *cis*-cyclooctene isomer by interactions with copper-containing proteins.[293] By attaching the TCO through a shorter linker to hamper interaction with the copper-binding site in albumin, the deactivation half-life of TCO in circulation in mice was enhanced to 4 days.[293] In another study, a pretargeting approach was developed for radioimmunotherapy using a ^{177}Lu-labelled tetrazine probe and the CC49–TCO antibody.[294] It was demonstrated that the use of a less hydrophobic tag (TCO–oxymethylbenzamide) afforded a CC49–TCO conjugate with a longer clearance half-life, improved tumour accumulation and markedly increased *in vivo* tag stability.[295] Very recently, the authors also successfully employed a TCO–tetrazine pretargeting approach with antibody fragments and affibodies.[296,297] In addition, a number of other groups, have reported the development of a pretargeted imaging strategy based on the IEDDA reaction. Lewis *et al.* described an A33 TCO–antibody for *in vivo* pretargeting with a ^{64}Cu-labelled tetrazine in SW1222 tumour-bearing mice.[298] Relatively low T/B ratios were observed caused by the reaction between the labelled tetrazine and the freely circulating A33-TCO.

To circumvent the high blood uptake, tetrazine-functionalized clearing agents were developed (*e.g.* galactose–albumin–tetrazine and polystyrene beads coated with tetrazine-conjugated albumin). These enable rapid reaction with and removal of the TCO-tagged antibody from blood resulting in a significant improvement of the tumour-to-blood (125-fold) ratios (Fig. 47a).[294] The utility of the IEDDA reaction for pretargeting extends beyond ^{111}In, ^{64}Cu and ^{89}Zr metals. Recently, a bisphosphonate-modified variant of TCO was used to pretarget bone and for subsequent bone imaging after *in vivo* labelling with a ^{99m}Tc–tetrazine (Fig. 47b). This approach explores the high avidity of bisphosphonates to osteoclasts. In the same study a therapeutic radioisotope was also used (^{177}Lu conjugated to a tetrazine).[299]

A robust and modular chemoenzymatic strategy was employed for the preparation of site-specifically modified antibody–TCO immunoconjugates on the glycans present in the heavy chain.[300] This approach relies on the enzymatic activity of β-1,4-galactosidase and galactosyltransferase [Gal-T(Y289L)] for the incorporation of azide-modified monosaccharides (GalNAz) into the oligosaccharide chain. The resulting azide-modified antibody was then conjugated to a dibenzocyclooctyne-bearing variant of TCO (DIBO–PEG_{12}–TCO) *via* SPAAC ligation. The site-specifically labelled huA33–TCO immunoconjugate was used for pretargeting PET imaging of colorectal cancer with a ^{64}Cu-labelled Tz radioligand (^{64}Cu–Tz–SarAr).[300] The same chemoenzymatic strategy was used to construct a TCO- and fluorophore-bearing immunoconjugate of the huA33 antibody (huA33–Dye800–TCO) for multimodal PET/NIRF imaging of colorectal cancer using a ^{64}Cu-labelled tetrazine (^{64}Cu–Tz–SarAr). Importantly, simulated tumour resections using a near-infrared fluorescence (NIRF) camera showed its potential for real-time delineation of malignant tissue during image-guided surgery.[301]

IEDDA ligation has also been successfully used in the synthesis of radioactive iodine labelled constructs.[302,303] For example, Valliant *et al.* developed a convenient method to prepare radioiodinated tetrazines that could be used for labelling a TCO–anti-VEGFR2 conjugate with iodine-125 for *in vivo* studies. The ^{125}I–tetrazine was prepared by employing an oxidative halo destannylation reaction. Under these conditions the tetrazine showed high stability resulting in high iodination yields (80% RCY, 15 min reaction).[303] Importantly, the ^{125}I–tetrazine labelled antibody was shown to be 10 times more stable to deiodination than the same antibody labelled through direct iodination of for example tyrosines using iodogen.

6.4.1 Expanding the scope of IEDDA for pretargeting with short-lived isotopes. The use of the tetrazine–TCO cycloaddition for pretargeted imaging has also been described with short-lived isotopes. For example, ^{18}F and ^{68}Ga are inappropriate for labelling intact antibodies because they would have decayed before optimal biodistribution of the targeting biomolecule occurs. Aboagye *et al.* developed a labelling procedure for imaging EGFR expression on cancer cells using the IEDDA reaction between a TCO-modified Cetuximab and a ^{68}Ga-labelled tetrazine.[304] In addition, Lewis *et al.* used a TCO-bearing immunoconjugate of the

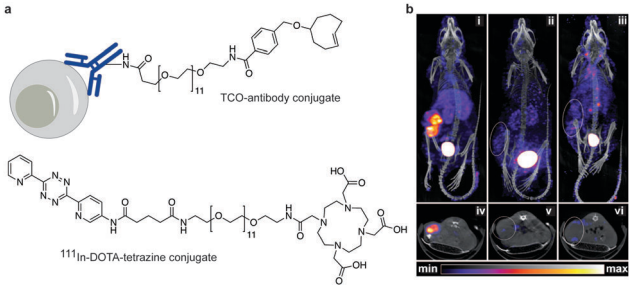

Fig. 46 (a) Pretargeting components: TCO–antibody conjugate and ^{111}In–DOTA–tetrazine conjugate. (b) SPECT/CT imaging of mice bearing colon carcinoma xenografts: SPECT images of mice preinjected with (i) TCO–antibody conjugate followed one day later by ^{111}In–DOTA–tetrazine conjugate. (ii) Mice treated with unmodified antibody (no TCO tag) followed one day later by ^{111}In–DOTA–tetrazine conjugate. (iii) Mice treated with TCO-modified rituximab, which lacks specificity for TAG72, followed by ^{111}In–DOTA–tetrazine conjugate. (iv)–(vi) Single transverse slices passing through the tumours in (i)–(iii). From ref. 266, Copyright © 2013 by John Wiley & Sons, Inc. Reprinted in part (panel b) by permission of John Wiley & Sons, Inc.

anti-CA19.9 antibody 5B1 and an ^{18}F-tetrazine radioligand for imaging of pancreatic cancer xenografts. A PEG_{11}–NOTA chelator coupled to a tetrazine was used for complexation of aluminum-[^{18}F]fluoride. The labelling was performed in 54–65% RCY in high purity (>96%) and a specific activity between 21.4 and 26.7 GBq μmol^{-1} was achieved within 15 min at 90 °C.[305] For pretargeted *in vivo* experiments, nude, athymic mice bearing subcutaneous CA19.9-expressing BxPC3 xenografts were injected with 5B1–TCO 72 h prior to the administration of Tz–PEG_{11}–Al[^{18}F]–NOTA (Fig. 48a). PET imaging showed tumoural activity concentrations of up to 6.4% ID per g at 4 h post-injection and low bone accumulation demonstrating the high stability of the Al[^{18}F]–NOTA complex.[305] Aimed to improve the *in vivo* labelling reaction in the tumour, Weissleder *et al.* have used ^{18}F-labelled dextran polymers modified with tetrazines for *in vivo* pretargeting with a TCO-antibody against A33.[306] The dextran polymer was envisaged to extend the circulation time of the ^{18}F-tetrazine *in vivo* and improve the labelling of the TCO-tagged tumours (Fig. 48b). In a similar study Devaraj *et al.* have used a ^{68}Ga–DTPA–dextran–tetrazine derivative to target a A33 TCO–antibody for imaging of implanted LS174T xenografts. PET imaging and biodistribution studies revealed a prolonged retention in blood and high liver uptake, possibly due to partial release of ^{68}Ga from DTPA *in vivo*.[307]

The fast rates of the IEDDA ligation has made this reaction so attractive that even labelling with ^{11}C (half-life of 20.3 min) was explored in pretargeting approaches. The first radiosynthesis of a ^{11}C-tetrazine was reported in 2013 by Kristensen *et al.* in moderate yields (33% RCY) in 2 min but with a total preparation time of 50–60 min that included HPLC purification. The final click ligation with TCO is completed within 20 seconds, however, imaging, biodistribution, and stability data were not reported using this probe.[308] More recently a new ^{11}C-tetrazine precursor was prepared in 50% RCY and an overall synthesis time of 30 min including purification. The *in vivo* profile of this tetrazine was investigated by dynamic PET/MR scanning and *ex vivo* biodistribution studies. These results

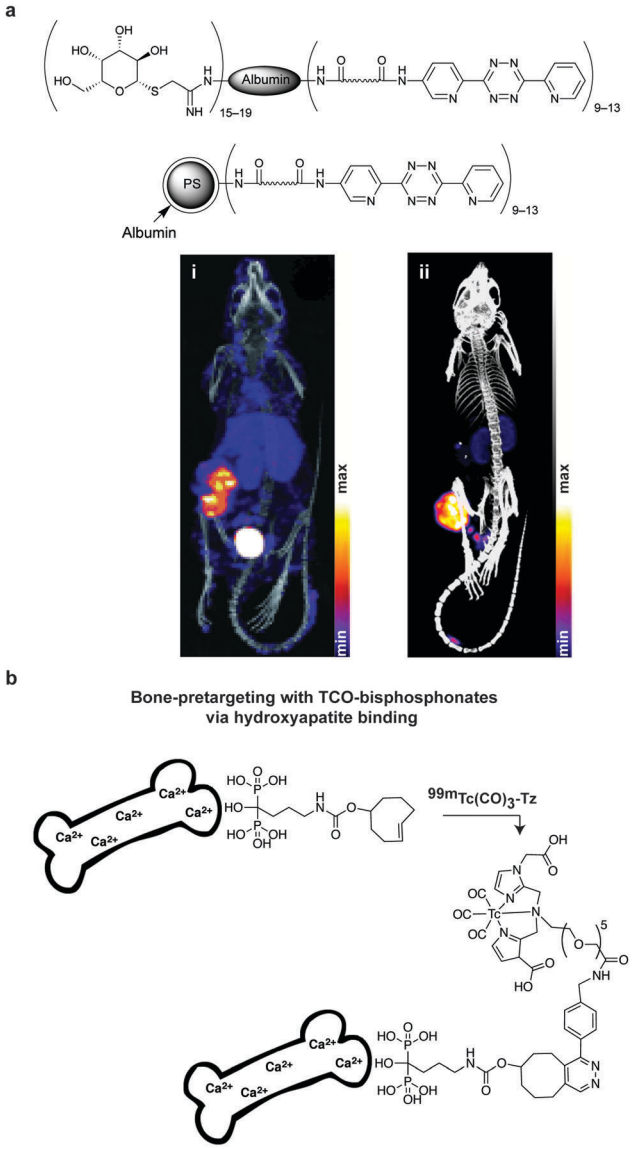

Fig. 47 Clearing agents and TCO–bisphophonates for pretargeting applications. (a) Schematic representations of galactose–albumin–tetrazine and polystyrene (PS) beads coated with tetrazine-conjugated albumin for rapid removal of freely circulating antibody–TCO. (i) SPECT/CT image of a CC49–TCO pretargeted mouse bearing LS174T xenograft, after 3 h injection of the ^{111}In–DOTA–tetrazine conjugate (24 h post-antibody injection).[266] (ii) SPECT/CT imaging using same animal model pretreated with CC49–TCO after two doses of the clearing agent galactose–albumin–tetrazine followed by ^{111}In–tetrazine injection.[294] (b) Bisphosphonate-modified TCO for bone pretargeting. Reprinted in part (panel a) with permission from ref. 266 and 294. Copyright (2010) by John Wiley & Sons, Inc. and Society of Nuclear Medicine and Molecular Imaging, Inc.

confirmed this ^{11}C-radiotetrazine as a promising tool for pretargeted PET imaging. To investigate the applicability of the ^{11}C-tetrazine for rapid *in vivo* pretargeting and PET imaging, mesoporous silica was functionalized with TCO. The TCO-modified silica was shown be localized in the lung by PET after *in vivo* click reaction with ^{11}C-tetrazine, demonstrating the potential of ^{11}C-labelled tetrazine for pretargeting applications.[309]

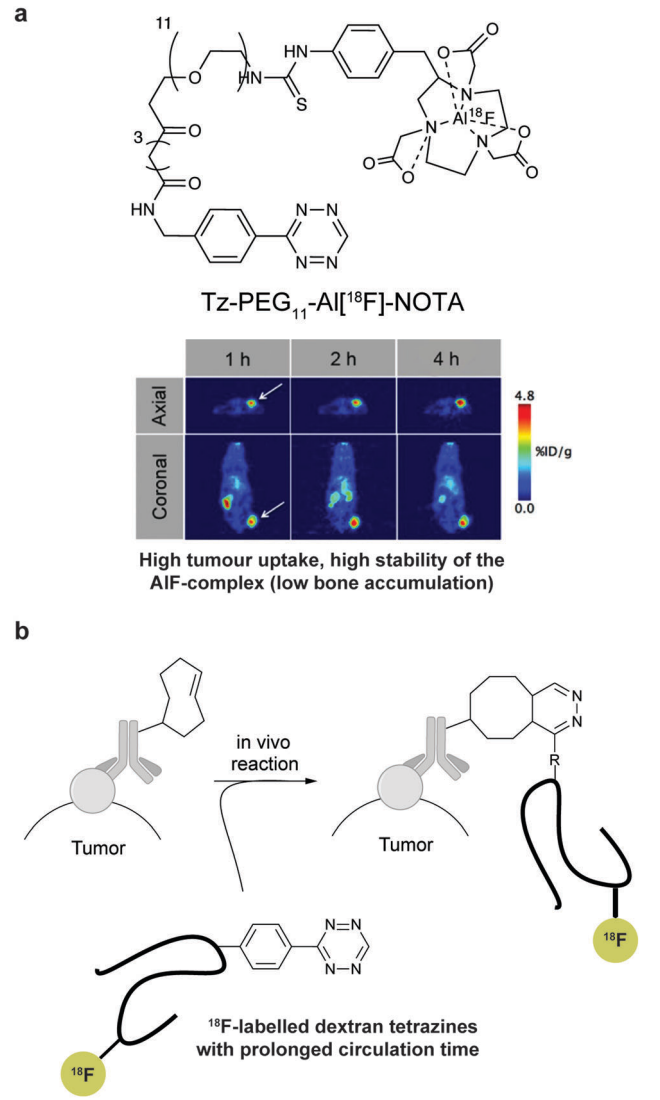

Fig. 48 IEDDA pretargeting with short-lived isotopes. (a) PET images of pretargeted subcutaneous xenograft tumour-bearing mice with Tz–PEG_{11}–Al[^{18}F]–NOTA/5B1–TCO. (b) ^{18}F-labelled dextran tetrazines with optimized pharmacokinetics. Reprinted in part (panel a) with permission from ref. 305. Copyright (2016) American Chemical Society.

7. Tetrazines – an emerging trigger for bioorthogonal cleavage reactions

Together with the explosion of bioorthogonal ligation reactions, using biocompatible reagents to trigger bond cleavage under physiological conditions has recently gained much attention.[4,5] Instead of attaching additional functionality on biomolecules of interest, bioorthogonal cleavage reactions offer an alternative way to restore function of protected motifs, such as caged-fluorophores, prodrugs or masked biomolecules. In order to induce such a gain-of-function event, not only the caging groups, but the trigger, should be bioorthogonal, non-toxic, stable and reactive in cellular environment. In this section, we report recent progress in bioorthogonal cleavage reactions drawing particular attention to tetrazine-mediated IEDDA decaging reactions and its application *in vitro* and *in vivo*.

7.1 Bioorthogonal bond cleavage chemistry

7.1.1 Photo decaging. Photo irradiation, as non-chemical stimuli, could serve as an orthogonal trigger for cleavage reaction. For example, the well-developed *o*-nitrobenzyl (ONB) ether derivative undergoes photo-deprotection to yield the free amine under UV light (Fig. 49a).[310,311] Additionally, Chin *et al.* have genetically encoded caged Tyr[312] and Cys[313] amino acid variants into proteins for protein photoactivation. Even though photodecaging could offer high temporal resolution and potential spatial control, the UV light may however cause photo toxicity and perturb cellular processes. Moreover, the nitrobenzyl-based photocaging proved to be not fully bioorthogonal and stable in cells.[310,311] Additionally, the poor penetration of ultraviolet radiation also hamper its compatibility in tissue and animal studies.

7.1.2 Metal mediated cleavage reactions. Molecule-based response systems have key advantages compared with other decaging approaches due to better biocompatibility and minimal perturbation of cellular processes. In this context, metal mediated cleavage reactions emerged as a powerful tool for decaging, with rapid turn-over and versatility towards various protecting groups. So far, Ru and Pd catalysts have been the two most explored triggers because of their efficiency and biocompatibility. The first example of the use of an organoruthenium complex to form amines from their respective allylcarbamates (alloc) under physiological conditions and in living cells was published in 2006 (Fig. 49b).[314] Based on this first report, the efficiency of the Ru catalyst was further optimized by ligand design, resulting in higher turnover number (TON) that could be used for decaging of fluorophores and the drug doxorubicin within mammalian cells.[315] Other interesting applications of Ru in this field include the introduction of lysine methylation on proteins by decaging of genetically encoded alloc-methyl Lys[316] and decaging of alloc-protected DNA-binding species to trigger DNA binding events in cells.[317] The same deallylation reaction was applied for supramolecular regulation of intracellular catalysis and catalytic activation of cellular bioluminescence.[318,319] Notably, this Ru-mediated deprotection could also embed spatial and temporal control with certain ligands and substrates.[320–322]

Apart from organoruthenium, Pd species have also been shown to be a useful catalyst for *O*-deallylation (Fig. 49c).[323,324] Using fluorescent polystyrene microspheres, Bradley *et al.* showed that Pd nanoparticles could cross cell membrane and cleave allylcarbamate linkages intracellularly on mammalian cells (Fig. 49c).[325] Additionally, propargyl groups (proc) could also be cleaved by Pd catalysts and used to activate anticancer drugs in cells and, most impressively, in zebrafish.[326–328] In a recent work, Chen *et al.* managed to restore the function of propargyl-carbamates (proc)-caged proteins by Pd catalysis *in vitro* and *in vivo*.[329] They also managed to manipulate cell-surface sugars by depropargylation of caged glycans using *in situ*-generated Pd nanoparticles.[330] Recently, novel cleavable groups such as an allenyl ether on Tyr and non-terminal allylcarbamate linkages were also developed to undergo decaging reactions catalysed by Pd.[331,332] Notably, other organometallic complexes, such as mercury,[333] copper,[334,335] iron[318,336] and cobalt

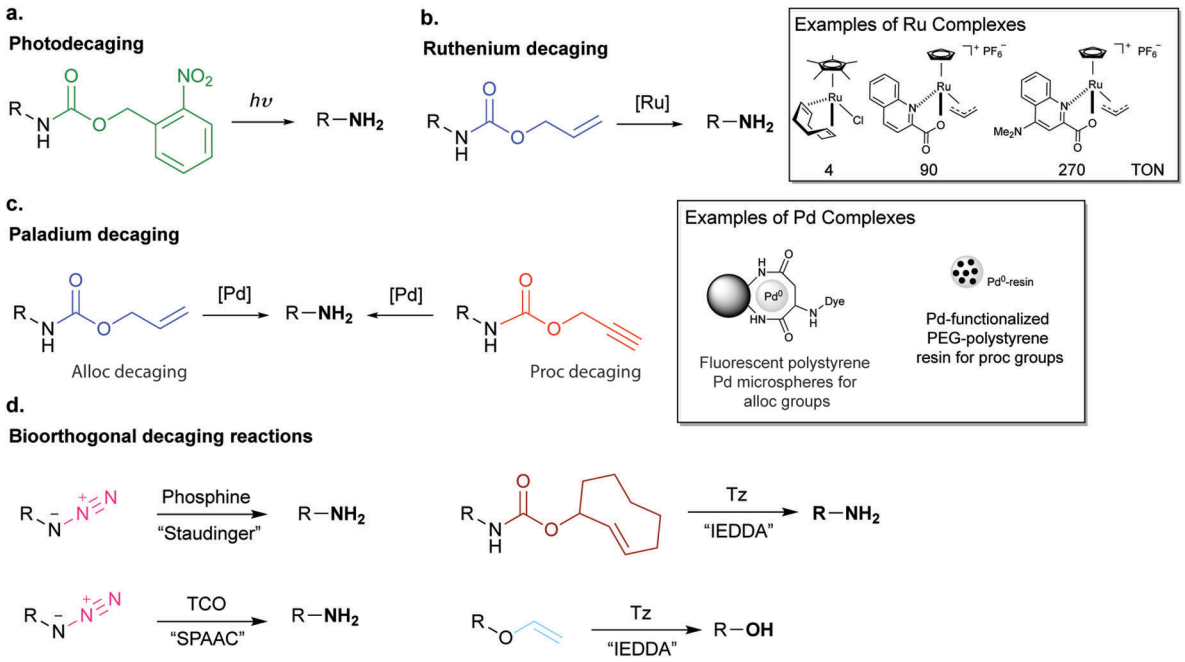

Fig. 49 Examples of bioorthogonal decaging methods.

species[337] were also found reactive for bond-cleavage reaction on allyl, propargyl and azide groups under physiological conditions, in living human cells and even in nematodes and zebrafish.

It is noteworthy that even though reaction proceeds efficiently at the small molecule level with 10% catalyst loading, when applied for protein and drug activation in cell studies, large amounts of catalyst is always required due to nonspecific binding of metal to proteins, especially for Pd catalysed reactions.[329] Despite the moderate to low toxicity of these metal catalysts, their use is still limited for *in vivo* applications. In addition, further studies are needed to understand the cellular uptake of these catalysts and their influence on normal cellular processes.

7.1.3 Non-metal mediated cleavage reactions. Alternatively, non-metal cleavage reactions, mediated by biocompatible chemicals, stand out due to their excellent biocompatibility and enhanced orthogonality (Fig. 49d). Interestingly, these metal-free cleavage reactions mostly derive from their parent ligation reactions. By employing readily developed bioorthogonal handles, reactions could be redesigned to induce subsequent rearrangement and bond cleavage on the unstable ligation product (Fig. 49d). Because the ligation step is usually very fast, the overall kinetics of such cleavage transformations should in principle be also rapid. Accordingly, emerging bioorthogonal cleavage reactions were developed based on IEDDA, strain-promoted 1,3-dipolar cycloaddition and the Staudinger reaction, along with novel reactions such as bond-cleaving reactions between *N*-oxide and boron reagents.[338] As an example, azide could serve as bioorthogonal protecting group for amines (Fig. 49d).[339] In this system, a biocompatible phosphine reacts with an azide forming an aza–ylide conjugate, which is prone to hydrolysis in aqueous media affording the corresponding unmasked amine. This azide-to-amine conversion was employed for the activation of a doxorubicin prodrug,[339] DNA-templated release of fluorophores and functional molecules,[340] as well as controlled activation of epitopes on the surface.[341] Apart from this bioorthogonal reductive transition, azide could also be decaged to give amines by reaction with TCO (Fig. 49d). Upon strain-promoted 1,3-dipolar cycloaddition, the resulting unstable 1,2,3-triazoline eliminates one molecule of nitrogen to generate an imine that undergoes hydrolysis to yield the free amine in aqueous solution. When combined with the self-immolative linker *p*-aminobenzyloxycarbonyl, the SPAAC reaction has been applied to chemically trigger the release of a caged doxorubicin[342] as well as the decaging of Lys residues site-selectively on proteins.[343] Among all these chemically-triggered bioorthogonal reactions, IEDDA mediated cleavage reactions outperform other examples due to their fast kinetics, catalyst-free nature and biocompatibility (Fig. 49d).[4] Herein, we will present applications of the IEDDA-triggered cleavage on both TCO and vinyl ether moieties.

7.2 IEDDA triggered "click-to-release" of TCO bearing molecules.

TCO pro-drug activation. Robillard *et al.* first demonstrated in 2013 that the superfast IEDDA reaction could serve as a cleavage reaction for drug activation (Fig. 50a).[65] By reacting a doxorubicin carbamate-linked TCO derivative with tetrazine, the resulting 1,4-dihydropyridazine product could undergo elimination of doxorubicin and CO_2 if TCO is modified at the allylic position (Fig. 50b). Notably, it was shown that the axially substituted TCO presents 156-fold higher reactivity than equatorial corresponding isomer (Fig. 50c), which presumably derives from the steric interaction between tetrazine and equatorial benzyl carbamate moiety.[65] In a recent example, this tetrazine-triggered reaction was used for pretargeting antibody–drug

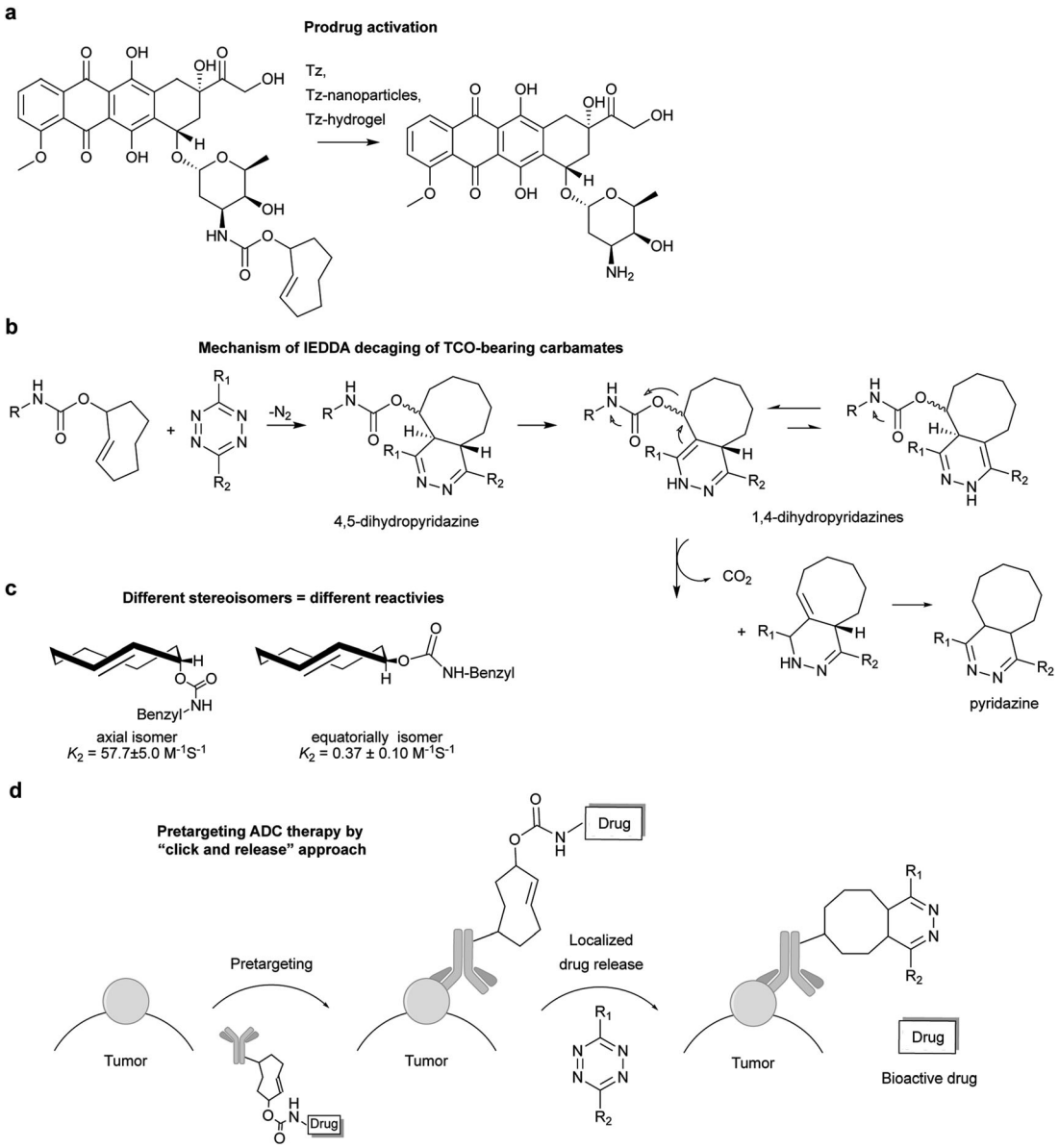

Fig. 50 (a) Non-metal cleavage reactions, mediated by bio-friendly chemicals. (b) Doxorubicin release upon tetrazine ligation. (c) Mechanism of decaging by IEDDA tetrazine reaction. (d) Equatorial and axial isomers of TCO carbamates and the respective reaction rates. (e) Triggered drug release from an ADC by tetrazine reaction.

conjugate (ADC) therapy. Here, the masked drug is conjugated to a tumour-homing antibody *via* a TCO linker (CC49-TCO-Dox), which could be readily released in antibody pretargeted tumour cells upon tetrazine decaging reaction (Fig. 50d). Indeed, *in vivo* studies in mice bearing colon carcinoma xenografts showed efficacious drug release and high tumour retention of doxorubicin as confirmed by *ex vivo* fluorescence RP-HPLC analysis of tumour homogenates. Of note the TCO linker displays high *in vivo* stability with a half-life of 5 days, comparable to conventional cleavable ADC linkers. Although some isomerisation of TCO is expected, this only results in loss of reactivity and not in non-specific payload release, and thus potential side-toxicity.[15]

Multivalence of nanoparticles and hydrogels enables the introduction of a high copy number of tetrazine motifs, enhancing activation efficiency and local drug concentration, and thus endow these materials as potential vectors for drug activation. In conventional chemotherapy, high doses of a drug need to be used because of the lack of specificity to the target diseased tissue. This leads to side toxicity and limits the general efficacy of the treatment. Royzen *et al.* envisioned that by systemic administration of non-toxic tetrazine-bearing magnetic nanoparticles (MNP), enhanced permeability and retention (EPR) effect would guide MNP accumulation in cancerous tissues, minimizing side effects by localized drug release. As a proof of concept, MNPs decorated with tetrazines and fluorescent probes could be used to image *in situ* prodrug activation of TCO-modified doxorubicin in cancer cells (Fig. 51a). Indeed, the pro-drug was activated completely after

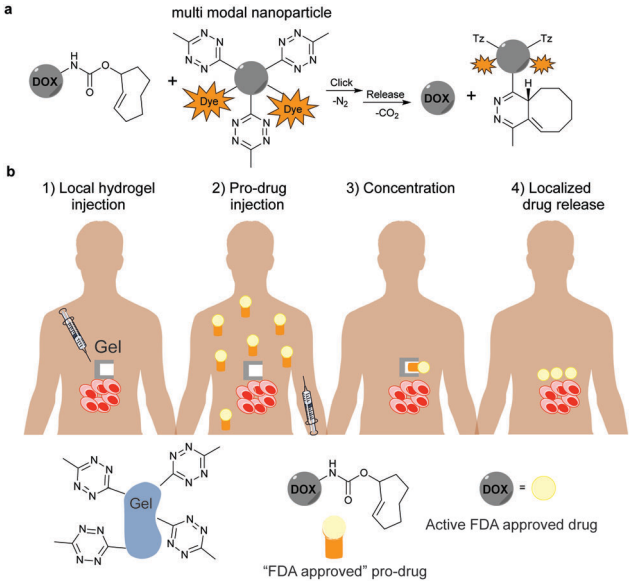

Fig. 51 (a) NP functionalization with tetrazines and fluorescent probes for image-guided prodrug activation. (b) "Click-to-release" for concentration and activation of pro-drugs at a diseased site.

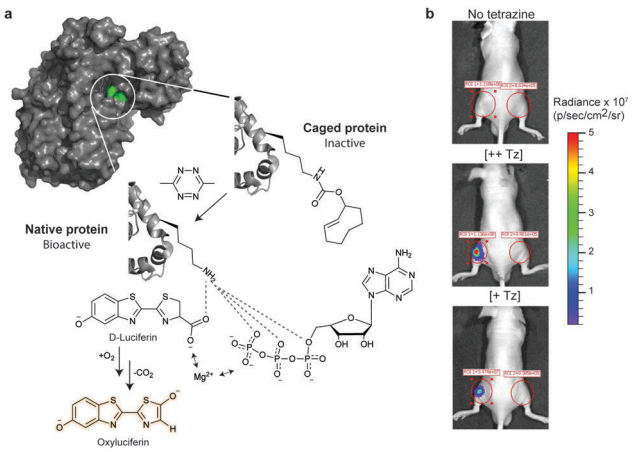

Fig. 52 (a) Schematic of the mechanism of protein gain-of-function. Caging the critical Lys residue of fLuc (TCOK-529) blocked protein function that could be restored by tetrazine cleavage and reformation of hydrogen bonding network between ε-amine of K529 and ATP. (b) Bioorthogonal chemical activation strategy in mice by using chemically caged fLuc as a model. HEK293T cells expressing the TCOK-a caged fLuc were injected into living mice subcutaneously (left legs), followed by the treatment of tetrazine (66 or 6.6 mg kg^{-1} body weight; [++Tz] and [+Tz], respectively) *via* tail vein injection. After *in vivo* decaging recover of luciferase bioluminescence was observed. Adapted in part with permission from ref. 311. Copyright 2016 American Chemical Society.

1 hour incubation of fluorescent tetrazine bearing MNP. This multi-model platform has potential for *in vivo* image-guided drug release either by fluorescence or magnetic resonance imaging.[344]

Similarly, a tetrazine-based hydrogel was synthesized for local drug activation. In contrast to systemic administration, the hydrogel could be injected directly into the tumour site, which allowed release of drug upon subsequent intravenously

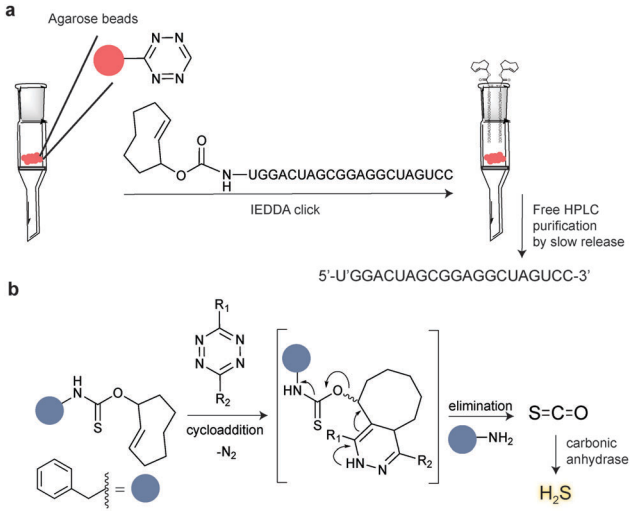

Fig. 53 (a) Click-to-release system for HPLC-free purification of RNAs bearing a TCO group. Prior generated failure capped sequences are collected in the early-eluted fractions before the slow release of TCO. (b) Self-immolative thiocarbamates triggered by tetrazines decompose and release SCO, which is rapidly converted to H_2S by the ubiquitous enzyme carbonic anhydrase.

injection of the TCO modified drug (Fig. 51b).[345] Animal studies revealed an increase in the efficacy of doxorubicin, minimizing systemic toxicity (no signs of toxicity, including weight loss, changes in coat texture and concentration of reticulocytes).

Protein gain-of-function. The potential of the bond cleaving IEDDA reaction to chemically activate caged enzymes was first reported by Chen *et al.* in 2015. In this work a TCO-bearing Lys analogue was genetically incorporated into the active site of firefly luciferase where the catalytic Lys is necessary to convert the non-luminescent luciferin to a highly luminescent product (Fig. 52a). The cleavage reaction with tetrazine was shown to restore the enzyme activity in both cells and animals (Fig. 52b).[311,346] As previously reported by Robillard *et al.* it was observed that the axial isomer showed faster kinetics relative to the equatorial isomer.[65,346] Tetrazines could also trigger gain-of-function to rescue the catalytic activity of a kinase in living mammalian cells.[311]

TCO decaging has not been limited only to drug release and protein gain-of-function studies. In another example, a tetrazine triggered approach has been described for the HPLC-free solid phase synthesis of RNA.[347] Additionally, a new strategy for bioorthogonal carbonyl sulphide and hydrogen sulphide (COS/H_2S) donation initiated by tetrazines has also been achieved (Fig. 53).[348]

Optimized tetrazine derivatives for faster TCO decaging. The electron properties of the substituents of tetrazines have proved essential for the efficiency of the decaging process (Fig. 54). Using a fluorogenic assay based on a TCO-coumarin derivative, it was possible to evaluate and optimize substituents of the tetrazine structure in order to achieve a superior decaging efficiency. By screening a range of tetrazines, it was found that EDG substituted tetrazines led to poor decaging due to slow cycloaddition. On the other hand, EWG, which are expected to accelerate the reaction due to the lowering of the LUMO energy

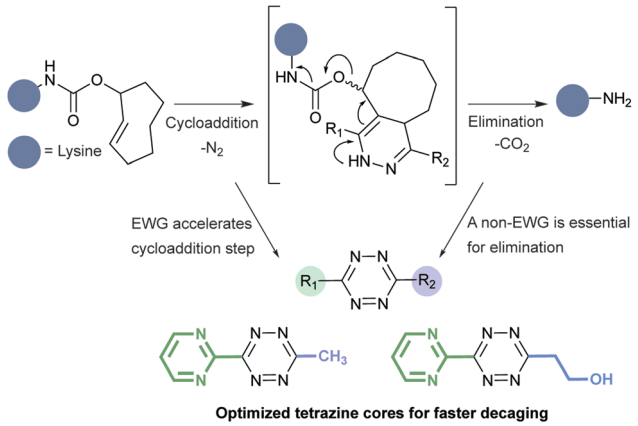

Fig. 54 Structure parameters determining the kinetics of TCO decaging.

of tetrazine suppress the elimination step by trapping the cycloaddition intermediate (Fig. 54). Based on these observations it was proposed that asymmetrical tetrazines with EWG and small-sized non-EWG could accelerate the cycloaddition and thus facilitate the elimination step. Remarkably, two pyrimidine substituted tetrazines showed excellent yields and very fast decaging efficiencies *in vitro* and in live cells. More than 90% decaging occurred after 5 min whereas the previously used dimethyl tetrazine gave only 58% decaged yield. The tetrazine TCO decaging reaction also outperformed the photo-decaging reaction in living cells, with 90% decaged protein after 4 min whereas only 38% decaged GFP was observed after 4 min UV irradiation.[349]

7.3 Vinyl-ether for function reactivation by IEDDA ligation

Apart from TCO derivatives, vinyl ethers could also serve as a masking group for alcohols.[350,351] Our group recently reported a vinyl ether decaging reaction on a cytotoxic drug for activation of a halogen-bearing duocarmycin derivative *via* a Winstein spirocyclization (Fig. 55). In cells the double prodrug showed similar cytotoxicity to the active drug. The broad applicability of this reaction on other chemotypes, including the protected amino acids serine and tyrosine, an 1,6-anhydro sugar, and a fluorophore, expand the scope and potential of this reaction for applications on proteins and glycans.[352]

Furthermore, based on the vinyl ether decaging chemistry, a tetrazine responsive self-immolative cleavable linker was developed by Bradley *et al.* to achieve molecular triggered drug delivery (Fig. 56a). Accordingly, the vinyl ether cleavable moiety

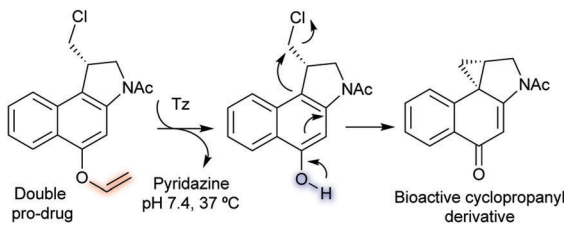

Fig. 55 The double pro-drug reacts with tetrazine leading to the formation of an intermediate that undergoes a Winstein spirocyclization to afford the bioactive cyclopropanyl duocarmycin analogue.

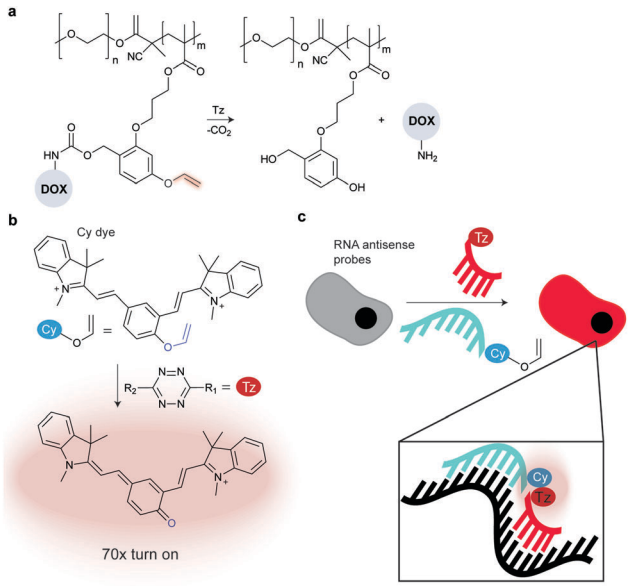

Fig. 56 (a) PEG polymer conjugated to a doxorubicin pro-drug through a self-immolative, which is eliminated upon reaction with tetrazine liberating the bioactive drug. (b) NIR-emitting vinyl ether cyanine dye activated by tetrazine reaction. (c) A fluorogenic NIR RNA-templated tetrazine uncaging probe could be used for cell imaging of mRNA.

was embedded on a PEG polymer and upon addition of tetrazine, the decaged prodrug could trigger 80% cell death with 48 h incubation.[353] Also recently, Devaraj *et al.* explored the vinyl ether decaging for mRNA detection. In particular, a caged near-infrared (NIR)-emitting cyanine dye was shown to restore the fluorescence by up to 70-fold after tetrazine reaction (Fig. 56b). Further this NIR fluorogenic probe was applied for mRNA detection *in vitro* and in cellular context (Fig. 56c).[354]

8. IEDDA reactions in materials and nanomaterials with biological applications

The aqueous compatibility of IEDDA reactions without involving any toxic catalyst or solvent makes it an optimal reaction for bio- and nanomaterial applications. Most importantly, due to its modular nature, IEDDA reactions allow the facile cross-linking of building blocks and thus enable an alternative way for the construction and modification of molecular structures. Another major advantage of IEDDA reactions is the facilitated purification since none of the conjugation partners has to be used in excess to reach fast reactions. Based on these favourable characteristics, the IEDDA reaction has been explored for biomaterials and nanomaterials preparation for applications in biology and medicine. Some examples of these applications are presented in the following sections.

8.1 Polymer hydrogel formation *via* IEDDA bioorthogonal reaction

Due to their high-water content, excellent mass transport properties, and tissue-like elasticity, ionically crosslinked

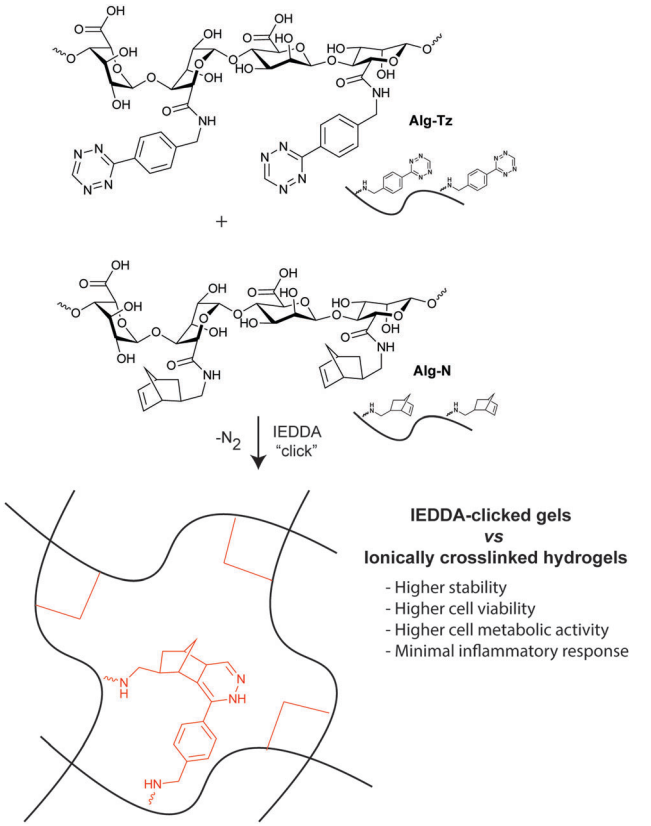

Fig. 57 Schematic of the click synthesis of alginate polymer. Coupling chemistry is used to modify alginate backbone carboxylic acids with tetrazine or norbornene, resulting in Alg–Tz or Alg–N polymers respectively. Alg–Tz and Alg–N polymers are reacted together to create a covalently crosslinked click alginate hydrogel network.

hydrogels have been used extensively to encapsulate cells and bioactive molecules (*e.g.* 3D cell culture and drug delivery *in vivo*) as well as for tissue engineering but so far, these polymers have been largely limited by low crosslinking efficiency and poor integrity of the resulting materials. To overcome these limitations, IEDDA ligation, along with other bioorthogonal reactions,[355] have been proposed as an alternative method for the synthesis of biocompatible hydrogels. In one example, Joshi *et al.* reported the synthesis of alginate hydrogels *via* tetrazine–norbornene bioorthogonal chemistry. By using tetrazine/norbornene alginate derivatives, the hydrogel could be prepared in 1 hour displaying tunable mechanical and swelling properties depending on the use of different tetrazine/norbornene alginate ratios (Fig. 57). Compared with the ionically crosslinked hydrogel, IEDDA-clicked gels showed higher cell viability and cell metabolic activity. Minimal inflammatory response and high stability was also observed after *in vivo* injections.

Furthermore, IEDDA combined with thiol–ene chemistry could serve as a robust reaction for further functionalization. Indeed, post-gelation modification could be introduced by functionalizing excess norbonene units with Cys-containing RGD peptide (RGDS) by thiol–ene chemistry. This construct showed 3-fold increase in cell adherence compared with unmodified gels.[356] In another example, Anseth *et al.* demonstrated that

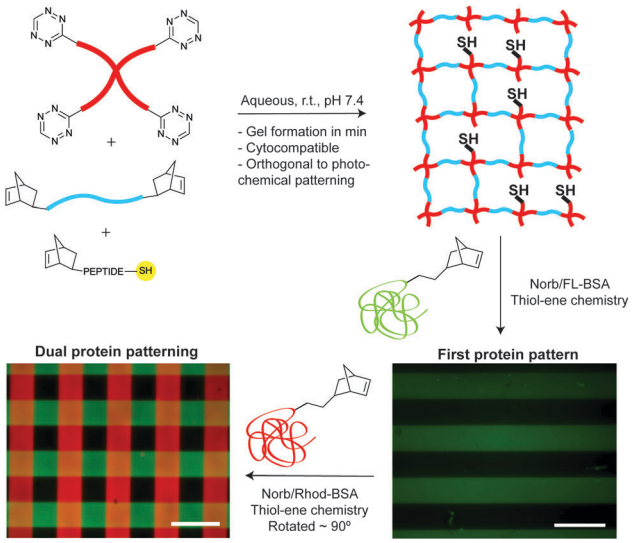

Fig. 58 Sequential biochemical patterning in tetrazine click gels. Tetrazine click hydrogels were formed to leave pendant thiols in the network for functionalization with fluorescent norbornene–BSA proteins by thiol–ene chemistry. Scalebars = 200 μm. Adapted with permission from ref. 357. Copyright 2013 American Chemical Society.

hydrogels formed by multi-functional PEG–tetrazine units could be functionalized with norbornene-containing peptides (*e.g.* an ECM mimetic cell degradable peptide, a RGDS peptide or a short peptide bearing a thiol group) for 3D cell culture. This hydrogel network formulated to have pendant thiols could be subsequently used for functionalization with fluorescein and rhodamine fluorescent norbornene-BSA proteins by photoinitiated thiol–ene click reaction with excellent pattern fidelity (Fig. 58).[357]

In order to develop a dual marking hydrogel system, Weissleder *et al.* encapsulated an X-ray radiography insoluble contrast agent and a pigment into a gelatin hydrogel, which was prepared by IEDDA reaction between tetrazine- and norbornene-modified gelatines. *In vivo* studies showed good performance for *in vivo* CT imaging and *ex vivo* visual localization of the radiopaque tinted hydrogel.[358] Double network (DN) hydrogels have also received much attention because of its high-water percentage (*ca.* 90 wt%) and high strength. In another work, Dove *et al.* reported the synthesis of a DN hydrogel in one-step under physiological conditions and within 3 min by using tetrazine–norbornene click reaction for formation of the loose network (norbornene-functionalized chitosan and a linear PEG ditetrazine) and thiol–ene chemistry for formation of the dense network (PEG–tetraalkyne and a linear PEG–dithiol). The resulting hydrogels exhibited excellent mechanical properties and display high cytocompatibility (>99% cell viability after 48 h).[359]

Due to its ability to coordinate with metal ions, PEG polymers terminally functionalized with bipyridyltetrazines could form multi-functional supermolecular gels in the presence of metal ions (Fe^{2+} and Ni^{2+}). This platform was explored to prepare metallo-hydrogel scaffolds for photo-triggered drug release (Fig. 59). This approach is, however, limited by slow photo release rates due to the competitive absorption from the dark-coloured gel, and thus, the development of new systems

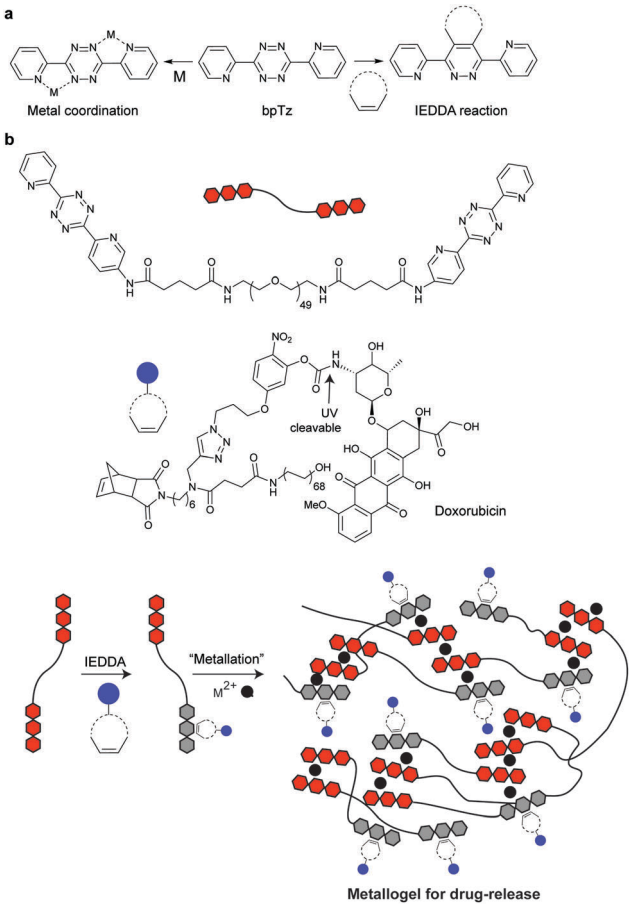

Fig. 59 Synthesis of metallo-hydrogels. (a) Diels–Alder reaction and metal coordination of bpTz. (b) Schematic representation of the drug release approach triggered by photo decaging from the metallo-hydrogel.

with alternative metals or ligands with desirable optical properties is demanded.[360]

The IEDDA reaction has also emerged as an important tool for producing microsphere hydrogels by interfacial crosslinking using a tetrazine-hyaluronic derivative (HA-Tz) and bis-TCO cross-linker (Fig. 60a and b). Covalent tagging with diffusible Alexa-TCO yielded shell- or core-labelled microspheres. Alternating the presence and absence of TCO-dye afford onion-like structures with 3, 5, and 7 layers (Fig. 60c). These 3D microspheres were tested for 3D culture of prostate cancer cells with good cell proliferation and viability (98% viable at 5 days). Notably, cells aggregated to form clusters instead of homogeneous disperse.[361]

8.2 Application of IEDDA reaction in polymer formation and modification

Tetrazine bioorthogonal reaction is increasingly being applied for polymer modification or polymer-polymer coupling. In 2011, O'Reilly demonstrated firstly the suitability of the IEDDA conjugation method for efficient synthesis of block copolymers.[362] Importantly, the norbornene–tetrazine combination was found to be compatible with the trithiocarbonate group in RAFT (reversible addition–fragmentation chain transfer polymerisation) chain transfer agents (Fig. 61).

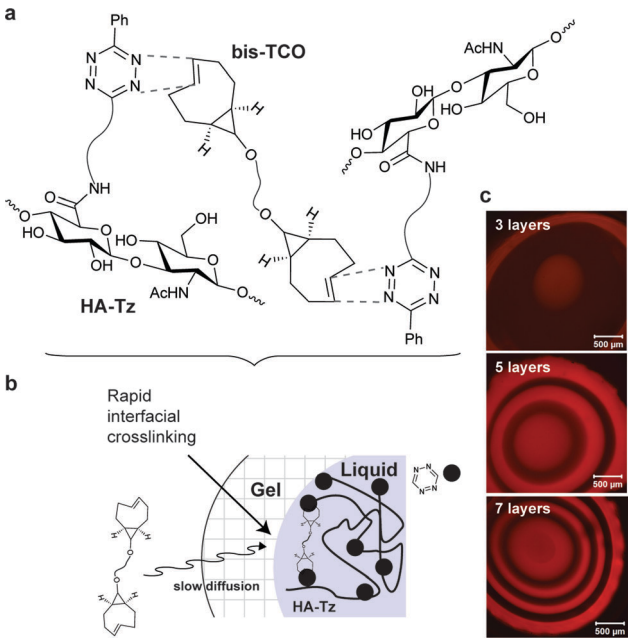

Fig. 60 Synthesis of microsphere hydrogels. (a) Instantaneous cross-linking *via* tetrazine–TCO ligation. (b) Gel interface forms when a droplet of tetrazine-modified hyaluronic (HA-Tz) contacts a solution of bis-TCO. Cross-linking at the gel/liquid interface is faster than the rate of diffusion through the gel interface. (c) Onion-like structures obtained by alternating the presence and absence of Alexa-TCO during the cross-linking procedure. Adapted with permission from ref. 361. Copyright 2014 American Chemical Society.

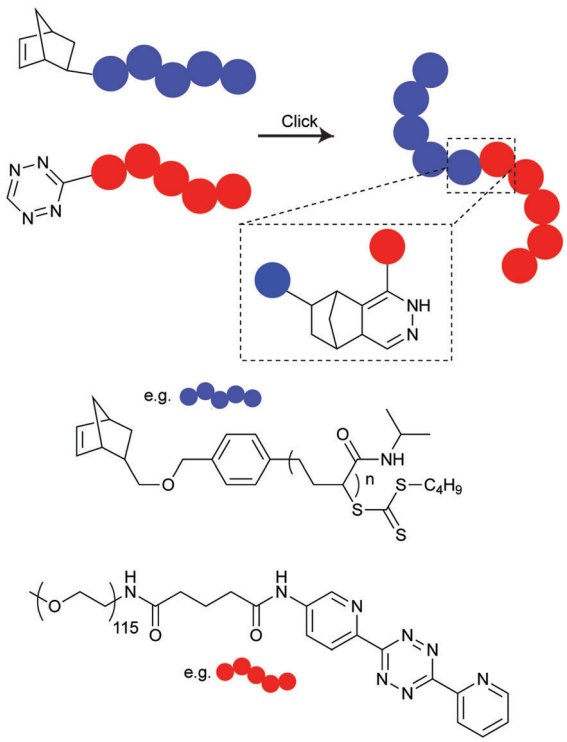

Fig. 61 Polymer–polymer coupling by norbornene–tetrazine reaction between norbornenyl-functionalized poly(styrene) trithiocarbonate and a tetrazine-functionalized PEG.

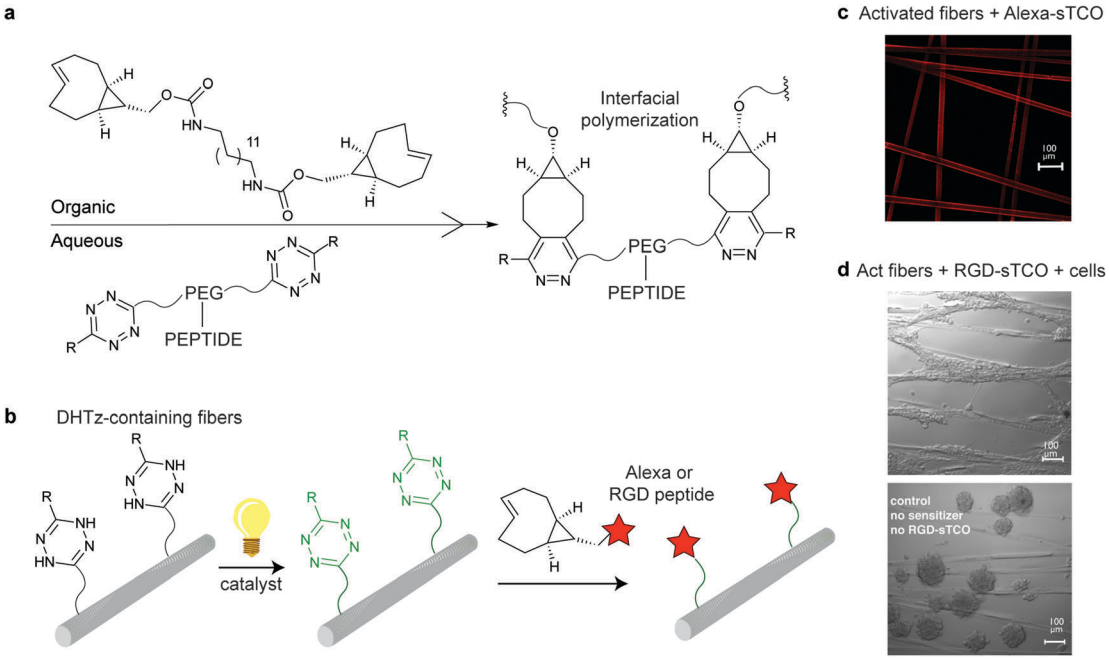

Fig. 62 Synthesis of copolymer fibres. (a) Interfacial polymerization between PEG tetrazine-derived monomer bearing peptides and bis-s-TCO. (b) Schematic representation of fibre photoactivation and subsequent conjugation. DHTz-containing fibres were irradiated with visible light and allowed to react with an s-TCO conjugate bearing fluorophores or cell adhesive peptides. (c) Confocal images (10×, scale bar 100 μm) of activated fibres that were treated with Alexa-s-TCO. (d) Confocal images (10×) of activated fibres that were treated with RGD-s-TCO. Cell culture with NIH 3T3 fibroblasts showed that the cells selectively adhered and spread on the fibres. Cell attachment and spreading on the fibres was not observed in control experiments. Adapted with permission from ref. 103. Copyright 2016 American Chemical Society.

Another application by Jia *et al.* describes the synthesis of multiblock copolymers through rapid tetrazine–TCO bioorthogonal polymerization (Fig. 62a). Further modification of the copolymer fibres with a fibronectin-derived cell adhesive peptide promotes the attachment and alignment of fibroblasts with various shapes and orientations, whereas when incubated with peptide-free fibres, cells remained round and unbound.[363] In a related paper, Fox *et al.* discovered that dihydrotetrazine could undergo photocatalytic oxidation to tetrazine thereby turning on its reactivity towards s-TCO (Fig. 62b). Interfacial polymerization between tetrazine-bearing monomers and bis-s-TCO monomers conjugated to dihydrotetrazine moieties (DHTz) produced dihydrotetrazine fibres (Fig. 62b), which could be further reacted with TCO bearing proteins, peptides and dyes (Fig. 62c) under irradiation with sensitizers. Notably, the fibres conjugated to a cell adhesive RGD peptide exhibited a dramatically increased ability to mediate contact guidance of cells (Fig. 62d).[103]

8.3 Application of IEDDA reaction in the synthesis of nanoparticles for biomedicine

Due to a large number of interesting properties (*e.g.* multivalent targeting capability, high payload, *etc.*), imaging and therapeutic nanoparticles have been widely used in nanomedicine research.[364] Quantum dots (QDs) are highly fluorescent nanoscale crystals with size-dependent emission spectra and excellent photophysical properties (*e.g.* high quantum yield, low photobleaching) that have been demonstrated to have several advantages over

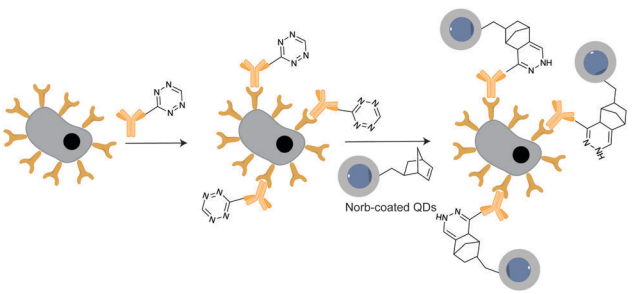

Fig. 63 Pre-targeting of EGFRs on live cells with a tetrazine-modified EGF antibody and labelling with norbornene-coated QDs.

fluorescent organic dyes for cell imaging.[365] The first proof of concept study using "bioorthogonal QD" was reported in 2010 by Bawendi *et al.* In this work norbornene-coated QDs were used to target cancer cells previously decorated with tetrazine-modified epidermal growth factor antibody (Fig. 63).[366] Similarly, Duda *et al.* conjugated tetrazine-modified antibodies to quantum dots modified with norbornene. Using these QD/antibody conjugates, the authors target a rare cell population in bone marrow at the single cell level in live animals using multiphoton microscopy.[367]

Beyond QDs Weissleder *et al.* described the use of magneto-fluorescent nanoparticles (MFNPs; fluorescent iron oxide nanoparticles) in different configurations to improve binding efficiency and cell detection for clinical diagnostics. This technique was referred to as 'bioorthogonal nanoparticle detection' (BOND).

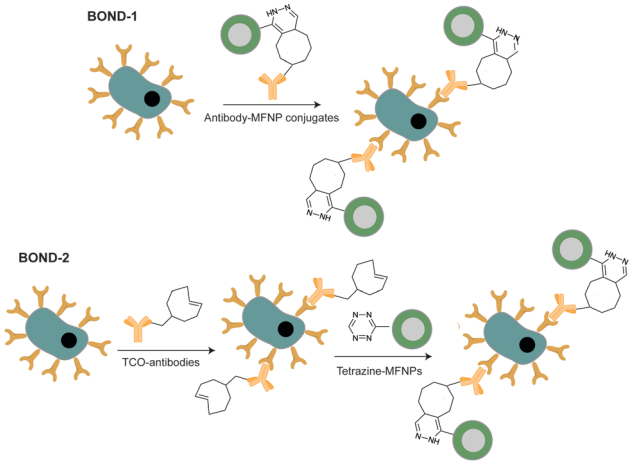

Fig. 64 "BOND" strategy. Antibodies against biomarkers are modified with TCO and used as scaffolds to deliver magnetic fluorescent nanoparticles (MFNPs) onto live cells through tetrazine reaction.

The rational for the development of this new methodology was that magnetic based sensing schemes benefit from high sensitivity, low cost, and the ability to perform measurements in samples that are not optically transparent. Their study compared two BOND assays to determine the ability to specifically target cancer cells. Cellular labelling was performed by exposing cells directly to antibody–MFNP conjugates (one step BOND-1 strategy) or by incubating cells first with TCO decorated antibodies, followed by tetrazine–MFNPs (two steps strategy: BOND-2) (Fig. 64).[288] The authors demonstrated that BOND-2 consistently yielded higher nanoparticle binding to cells by a factor of 10 to 15 compared to direct immuno-conjugates obtained from BOND-1 method.

Importantly, a similar two-step targeting strategy using avidin/biotin, although exceeds the direct "BOND-1 conjugate", falls behind BOND-2, which was attributed to the large size of avidin proteins blocking neighbouring biotin binding sites and potential constraining binding configurations. Using this system, different biomarkers of human circulating tumour cells were detected and evaluated *via* μ-nuclear magnetic resonance on clinical samples.[368–371] Alternatively, the Hall effect of MNP enables rapid and sensitive high-throughput screening on mammalian cells and bacteria.[372,373] Other medical applications of BOND-2 technique are on-chip detection of microvesicles liberated into the blood circulation from glioblastomas,[374] detection of microvesicle urinary markers,[375,376] and detection of mammalian and bacteria cells for diagnosis of infectious disease.[377–379] BOND-2 was also evaluated for cell tracking by spatiotemporally labelling with photoactivatable fluorophores,[380] and for targeting intracellular biomarkers in permeabilized and fixed cells by confocal fluorescence imaging and diagnostic magnetic resonance.[381] In one attempt to improve BOND-2 assay sensitivity and robustness, multiple consecutive conjugation steps of fluorescent nanoparticles containing TCO and tetrazine groups were used to amplify the corresponding signals.[382] Detection sensitivity could be increased up to 2 orders of magnitude over current method.

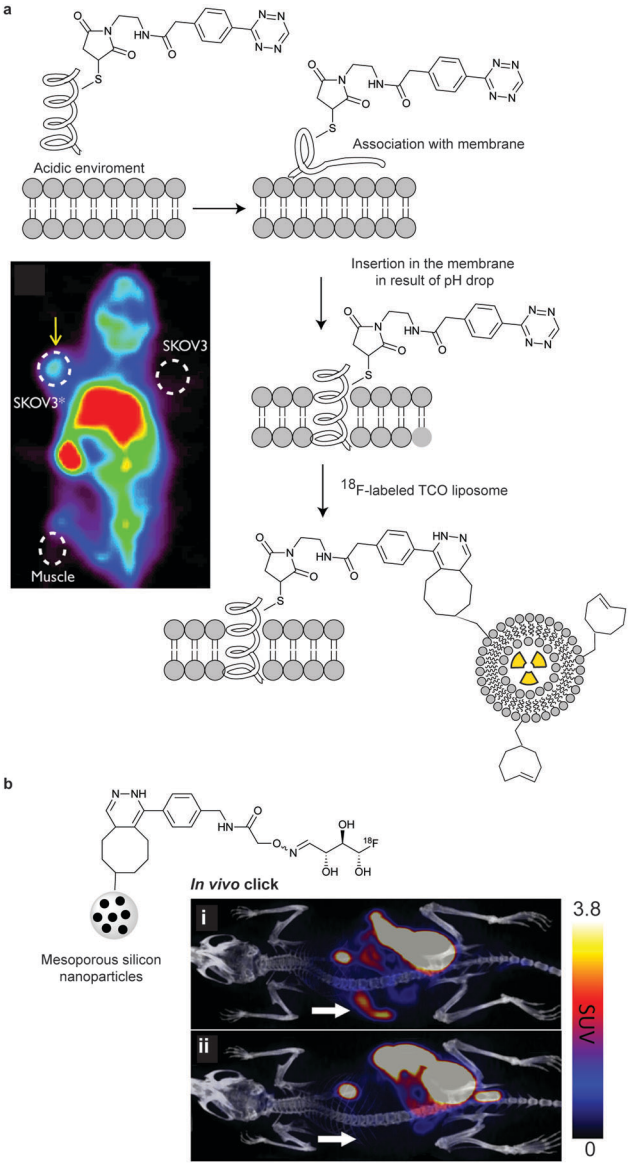

Fig. 65 Nanoparticle systems for radionuclide imaging. (a) *In vivo* pretargeting with liposomes. At low pH levels, the polar C-terminus of the peptide pHLIP–Tz changes its conformation to a helical structure, resulting in the insertion of the peptide into the cellular membrane. The tetrazine on the tumour surface can then be targeted by ^{18}F-labelled bioorthogonal liposomes bearing TCO groups (left shoulder, pre-injected intra-tumourally with pHLIP–Tz, SKOV3; right shoulder, untreated; bioorthogonally TCO liposomes encapsulating ^{18}F PET isotope were administered intravenously). Reprinted in part with permission from ref. 383. Copyright 2013 American Chemical Society. (b) Pretargeted PET–CT tracing of mesoporous silicon nanoparticles. (i) TCO-modified PSi-NPs were administered 15 min before the intravenous injection of the ^{18}F-tetrazine probe. (ii) Controls were injected only with ^{18}F-tetrazine. The arrows indicate the location of spleen, the expected target organ. Reprinted in part with permission from ref. 309. Copyright 2017 American Chemical Society.

There have also been many advances in the development of nanoparticle systems for *in vivo* radionuclide imaging. Liposomes are attractive nanoparticle vesicles considered promising systems for controlled drug delivery. Reiner *et al.* introduced in

2013 a dual-delivery pretargeting approach using a pH low insertion peptide conjugated to a tetrazine (pHLIP–Tz) to tether "TCO-liposomes" to tumour tissue in live animals (Fig. 65). The long circulating radiolabelled liposomes showed a significant accumulation in tumour sites mainly *via* enhanced permeability and retention (EPR) effect, after *in vivo* IEDDA click reaction between pHLIP–tetrazine and the ^{18}F-labelled liposomes bearing TCO lipids.[383] The described liposomes might be particularly useful for imaging the delivery of drugs immobilized either on the liposomal surface or in the endoliposomal space. Similarly, mesoporous silicon (PSi) is a very attractive material for targeted drug delivery in nanomedicine due to their biodegradability, low toxicity, and high drug loading capacity. Recently, Airaksinen *et al.* reported the first successful pretargeted PET imaging of TCO-modified mesoporous silicon nanoparticles (PSi-NPs), using ^{18}F-labelled tetrazine as a tracer. *In vivo* IEDDA reaction between the ^{18}F-Tz and TCOs on the surface of the PSi-NPs was fast and occurred within the first 10 min. Unfortunately, administration of the ^{18}F-Tz tracer 24 h after the injection of the nanoparticles, resulted in no reaction, suggesting *cis–trans* isomerisation *in vivo* of the TCO groups. Further optimization is still needed to maintain the high reactivity of TCO groups to permit pretargeted imaging over the course of days, which would be relevant for longer-circulating nanotheranostic agents.[309]

Carbon nanotubes (CNT) and graphene are another class of nanoparticles that have potential for biomedical applications. Functionalization of these nanocomposites using tetrazine-chemistry is described as a promising approach to control and manipulate their characteristics.[384–386] To the best of our knowledge, application of these constructs in a biomedical context is still to be explored.

Conclusions

Owing to its high selectivity, unparalleled fast kinetics, and free catalyst nature, the IEDDA reactions have emerged during the last decade as the state-of-the-art approach for selective modification of proteins in live cells and notably in animals. Herein we reviewed recent advances in this field with a focus on examples that highlight the utility of IEDDA ligations over other bioorthogonal reactions. The superfast kinetics and unique fluorogenicity makes IEDDA particularly suitable for super resolution imaging and tracking fast dynamics process in cells with minimal background. In addition, with the deepening understanding of IEDDA reactivity, researchers have realized that by choosing a fine-tuned tetrazine-dienophile pair, two parallel IEDDA reactions can be orthogonal to each other, which allows fast simultaneous multicolour labelling. Although recent developments are very promising a number of key challenges can be envisaged that must be addressed in the future. The fastest IEDDA ligations usually involve relatively large reactive groups, leading to higher chances of influencing biological processes. In addition, the hydrophobicity of large reporting groups could also be disadvantageous in certain circumstances, affording high nonspecific labelling. To circumvent this, a challenge lies in the development of small, reactive and hydrophilic dienophiles that possess at the same time high stability and permeability to achieve fast and selective labelling with minimal background. In this regard, the troublesome synthesis of the tetrazine and dienophiles partners, combined with their limited commercial availability, is still restraining IEDDA as a widely used tool.

In terms of pretargeting, the development of clearing agents introduced before administration of the radiolabelled probe results in improved tissue to non-tissue ratios with pronounced localization of radioactivity in the tumour. However, the next challenges lie in the modulation of the pharmacokinetics of the Tz/TCO components to reduce *in vivo* nonspecific accumulation of the IEDDA radio ligands. More attention should be also given to the therapeutic potential of pretargeted radio immunotherapy. It is envisaging that the use of radioligands with optimum pharmacokinetic profiles combined with clearing agents would substantially reduce accumulation in healthy tissues, maximizing the therapeutic efficacy and minimizing side effects. Regarding future perspectives, we anticipate the use of IEDDA reactions will go beyond the straightforward attachment of a given functional moiety to a protein of interest. There are already published work supporting that tetrazine decaging reactions will emerge as efficient tools for study for example the effect of PTMs on protein function and bioorthogonal drug activation. *In vivo* examples of ADCs containing a dienophile chemically linked to a prodrug could be already used for direct release of the drug after tumour binding triggered by the IEDDA reaction. Future studies will aim to optimize the therapeutic effect of this class of ADCs for pretargeting tumour treatment. In resume, the potential of IEDDA reactions are enormous and suggest a rich future of this bioorthogonal reaction in the field of chemical biology.

Acknowledgements

We thank the European Commission (Marie Skłodowska-Curie ITN Protein Conjugates; Marie Skłodowska-Curie IEF to B. L. O.), China Scholarship Council (PhD studentship to Z. G.), FCT Portugal (FCT Investigator to G. J. L. B.), and the EPSRC for financial support. We also thank Lavinia Dunsmore, Sarah Davies and Benjamin Stenton for helpful carefully reading the manuscript. G. J. L. B. is a Royal Society University Research Fellow and the recipient of a European Research Council Starting Grant (*TagIt*).

Notes and references

1 K. Lang and J. W. Chin, *Chem. Rev.*, 2014, **114**, 4764–4806.
2 O. Boutureira and G. J. L. Bernardes, *Chem. Rev.*, 2015, **115**, 2174–2195.
3 L. Xue, I. A. Karpenko, J. Hiblot and K. Johnsson, *Nat. Chem. Biol.*, 2015, **11**, 917–923.
4 J. Li and P. R. Chen, *Nat. Chem. Biol.*, 2016, **12**, 129–137.

5 N. Krall, F. P. da Cruz, O. Boutureira and G. J. L. Bernardes, *Nat. Chem.*, 2016, **8**, 103–113.
6 C. D. Spicer and B. G. Davis, *Nat. Commun.*, 2014, **5**, 4740.
7 O. S. Walker, S. J. Elsasser, M. Mahesh, M. Bachman, S. Balasubramanian and J. W. Chin, *J. Am. Chem. Soc.*, 2016, **138**, 718–721.
8 I. Nikic, T. Plass, O. Schraidt, J. Szymanski, J. A. Briggs, C. Schultz and E. A. Lemke, *Angew. Chem., Int. Ed.*, 2014, **53**, 2245–2249.
9 T. H. Wright, B. J. Bower, J. M. Chalker, G. J. L. Bernardes, R. Wiewiora, W. L. Ng, R. Raj, S. Faulkner, M. R. Vallee, A. Phanumartwiwath, O. D. Coleman, M. L. Thezenas, M. Khan, S. R. Galan, L. Lercher, M. W. Schombs, S. Gerstberger, M. E. Palm-Espling, A. J. Baldwin, B. M. Kessler, T. D. Claridge, S. Mohammed and B. G. Davis, *Science*, 2016, **354**, 597.
10 P. V. Robinson, C. T. Tsai, A. E. de Groot, J. L. McKechnie and C. R. Bertozzi, *J. Am. Chem. Soc.*, 2016, **138**, 10722–10725.
11 M. H. Wright, B. Clough, M. D. Rackham, K. Rangachari, J. A. Brannigan, M. Grainger, D. K. Moss, A. R. Bottrill, W. P. Heal, M. Broncel, R. A. Serwa, D. Brady, D. J. Mann, R. J. Leatherbarrow, R. Tewari, A. J. Wilkinson, A. A. Holder and E. W. Tate, *Nat. Chem.*, 2014, **6**, 112–121.
12 D. Rosner, T. Schneider, D. Schneider, M. Scheffner and A. Marx, *Nat. Protoc.*, 2015, **10**, 1594–1611.
13 N. Stefan, M. Zimmermann, M. Simon, U. Zangemeister-Wittke and A. Pluckthun, *Bioconjugate Chem.*, 2014, **25**, 2144–2156.
14 P. C. Trippier, *ChemMedChem*, 2013, **8**, 190–203.
15 R. Rossin, S. M. van Duijnhoven, W. Ten Hoeve, H. M. Janssen, L. H. Kleijn, F. J. Hoeben, R. M. Versteegen and M. S. Robillard, *Bioconjugate Chem.*, 2016, **27**, 1697–1706.
16 V. V. Rostovtsev, L. G. Green, V. V. Fokin and K. B. Sharpless, *Angew. Chem., Int. Ed.*, 2002, **41**, 2596–2599.
17 C. W. Tornoe, C. Christensen and M. Meldal, *J. Org. Chem.*, 2002, **67**, 3057–3064.
18 N. J. Agard, J. A. Prescher and C. R. Bertozzi, *J. Am. Chem. Soc.*, 2004, **126**, 15046–15047.
19 K. E. Beatty, J. D. Fisk, B. P. Smart, Y. Y. Lu, J. Szychowski, M. J. Hangauer, J. M. Baskin, C. R. Bertozzi and D. A. Tirrell, *Chembiochem*, 2010, **11**, 2092–2095.
20 B. Amgarten, R. Rajan, N. Martinez-Saez, B. L. Oliveira, I. S. Albuquerque, R. A. Brooks, D. G. Reid, M. J. Duer and G. J. L. Bernardes, *Chem. Commun.*, 2015, **51**, 5250–5252.
21 E. M. Sletten and C. R. Bertozzi, *Angew. Chem., Int. Ed.*, 2009, **48**, 6974–6998.
22 S. I. Presolski, V. Hong, S. H. Cho and M. G. Finn, *J. Am. Chem. Soc.*, 2010, **132**, 14570–14576.
23 D. Soriano Del Amo, W. Wang, H. Jiang, C. Besanceney, A. C. Yan, M. Levy, Y. Liu, F. L. Marlow and P. Wu, *J. Am. Chem. Soc.*, 2010, **132**, 16893–16899.
24 J. Dommerholt, F. P. Rutjes and F. L. van Delft, *Top. Curr. Chem.*, 2016, **374**, 16.
25 E. Saxon and C. R. Bertozzi, *Science*, 2000, **287**, 2007–2010.
26 B. L. Nilsson, L. L. Kiessling and R. T. Raines, *Org. Lett.*, 2000, **2**, 1939–1941.
27 E. Saxon, J. I. Armstrong and C. R. Bertozzi, *Org. Lett.*, 2000, **2**, 2141–2143.
28 S. S. van Berkel, M. B. van Eldijk and J. C. van Hest, *Angew. Chem., Int. Ed.*, 2011, **50**, 8806–8827.
29 J. Y. Axup, K. M. Bajjuri, M. Ritland, B. M. Hutchins, C. H. Kim, S. A. Kazane, R. Halder, J. S. Forsyth, A. F. Santidrian, K. Stafin, Y. Lu, H. Tran, A. J. Seller, S. L. Biroc, A. Szydlik, J. K. Pinkstaff, F. Tian, S. C. Sinha, B. Felding-Habermann, V. V. Smider and P. G. Schultz, *Proc. Natl. Acad. Sci. U. S. A.*, 2012, **109**, 16101–16106.
30 W. Song, Y. Wang, J. Qu, M. M. Madden and Q. Lin, *Angew. Chem., Int. Ed.*, 2008, **47**, 2832–2835.
31 A. Herner and Q. Lin, *Top. Curr. Chem.*, 2016, **374**, 1.
32 D. A. MacKenzie, A. R. Sherratt, M. Chigrinova, L. L. Cheung and J. P. Pezacki, *Curr. Opin. Chem. Biol.*, 2014, **21**, 81–88.
33 J. M. Chalker, C. S. Wood and B. G. Davis, *J. Am. Chem. Soc.*, 2009, **131**, 16346–16347.
34 N. Li, R. K. Lim, S. Edwardraja and Q. Lin, *J. Am. Chem. Soc.*, 2011, **133**, 15316–15319.
35 Y. A. Lin, J. M. Chalker, N. Floyd, G. J. L. Bernardes and B. G. Davis, *J. Am. Chem. Soc.*, 2008, **130**, 9642–9643.
36 M. Yang, J. Li and P. R. Chen, *Chem. Soc. Rev.*, 2014, **43**, 6511–6526.
37 R. A. Carboni and R. V. Lindsey, *J. Am. Chem. Soc.*, 1959, **81**, 4342–4346.
38 D. L. Boger, R. P. Schaum and R. M. Garbaccio, *J. Org. Chem.*, 1998, **63**, 6329–6337.
39 A. Hamasaki, R. Ducray and D. L. Boger, *J. Org. Chem.*, 2006, **71**, 185–193.
40 M. R. Karver, R. Weissleder and S. A. Hilderbrand, *Bioconjugate Chem.*, 2011, **22**, 2263–2270.
41 S. Jain, K. Neumann, Y. Zhang, J. Geng and M. Bradley, *Macromolecules*, 2016, **49**, 5438–5443.
42 D. Wang, W. Chen, Y. Zheng, C. Dai, K. Wang, B. Ke and B. Wang, *Org. Biomol. Chem.*, 2014, **12**, 3950–3955.
43 C. Li, H. X. Ge, B. Yin, M. Y. She, P. Liu, X. D. Li and J. L. Li, *RSC Adv.*, 2015, **5**, 12277–12286.
44 J. Balcar, G. Chrisam, F. X. Huber and J. Sauer, *Tetrahedron Lett.*, 1983, **24**, 1481–1484.
45 D. N. Kamber, Y. Liang, R. J. Blizzard, F. Liu, R. A. Mehl, K. N. Houk and J. A. Prescher, *J. Am. Chem. Soc.*, 2015, **137**, 8388–8391.
46 K. A. Horner, N. M. Valette and M. E. Webb, *Chem. – Eur. J.*, 2015, **21**, 14376–14381.
47 L. R. Domingo, M. T. Picher and J. A. Saez, *J. Org. Chem.*, 2009, **74**, 2726–2735.
48 J. Sauer and D. Lang, *Angew. Chem., Int. Ed. Engl.*, 1964, **76**, 603.
49 J. Sauer, D. K. Heldmann, J. Hetzenegger, J. Krauthan, H. Sichert and J. Schuster, *Eur. J. Org. Chem.*, 1998, 2885–2896.
50 J. Sauer, D. Lang and H. Wiest, *Chem. Ber.*, 1964, **97**, 3208–3218.
51 J. Sauer and G. Heinrichs, *Tetrahedron Lett.*, 1966, **7**, 4979.
52 D. K. Heldmann and J. Sauer, *Tetrahedron Lett.*, 1997, **38**, 5791–5794.

53 A. Meier and J. Sauer, *Tetrahedron Lett.*, 1990, **31**, 6855–6858.
54 K. Müller and J. Sauer, *Tetrahedron Lett.*, 1984, **25**, 2541–2544.
55 D. R. Soenen, J. M. Zimpleman and D. L. Boger, *J. Org. Chem.*, 2003, **68**, 3593–3598.
56 F. Thalhammer, U. Wallfahrer and J. Sauer, *Tetrahedron Lett.*, 1990, **31**, 6851–6854.
57 F. Liu, Y. Liang and K. N. Houk, *J. Am. Chem. Soc.*, 2014, **136**, 11483–11493.
58 F. Liu, R. S. Paton, S. Kim, Y. Liang and K. N. Houk, *J. Am. Chem. Soc.*, 2013, **135**, 15642–15649.
59 M. T. Taylor, M. L. Blackman, O. Dmitrenko and J. M. Fox, *J. Am. Chem. Soc.*, 2011, **133**, 9646–9649.
60 A. Darko, S. Wallace, O. Dmitrenko, M. M. Machovina, R. A. Mehl, J. W. Chin and J. M. Fox, *Chem. Sci.*, 2014, **5**, 3770–3776.
61 W. Chen, D. Wang, C. Dai, D. Hamelberg and B. Wang, *Chem. Commun.*, 2012, **48**, 1736–1738.
62 J. A. Wagner, D. Mercadante, I. Nikic, E. A. Lemke and F. Grater, *Chem. – Eur. J.*, 2015, **21**, 12431–12435.
63 J. E. Hoffmann, T. Plass, I. Nikic, I. V. Aramburu, C. Koehler, H. Gillandt, E. A. Lemke and C. Schultz, *Chem. – Eur. J.*, 2015, **21**, 12266–12270.
64 J. Li, S. Jia and P. R. Chen, *Nat. Chem. Biol.*, 2014, **10**, 1003–1005.
65 R. M. Versteegen, R. Rossin, W. ten Hoeve, H. M. Janssen and M. S. Robillard, *Angew. Chem., Int. Ed.*, 2013, **52**, 14112–14116.
66 M. Vrabel, P. Kolle, K. M. Brunner, M. J. Gattner, V. Lopez-Carrillo, R. de Vivie-Riedle and T. Carell, *Chem. – Eur. J.*, 2013, **19**, 13309–13312.
67 I. Nikic, J. H. Kang, G. E. Girona, I. V. Aramburu and E. A. Lemke, *Nat. Protoc.*, 2015, **10**, 780–791.
68 G. B. Cserep, O. Demeter, E. Batzner, M. Kallay, H. A. Wagenknecht and P. Kele, *Synthesis*, 2015, 2738–2744.
69 J. Yang, Y. Liang, J. Seckute, K. N. Houk and N. K. Devaraj, *Chem. – Eur. J.*, 2014, **20**, 3365–3375.
70 A. Meijer, S. Otto and J. B. F. N. Engberts, *J. Org. Chem.*, 1998, **63**, 8989–8994.
71 J. W. Wijnen, S. Zavarise, J. B. F. N. Engberts and M. Charton, *J. Org. Chem.*, 1996, **61**, 2001–2005.
72 K. Lang, L. Davis, J. Torres-Kolbus, C. Chou, A. Deiters and J. W. Chin, *Nat. Chem.*, 2012, **4**, 298–304.
73 M. A. Grishina, V. A. Potemkin, E. V. Bartashevich, A. N. Sinyaev, G. L. Rusinov, N. I. Latosh, I. N. Ganebnykh, O. V. Koryakova and R. I. Ishmetova, *J. Struct. Chem.*, 2006, **47**, 1155–1160.
74 A. Pinner, *Ber. Dtsch. Chem. Ges.*, 1893, **26**, 2126–2135.
75 P. Audebert, S. Sadki, F. Miomandre, G. Clavier, M. C. Vernieres, M. Saoud and P. Hapiot, *New J. Chem.*, 2004, **28**, 387–392.
76 N. O. Abdel, M. A. Kira and M. N. Tolba, *Tetrahedron Lett.*, 1968, **9**, 3871–3872.
77 J. F. Ding, Z. Li, Z. Cui, G. P. Robertson, N. H. Song, X. M. Du and L. Scoles, *J. Polym. Sci., Part A: Polym. Chem.*, 2011, **49**, 3374–3386.
78 M. Savastano, C. Bazzicalupi, C. Giorgi, C. Garcia-Gallarin, M. D. Lopez de la Torre, F. Pichierri, A. Bianchi and M. Melguizo, *Inorg. Chem.*, 2016, **55**, 8013–8024.
79 J. Yang, M. R. Karver, W. Li, S. Sahu and N. K. Devaraj, *Angew. Chem., Int. Ed.*, 2012, **51**, 5222–5225.
80 D. L. Alge, D. F. Donohue and K. S. Anseth, *Tetrahedron Lett.*, 2013, **54**, 5639–5641.
81 L. G. Meimetis, J. C. Carlson, R. J. Giedt, R. H. Kohler and R. Weissleder, *Angew. Chem., Int. Ed.*, 2014, **53**, 7531–7534.
82 J. C. Carlson, L. G. Meimetis, S. A. Hilderbrand and R. Weissleder, *Angew. Chem., Int. Ed.*, 2013, **52**, 6917–6920.
83 D. S. Liu, A. Tangpeerachaikul, R. Selvaraj, M. T. Taylor, J. M. Fox and A. Y. Ting, *J. Am. Chem. Soc.*, 2012, **134**, 792–795.
84 R. Stollé, *J. Prakt. Chem.*, 1906, **73**, 277–287.
85 D. Z. Wang, W. X. Chena, Y. Q. Zheng, C. F. Dai, L. F. Wang and B. H. Wang, *Heterocycl. Commun.*, 2013, **19**, 171–177.
86 E. Sagot, A. Le Roux, C. Soulivet, E. Pasquinet, D. Poullain, E. Girard and P. Palmas, *Tetrahedron*, 2007, **63**, 11189–11194.
87 S. G. Tolshchina, G. L. Rusinov and V. N. Charushin, *Chem. Heterocycl. Compd.*, 2013, **49**, 66–91.
88 Z. Novak and A. Kotschy, *Org. Lett.*, 2003, **5**, 3495–3497.
89 F. Suzenet, N. Leconte, A. Keromnes-Wuillaume and G. Guillaumet, *Synlett*, 2007, 0204–0210.
90 A. Wieczorek, P. Werther, J. Euchner and R. Wombacher, *Chem. Sci.*, 2017, **8**, 1506–1510.
91 Q. Zhou, P. Audebert, G. Clavier, F. Miomandre and J. Tang, *RSC Adv.*, 2014, **4**, 7193–7195.
92 C. Quinton, V. Alain-Rizzo, C. Dumas-Verdes, G. Clavier, L. Vignau and P. Audebert, *New J. Chem.*, 2015, **39**, 9700–9713.
93 H. Wu, J. Yang, J. Seckute and N. K. Devaraj, *Angew. Chem., Int. Ed.*, 2014, **53**, 5805–5809.
94 A. Wieczorek, T. Buckup and R. Wombacher, *Org. Biomol. Chem.*, 2014, **12**, 4177–4185.
95 G. Knorr, E. Kozma, A. Herner, E. A. Lemke and P. Kele, *Chem. – Eur. J.*, 2016, **22**, 8972–8979.
96 D. Nhu, S. Duffy, V. M. Avery, A. Hughes and J. B. Baell, *Bioorg. Med. Chem. Lett.*, 2010, **20**, 4496–4498.
97 J. Sauer, G. R. Pabst, U. Holland, H. S. Kim and S. Loebbecke, *Eur. J. Org. Chem.*, 2001, 697–706.
98 S. Pican, V. Lapinte, J. F. Pilard, E. Pasquinet, L. Beller, L. Fontaine and D. Poullain, *Synlett*, 2009, 731–734.
99 R. Selvaraj and J. M. Fox, *Tetrahedron Lett.*, 2014, **55**, 4795–4797.
100 M. L. Blackman, M. Royzen and J. M. Fox, *J. Am. Chem. Soc.*, 2008, **130**, 13518–13519.
101 S. A. Albu, S. A. Al-Karmi, A. Vito, J. P. Dzandzi, A. Zlitni, D. Beckford-Vera, M. Blacker, N. Janzen, R. M. Patel, A. Capretta and J. F. Valliant, *Bioconjugate Chem.*, 2016, **27**, 207–216.
102 J. P. Dzandzi, D. R. Beckford Vera, A. R. Genady, S. A. Albu, L. J. Eltringham-Smith, A. Capretta, W. P. Sheffield and J. F. Valliant, *J. Org. Chem.*, 2015, **80**, 7117–7125.
103 H. Zhang, W. S. Trout, S. Liu, G. A. Andrade, D. A. Hudson, S. L. Scinto, K. T. Dicker, Y. Li, N. Lazouski, J. Rosenthal, C. Thorpe, X. Jia and J. M. Fox, *J. Am. Chem. Soc.*, 2016, **138**, 5978–5983.
104 J. Yang, J. Seckute, C. M. Cole and N. K. Devaraj, *Angew. Chem., Int. Ed.*, 2012, **51**, 7476–7479.

105 D. N. Kamber, L. A. Nazarova, Y. Liang, S. A. Lopez, D. M. Patterson, H. W. Shih, K. N. Houk and J. A. Prescher, *J. Am. Chem. Soc.*, 2013, **135**, 13680–13683.
106 D. M. Patterson, L. A. Nazarova, B. Xie, D. N. Kamber and J. A. Prescher, *J. Am. Chem. Soc.*, 2012, **134**, 18638–18643.
107 A. K. Spate, H. Busskamp, A. Niederwieser, V. F. Schart, A. Marx and V. Wittmann, *Bioconjugate Chem.*, 2014, **25**, 147–154.
108 M. Royzen, G. P. Yap and J. M. Fox, *J. Am. Chem. Soc.*, 2008, **130**, 3760–3761.
109 D. Svatunek, C. Denk, V. Rosecker, B. Sohr, C. Hametner, G. Allmaier, J. Fröhlich and H. Mikula, *Monatsh. Chem.*, 2016, **147**, 579–585.
110 R. Rossin, S. M. van den Bosch, W. Ten Hoeve, M. Carvelli, R. M. Versteegen, J. Lub and M. S. Robillard, *Bioconjugate Chem.*, 2013, **24**, 1210–1217.
111 H. E. Murrey, J. C. Judkins, C. W. Am Ende, T. E. Ballard, Y. Fang, K. Riccardi, L. Di, E. R. Guilmette, J. W. Schwartz, J. M. Fox and D. S. Johnson, *J. Am. Chem. Soc.*, 2015, **137**, 11461–11475.
112 K. Lang, L. Davis, S. Wallace, M. Mahesh, D. J. Cox, M. L. Blackman, J. M. Fox and J. W. Chin, *J. Am. Chem. Soc.*, 2012, **134**, 10317–10320.
113 S. Eising, F. Lelivelt and K. M. Bonger, *Angew. Chem., Int. Ed.*, 2016, **55**, 12243–12247.
114 N. K. Devaraj, R. Weissleder and S. A. Hilderbrand, *Bioconjugate Chem.*, 2008, **19**, 2297–2299.
115 U. Rieder and N. W. Luedtke, *Angew. Chem., Int. Ed.*, 2014, **53**, 9168–9172.
116 J. M. Holstein, D. Stummer and A. Rentmeister, *Chem. Sci.*, 2015, **6**, 1362–1369.
117 A. Niederwieser, A. K. Spate, L. D. Nguyen, C. Jungst, W. Reutter and V. Wittmann, *Angew. Chem., Int. Ed.*, 2013, **52**, 4265–4268.
118 B. L. Oliveira, Z. Guo, O. Boutureira, A. Guerreiro, G. Jimenez-Oses and G. J. L. Bernardes, *Angew. Chem., Int. Ed.*, 2016, **55**, 14683–14687.
119 A. Borrmann, S. Milles, T. Plass, J. Dommerholt, J. M. Verkade, M. Wiessler, C. Schultz, J. C. van Hest, F. L. van Delft and E. A. Lemke, *ChemBioChem*, 2012, **13**, 2094–2099.
120 E. Kozma, I. Nikic, B. R. Varga, I. V. Aramburu, J. H. Kang, O. T. Fackler, E. A. Lemke and P. Kele, *ChemBioChem*, 2016, **17**, 1518–1524.
121 R. J. Blizzard, D. R. Backus, W. Brown, C. G. Bazewicz, Y. Li and R. A. Mehl, *J. Am. Chem. Soc.*, 2015, **137**, 10044–10047.
122 X. Li, X. Gao, W. Shi and H. Ma, *Chem. Rev.*, 2014, **114**, 590–659.
123 K. Sivakumar, F. Xie, B. M. Cash, S. Long, H. N. Barnhill and Q. Wang, *Org. Lett.*, 2004, **6**, 4603–4606.
124 J. J. Shie, Y. C. Liu, Y. M. Lee, C. Lim, J. M. Fang and C. H. Wong, *J. Am. Chem. Soc.*, 2014, **136**, 9953–9961.
125 Y. C. Chen, K. Tsao and J. W. Keillor, *Can. J. Chem.*, 2015, **93**, 389–398.
126 Z. Zhou and C. J. Fahrni, *J. Am. Chem. Soc.*, 2004, **126**, 8862–8863.
127 J. C. Jewett and C. R. Bertozzi, *Org. Lett.*, 2011, **13**, 5937–5939.
128 F. Friscourt, C. J. Fahrni and G. J. Boons, *J. Am. Chem. Soc.*, 2012, **134**, 18809–18815.
129 G. A. Lemieux, C. L. De Graffenried and C. R. Bertozzi, *J. Am. Chem. Soc.*, 2003, **125**, 4708–4709.
130 B. C. Gergely, H. András and K. Péter, *Methods Appl. Fluoresc.*, 2015, **3**, 042001.
131 P. Audebert, F. Miomandre, G. Clavier, M. C. Vernieres, S. Badre and R. Meallet-Renault, *Chem. – Eur. J.*, 2005, **11**, 5667–5673.
132 Yong-Hua Gong, Fabien Miomandre, R. Méallet-Renault, S. Badré, L. Galmiche, J. Tang, P. Audebert and G. Clavier, *Eur. J. Org. Chem.*, 2009, 6121–6128.
133 N. K. Devaraj, S. Hilderbrand, R. Upadhyay, R. Mazitschek and R. Weissleder, *Angew. Chem., Int. Ed.*, 2010, **49**, 2869–2872.
134 T. G. Kim, J. C. Castro, A. Loudet, J. G. Jiao, R. M. Hochstrasser, K. Burgess and M. R. Topp, *J. Phys. Chem. A*, 2006, **110**, 20–27.
135 X. Shang, X. Song, C. Faller, R. Lai, H. Li, R. Cerny, W. Niu and J. Guo, *Chem. Sci.*, 2017, **8**, 1141–1145.
136 A. Vazquez, R. Dzijak, M. Dracinsky, R. Rampmaier, S. J. Siegl and M. Vrabel, *Angew. Chem., Int. Ed.*, 2017, **56**, 1334–1337.
137 C. C. Liu and P. G. Schultz, *Annu. Rev. Biochem.*, 2010, **79**, 413–444.
138 J. Xie and P. G. Schultz, *Nat. Rev. Mol. Cell Biol.*, 2006, **7**, 775–782.
139 L. Davis and J. W. Chin, *Nat. Rev. Mol. Cell Biol.*, 2012, **13**, 168–182.
140 A. Gautier, D. P. Nguyen, H. Lusic, W. An, A. Deiters and J. W. Chin, *J. Am. Chem. Soc.*, 2010, **132**, 4086–4088.
141 A. Bianco, F. M. Townsley, S. Greiss, K. Lang and J. W. Chin, *Nat. Chem. Biol.*, 2012, **8**, 748–750.
142 S. Greiss and J. W. Chin, *J. Am. Chem. Soc.*, 2011, **133**, 14196–14199.
143 W. Wan, J. M. Tharp and W. R. Liu, *Biochim. Biophys. Acta*, 2014, **1844**, 1059–1070.
144 A. Dumas, L. Lercher, C. D. Spicer and B. G. Davis, *Chem. Sci.*, 2015, **6**, 50–69.
145 E. Kaya, M. Vrabel, C. Deiml, S. Prill, V. S. Fluxa and T. Carell, *Angew. Chem., Int. Ed.*, 2012, **51**, 4466–4469.
146 S. Schneider, M. J. Gattner, M. Vrabel, V. Flugel, V. Lopez-Carrillo, S. Prill and T. Carell, *ChemBioChem*, 2013, **14**, 2114–2118.
147 J. R. Kramer, B. Onoa, C. Bustamante and C. R. Bertozzi, *Proc. Natl. Acad. Sci. U. S. A.*, 2015, **112**, 12574–12579.
148 Y. Kurra, K. A. Odoi, Y. J. Lee, Y. Yang, T. Lu, S. E. Wheeler, J. Torres-Kolbus, A. Deiters and W. R. Liu, *Bioconjugate Chem.*, 2014, **25**, 1730–1738.
149 T. Plass, S. Milles, C. Koehler, J. Szymanski, R. Mueller, M. Wiessler, C. Schultz and E. A. Lemke, *Angew. Chem., Int. Ed.*, 2012, **51**, 4166–4170.
150 M. Baumdick, Y. Bruggemann, M. Schmick, G. Xouri, O. Sabet, L. Davis, J. W. Chin and P. I. Bastiaens, *eLife*, 2015, **4**, e12223.
151 A. Rutkowska, T. Plass, J. E. Hoffmann, D. A. Yushchenko, S. Feng and C. Schultz, *ChemBioChem*, 2014, **15**, 1765–1768.

152 C. Uttamapinant, J. D. Howe, K. Lang, V. Beranek, L. Davis, M. Mahesh, N. P. Barry and J. W. Chin, *J. Am. Chem. Soc.*, 2015, **137**, 4602–4605.
153 R. B. Cooley, P. A. Karplus and R. A. Mehl, *ChemBioChem*, 2014, **15**, 1810–1819.
154 Z. Yu, Y. Pan, Z. Wang, J. Wang and Q. Lin, *Angew. Chem., Int. Ed.*, 2012, **51**, 10600–10604.
155 T. S. Elliott, F. M. Townsley, A. Bianco, R. J. Ernst, A. Sachdeva, S. J. Elsasser, L. Davis, K. Lang, R. Pisa, S. Greiss, K. S. Lilley and J. W. Chin, *Nat. Biotechnol.*, 2014, **32**, 465–472.
156 T. S. Elliott, A. Bianco, F. M. Townsley, S. D. Fried and J. W. Chin, *Cell Chem. Biol.*, 2016, **23**, 805–815.
157 Y. J. Lee, Y. Kurra, Y. Yang, J. Torres-Kolbus, A. Deiters and W. R. Liu, *Chem. Commun.*, 2014, **50**, 13085–13088.
158 W. W. Wang, Y. Zeng, B. Wu, A. Deiters and W. R. Liu, *ACS Chem. Biol.*, 2016, **11**, 1973–1981.
159 Y. Yang, S. Lin, W. Lin and P. R. Chen, *ChemBioChem*, 2014, **15**, 1738–1743.
160 S. Lin, H. Yan, L. Li, M. Yang, B. Peng, S. Chen, W. Li and P. R. Chen, *Angew. Chem., Int. Ed.*, 2013, **52**, 13970–13974.
161 Y. H. Tsai, S. Essig, J. R. James, K. Lang and J. W. Chin, *Nat. Chem.*, 2015, **7**, 554–561.
162 T. Machida, K. Lang, L. Xue, J. W. Chin and N. Winssinger, *Bioconjugate Chem.*, 2015, **26**, 802–806.
163 T. Plass, S. Milles, C. Koehler, C. Schultz and E. A. Lemke, *Angew. Chem., Int. Ed.*, 2011, **50**, 3878–3881.
164 J. L. Seitchik, J. C. Peeler, M. T. Taylor, M. L. Blackman, T. W. Rhoads, R. B. Cooley, C. Refakis, J. M. Fox and R. A. Mehl, *J. Am. Chem. Soc.*, 2012, **134**, 2898–2901.
165 H. Neumann, K. Wang, L. Davis, M. Garcia-Alai and J. W. Chin, *Nature*, 2010, **464**, 441–444.
166 A. Sachdeva, K. Wang, T. Elliott and J. W. Chin, *J. Am. Chem. Soc.*, 2014, **136**, 7785–7788.
167 K. Wang, A. Sachdeva, D. J. Cox, N. M. Wilf, K. Lang, S. Wallace, R. A. Mehl and J. W. Chin, *Nat. Chem.*, 2014, **6**, 393–403.
168 C. Meyer, S. Liebscher and F. Bordusa, *Bioconjugate Chem.*, 2016, **27**, 47–53.
169 M. Best, A. Degen, M. Baalmann, T. T. Schmidt and R. Wombacher, *ChemBioChem*, 2015, **16**, 1158–1162.
170 J. K. Dozier, S. L. Khatwani, J. W. Wollack, Y. C. Wang, C. Schmidt-Dannert and M. D. Distefano, *Bioconjugate Chem.*, 2014, **25**, 1203–1212.
171 M. Rashidian, E. Keliher, M. Dougan, P. K. Juras, M. Cavallari, G. R. Wojtkiewicz, J. Jacobsen, J. G. Edens, J. M. Tas, G. Victora, R. Weissleder and H. Ploegh, *ACS Cent. Sci.*, 2015, **1**, 142–147.
172 M. Rashidian, E. J. Keliher, A. M. Bilate, J. N. Duarte, G. R. Wojtkiewicz, J. T. Jacobsen, J. Cragnolini, L. K. Swee, G. D. Victora, R. Weissleder and H. L. Ploegh, *Proc. Natl. Acad. Sci. U. S. A.*, 2015, **112**, 6146–6151.
173 J. E. Glasgow, M. L. Salit and J. R. Cochran, *J. Am. Chem. Soc.*, 2016, **138**, 7496–7499.
174 J. J. Gruskos, G. Zhang and D. Buccella, *J. Am. Chem. Soc.*, 2016, **138**, 14639–14649.
175 D. Schulz and A. Rentmeister, *Chembiochem*, 2014, **15**, 2342–2347.
176 S. Kath-Schorr, *Top. Curr. Chem.*, 2016, **374**, 4.
177 K. Gutsmiedl, C. T. Wirges, V. Ehmke and T. Carell, *Org. Lett.*, 2009, **11**, 2405–2408.
178 J. Schoch, S. Ameta and A. Jaschke, *Chem. Commun.*, 2011, **47**, 12536–12537.
179 A. M. Pyka, C. Domnick, F. Braun and S. Kath-Schorr, *Bioconjugate Chem.*, 2014, **25**, 1438–1443.
180 J. Schoch, M. Staudt, A. Samanta, M. Wiessler and A. Jaschke, *Bioconjugate Chem.*, 2012, **23**, 1382–1386.
181 J. M. Holstein and A. Rentmeister, *Methods*, 2016, **98**, 18–25.
182 S. Ameta, J. Becker and A. Jaschke, *Org. Biomol. Chem.*, 2014, **12**, 4701–4707.
183 P. N. Asare-Okai, E. Agustin, D. Fabris and M. Royzen, *Chem. Commun.*, 2014, **50**, 7844–7847.
184 J. M. Holstein, L. Anhauser and A. Rentmeister, *Angew. Chem., Int. Ed.*, 2016, **55**, 10899–10903.
185 J. M. Holstein, F. Muttach, S. H. H. Schiefelbein and A. Rentmeister, *Chem. – Eur. J.*, 2017, **23**, 6165–6173.
186 H. Busskamp, E. Batroff, A. Niederwieser, O. S. Abdel-Rahman, R. F. Winter, V. Wittmann and A. Marx, *Chem. Commun.*, 2014, **50**, 10827–10829.
187 M. Merkel, S. Arndt, D. Ploschik, G. B. Cserep, U. Wenge, P. Kele and H. A. Wagenknecht, *J. Org. Chem.*, 2016, **81**, 7527–7538.
188 J. Schoch and A. Jaschke, *RSC Adv.*, 2013, **3**, 4181–4183.
189 K. Wang, D. Wang, K. Ji, W. Chen, Y. Zheng, C. Dai and B. Wang, *Org. Biomol. Chem.*, 2015, **13**, 909–915.
190 X. Ren, A. H. El-Sagheer and T. Brown, *Analyst*, 2015, **140**, 2671–2678.
191 J. Schoch, M. Wiessler and A. Jaschke, *J. Am. Chem. Soc.*, 2010, **132**, 8846–8847.
192 M. L. Winz, E. C. Linder, T. Andre, J. Becker and A. Jaschke, *Nucleic Acids Res.*, 2015, **43**, e110.
193 C. Domnick, F. Eggert and S. Kath-Schorr, *Chem. Commun.*, 2015, **51**, 8253–8256.
194 F. Eggert and S. Kath-Schorr, *Chem. Commun.*, 2016, **52**, 7284–7287.
195 J. A. Prescher and C. R. Bertozzi, *Nat. Chem. Biol.*, 2005, **1**, 13–21.
196 A. Varki, *Glycobiology*, 2017, **27**, 3–49.
197 K. Ohtsubo and J. D. Marth, *Cell*, 2006, **126**, 855–867.
198 T. J. Sminia, H. Zuilhof and T. Wennekes, *Carbohydr. Res.*, 2016, **435**, 121–141.
199 C. M. Cole, J. Yang, J. Seckute and N. K. Devaraj, *ChemBioChem*, 2013, **14**, 205–208.
200 D. M. Patterson, K. A. Jones and J. A. Prescher, *Mol. BioSyst.*, 2014, **10**, 1693–1697.
201 D. C. Xiong, J. Zhu, M. J. Han, H. X. Luo, C. Wang, Y. Yu, Y. Ye, G. Tai and X. S. Ye, *Org. Biomol. Chem.*, 2015, **13**, 3911–3917.
202 A. K. Spate, V. F. Schart, J. Hafner, A. Niederwieser, T. U. Mayer and V. Wittmann, *Beilstein J. Org. Chem.*, 2014, **10**, 2235–2242.
203 F. Doll, A. Buntz, A. K. Spate, V. F. Schart, A. Timper, W. Schrimpf, C. R. Hauck, A. Zumbusch and V. Wittmann, *Angew. Chem., Int. Ed.*, 2016, **55**, 2262–2266.

204 A. K. Spate, V. F. Schart, S. Schollkopf, A. Niederwieser and V. Wittmann, *Chem. – Eur. J.*, 2014, **20**, 16502–16508.
205 A. K. Spate, J. E. Dold, E. Batroff, V. F. Schart, D. E. Wieland, O. R. Baudendistel and V. Wittmann, *ChemBioChem*, 2016, **17**, 1374–1383.
206 A. A. Neves, H. Stöckmann, Y. A. Wainman, J. C. H. Kuo, S. Fawcett, F. J. Leeper and K. M. Brindle, *Bioconjugate Chem.*, 2013, **24**, 934–941.
207 P. Agarwal, B. J. Beahm, P. Shieh and C. R. Bertozzi, *Angew. Chem., Int. Ed.*, 2015, **54**, 11504–11510.
208 S. E. Pidgeon and M. M. Pires, *Chem. Commun.*, 2015, **51**, 10330–10333.
209 H. C. Hang, J. P. Wilson and G. Charron, *Acc. Chem. Res.*, 2011, **44**, 699–708.
210 R. S. Erdmann, H. Takakura, A. D. Thompson, F. Rivera-Molina, E. S. Allgeyer, J. Bewersdorf, D. Toomre and A. Schepartz, *Angew. Chem., Int. Ed.*, 2014, **53**, 10242–10246.
211 S. P. Brown and A. B. Smith, 3rd, *J. Am. Chem. Soc.*, 2015, **137**, 4034–4037.
212 J. D. Thomas, H. Cui, P. J. North, T. Hofer, C. Rader and T. R. Burke, *Bioconjugate Chem.*, 2012, **23**, 2007–2013.
213 T. Peng and H. C. Hang, *J. Am. Chem. Soc.*, 2016, **138**, 14423–14433.
214 Z. Li, D. Wang, L. Li, S. Pan, Z. Na, C. Y. Tan and S. Q. Yao, *J. Am. Chem. Soc.*, 2014, **136**, 9990–9998.
215 J. Seckute, J. Yang and N. K. Devaraj, *Nucleic Acids Res.*, 2013, **41**, e148.
216 K. M. Dean and A. E. Palmer, *Nat. Chem. Biol.*, 2014, **10**, 512–523.
217 G. Lukinavicius, K. Umezawa, N. Olivier, A. Honigmann, G. Yang, T. Plass, V. Mueller, L. Reymond, I. R. Correa, Jr., Z. G. Luo, C. Schultz, E. A. Lemke, P. Heppenstall, C. Eggeling, S. Manley and K. Johnsson, *Nat. Chem.*, 2013, **5**, 132–139.
218 G. Lukinavicius, L. Reymond, E. D'Este, A. Masharina, F. Gottfert, H. Ta, A. Guther, M. Fournier, S. Rizzo, H. Waldmann, C. Blaukopf, C. Sommer, D. W. Gerlich, H. D. Arndt, S. W. Hell and K. Johnsson, *Nat. Methods*, 2014, **11**, 731–733.
219 T. S. Elliott, A. Bianco and J. W. Chin, *Curr. Opin. Chem. Biol.*, 2014, **21**, 154–160.
220 J. B. Grimm, B. P. English, J. Chen, J. P. Slaughter, Z. Zhang, A. Revyakin, R. Patel, J. J. Macklin, D. Normanno, R. H. Singer, T. Lionnet and L. D. Lavis, *Nat. Methods*, 2015, **12**, 244–250.
221 I. Nikic and E. A. Lemke, *Curr. Opin. Chem. Biol.*, 2015, **28**, 164–173.
222 I. Nikic, G. Estrada Girona, J. H. Kang, G. Paci, S. Mikhaleva, C. Koehler, N. V. Shymanska, C. Ventura Santos, D. Spitz and E. A. Lemke, *Angew. Chem., Int. Ed.*, 2016, **55**, 16172–16176.
223 M. Schurmann, P. Janning, S. Ziegler and H. Waldmann, *Cell Chem. Biol.*, 2016, **23**, 435–441.
224 A. Rutkowska, D. W. Thomson, J. Vappiani, T. Werner, K. M. Mueller, L. Dittus, J. Krause, M. Muelbaier, G. Bergamini and M. Bantscheff, *ACS Chem. Biol.*, 2016, **11**, 2541–2550.
225 K. S. Yang, G. Budin, T. Reiner, C. Vinegoni and R. Weissleder, *Angew. Chem., Int. Ed.*, 2012, **51**, 6598–6603.
226 J. T. Ngo and D. A. Tirrell, *Acc. Chem. Res.*, 2011, **44**, 677–685.
227 D. C. Dieterich, A. J. Link, J. Graumann, D. A. Tirrell and E. M. Schuman, *Proc. Natl. Acad. Sci. U. S. A.*, 2006, **103**, 9482–9487.
228 H. Wu, B. T. Cisneros, C. M. Cole and N. K. Devaraj, *J. Am. Chem. Soc.*, 2014, **136**, 17942–17945.
229 R. Weissleder and M. J. Pittet, *Nature*, 2008, **452**, 580–589.
230 M. L. James and S. S. Gambhir, *Physiol. Rev.*, 2012, **92**, 897–965.
231 J. R. Ballinger, *Semin. Nucl. Med.*, 2015, **45**, 470–478.
232 M. M. Khalil, J. L. Tremoleda, T. B. Bayomy and W. Gsell, *Int. J. Mol. Imaging*, 2011, **2011**, 796025.
233 O. Jacobson, D. O. Kiesewetter and X. Chen, *Bioconjugate Chem.*, 2015, **26**, 1–18.
234 E. W. Price and C. Orvig, *Chem. Soc. Rev.*, 2014, **43**, 260–290.
235 J. P. Holland, M. J. Williamson and J. S. Lewis, *Mol. Imaging*, 2010, **9**, 1–20.
236 C. Kai and C. Xiaoyuan, *Curr. Top. Med. Chem.*, 2010, **10**, 1227–1236.
237 S. Richter and F. Wuest, *Molecules*, 2014, **19**, 20536.
238 S. Preshlock, M. Tredwell and V. Gouverneur, *Chem. Rev.*, 2016, **116**, 719–766.
239 M. J. Adam and D. S. Wilbur, *Chem. Soc. Rev.*, 2005, **34**, 153–163.
240 D. Zeng, B. M. Zeglis, J. S. Lewis and C. J. Anderson, *J. Nucl. Med.*, 2013, **54**, 829–832.
241 J. Y. Choi and B. C. Lee, *Nucl. Med. Mol. Imaging*, 2015, **49**, 258–267.
242 J. Marik and J. L. Sutcliffe, *Tetrahedron Lett.*, 2006, **47**, 6681–6684.
243 H. S. Gill and J. Marik, *Nat. Protoc.*, 2011, **6**, 1718–1725.
244 S. Maschauer and O. Prante, *Carbohydr. Res.*, 2009, **344**, 753–761.
245 B. H. Rotstein, N. A. Stephenson, N. Vasdev and S. H. Liang, *Nat. Commun.*, 2014, **5**, 4365.
246 L. Mirfeizi, J. Walsh, H. Kolb, L. Campbell-Verduyn, R. A. Dierckx, B. L. Feringa, P. H. Elsinga, T. de Groot, I. Sannen, G. Bormans and S. Celen, *Nucl. Med. Biol.*, 2013, **40**, 710–716.
247 T. L. Mindt, H. Struthers, L. Brans, T. Anguelov, C. Schweinsberg, V. Maes, D. Tourwé and R. Schibli, *J. Am. Chem. Soc.*, 2006, **128**, 15096–15097.
248 V. Bouvet, M. Wuest and F. Wuest, *Org. Biomol. Chem.*, 2011, **9**, 7393–7399.
249 L. S. Campbell-Verduyn, L. Mirfeizi, A. K. Schoonen, R. A. Dierckx, P. H. Elsinga and B. L. Feringa, *Angew. Chem., Int. Ed.*, 2011, **50**, 11117–11120.
250 M. E. Martin, S. G. Parameswarappa, M. S. O'Dorisio, F. C. Pigge and M. K. Schultz, *Bioorg. Med. Chem. Lett.*, 2010, **20**, 4805–4807.
251 N. J. Baumhover, M. E. Martin, S. G. Parameswarappa, K. C. Kloepping, M. S. O'Dorisio, F. C. Pigge and

M. K. Schultz, *Bioorg. Med. Chem. Lett.*, 2011, **21**, 5757–5761.
252 R. D. Carpenter, S. H. Hausner and J. L. Sutcliffe, *ACS Med. Chem. Lett.*, 2011, **2**, 885–889.
253 K. Sachin, V. H. Jadhav, E.-M. Kim, H. L. Kim, S. B. Lee, H.-J. Jeong, S. T. Lim, M.-H. Sohn and D. W. Kim, *Bioconjugate Chem.*, 2012, **23**, 1680–1686.
254 J. M. Baskin, J. A. Prescher, S. T. Laughlin, N. J. Agard, P. V. Chang, I. A. Miller, A. Lo, J. A. Codelli and C. R. Bertozzi, *Proc. Natl. Acad. Sci. U. S. A.*, 2007, **104**, 16793–16797.
255 J. A. Codelli, J. M. Baskin, N. J. Agard and C. R. Bertozzi, *J. Am. Chem. Soc.*, 2008, **130**, 11486–11493.
256 B. L. Nilsson, L. L. Kiessling and R. T. Raines, *Org. Lett.*, 2000, **2**, 1939–1941.
257 M. Pretze, F. Wuest, T. Peppel, M. Köckerling and C. Mamat, *Tetrahedron Lett.*, 2010, **51**, 6410–6414.
258 L. Carroll, S. Boldon, R. Bejot, J. E. Moore, J. Declerck and V. Gouverneur, *Org. Biomol. Chem.*, 2011, **9**, 136–140.
259 M. Pretze, D. Pietzsch and C. Mamat, *Molecules*, 2013, **18**, 8618–8665.
260 M. Namavari, Z. Cheng, R. Zhang, A. De, J. Levi, J. K. Hoerner, S. S. Yaghoubi, F. A. Syud and S. S. Gambhir, *Bioconjugate Chem.*, 2009, **20**, 432–436.
261 R. R. Flavell, P. Kothari, M. Bar-Dagan, M. Synan, S. Vallabhajosula, J. M. Friedman, T. W. Muir and G. Ceccarini, *J. Am. Chem. Soc.*, 2008, **130**, 9106–9112.
262 M. Glaser, P. Iveson, S. Hoppmann, B. Indrevoll, A. Wilson, J. Arukwe, A. Danikas, R. Bhalla and D. Hiscock, *J. Nucl. Med.*, 2013, **54**, 1981–1988.
263 J. Jeon, B. Shen, L. Xiong, Z. Miao, K. H. Lee, J. Rao and F. T. Chin, *Bioconjugate Chem.*, 2012, **23**, 1902–1908.
264 J. A. H. Inkster, D. J. Colin and Y. Seimbille, *Org. Biomol. Chem.*, 2015, **13**, 3667–3676.
265 X. Su, K. Cheng, J. Jeon, B. Shen, G. T. Venturin, X. Hu, J. Rao, F. T. Chin, H. Wu and Z. Cheng, *Mol. Pharmaceutics*, 2014, **11**, 3947–3956.
266 R. Rossin, P. Renart Verkerk, S. M. van den Bosch, R. C. M. Vulders, I. Verel, J. Lub and M. S. Robillard, *Angew. Chem., Int. Ed.*, 2010, **49**, 3375–3378.
267 Z. Li, H. Cai, M. Hassink, M. L. Blackman, R. C. D. Brown, P. S. Conti and J. M. Fox, *Chem. Commun.*, 2010, **46**, 8043–8045.
268 L. Wyffels, D. Thomae, A. M. Waldron, J. Fissers, S. Dedeurwaerdere, P. Van der Veken, J. Joossens, S. Stroobants, K. Augustyns and S. Staelens, *Nucl. Med. Biol.*, 2014, **41**, 513–523.
269 R. Selvaraj, S. Liu, M. Hassink, C.-w. Huang, L.-p. Yap, R. Park, J. M. Fox, Z. Li and P. S. Conti, *Bioorg. Med. Chem. Lett.*, 2011, **21**, 5011–5014.
270 S. Liu, M. Hassink, R. Selvaraj, L.-P. Yap, R. Park, H. Wang, X. Chen, J. M. Fox, Z. Li and P. S. Conti, *Mol. Imaging*, 2013, **12**, 121–128.
271 Z. Wu, S. Liu, M. Hassink, I. Nair, R. Park, L. Li, I. Todorov, J. M. Fox, Z. Li, J. E. Shively, P. S. Conti and F. Kandeel, *J. Nucl. Med.*, 2013, **54**, 244–251.
272 Y. Wang, K. Lim, M. Normandin, X. Zhao, G. W. Cline and Y.-S. Ding, *Nucl. Med. Biol.*, 2012, **39**, 167–176.
273 B. Bernardim, P. M. S. D. Cal, M. J. Matos, B. L. Oliveira, N. Martínez-Sáez, I. S. Albuquerque, E. Perkins, F. Corzana, A. C. B. Burtoloso, G. Jiménez-Osés and G. J. L. Bernardes, *Nat. Commun.*, 2016, **7**, 13128.
274 P. M. S. D. Cal, G. J. L. Bernardes and P. M. P. Gois, *Angew. Chem., Int. Ed.*, 2014, **53**, 10585–10587.
275 T. Reiner, E. J. Keliher, S. Earley, B. Marinelli and R. Weissleder, *Angew. Chem., Int. Ed.*, 2011, **50**, 1922–1925.
276 M. T. Taylor, M. L. Blackman, O. Dmitrenko and J. M. Fox, *J. Am. Chem. Soc.*, 2011, **133**, 9646–9649.
277 M. Wang, D. Svatunek, K. Rohlfing, Y. Liu, H. Wang, B. Giglio, H. Yuan, Z. Wu, Z. Li and J. Fox, *Theranostics*, 2016, **6**, 887–895.
278 E. M. F. Billaud, E. Shahbazali, M. Ahamed, F. Cleeren, T. Noel, M. Koole, A. Verbruggen, V. Hessel and G. Bormans, *Chem. Sci.*, 2017, **8**, 1251–1258.
279 J. C. Knight, S. Richter, M. Wuest, J. D. Way and F. Wuest, *Org. Biomol. Chem.*, 2013, **11**, 3817–3825.
280 C. Denk, D. Svatunek, T. Filip, T. Wanek, D. Lumpi, J. Fröhlich, C. Kuntner and H. Mikula, *Angew. Chem., Int. Ed.*, 2014, **53**, 9655–9659.
281 J. Zhu, S. Li, C. Wangler, B. Wangler, R. Bruce Lennox and R. Schirrmacher, *Chem. Commun.*, 2015, **51**, 12415–12418.
282 O. Keinänen, X.-G. Li, N. K. Chenna, D. Lumen, J. Ott, C. F. M. Molthoff, M. Sarparanta, K. Helariutta, T. Vuorinen, A. D. Windhorst and A. J. Airaksinen, *ACS Med. Chem. Lett.*, 2016, **7**, 62–66.
283 M. Rashidian, L. Wang, J. G. Edens, J. T. Jacobsen, I. Hossain, Q. Wang, G. D. Victora, N. Vasdev, H. Ploegh and S. H. Liang, *Angew. Chem., Int. Ed.*, 2016, **55**, 528–533.
284 B. M. Zeglis, P. Mohindra, G. I. Weissmann, V. Divilov, S. A. Hilderbrand, R. Weissleder and J. S. Lewis, *Bioconjugate Chem.*, 2011, **22**, 2048–2059.
285 L. G. Meimetis, E. Boros, J. C. Carlson, C. Ran, P. Caravan and R. Weissleder, *Bioconjugate Chem.*, 2016, **27**, 257–263.
286 H. L. Evans, L. Carroll, E. O. Aboagye and A. C. Spivey, *J. Labelled Compd. Radiopharm.*, 2014, **57**, 291–297.
287 B. M. Zeglis, F. Emmetiere, N. Pillarsetty, R. Weissleder, J. S. Lewis and T. Reiner, *ChemistryOpen*, 2014, **3**, 48–53.
288 J. B. Haun, N. K. Devaraj, S. A. Hilderbrand, H. Lee and R. Weissleder, *Nat. Nanotechnol.*, 2010, **5**, 660–665.
289 T. Plass, S. Milles, C. Koehler, J. Szymański, R. Mueller, M. Wießler, C. Schultz and E. A. Lemke, *Angew. Chem., Int. Ed.*, 2012, **51**, 4166–4170.
290 J. C. Knight and B. Cornelissen, *Am. J. Nucl. Med. Mol. Imaging*, 2014, **4**, 96–113.
291 R. Rossin and M. S. Robillard, *Curr. Opin. Chem. Biol.*, 2014, **21**, 161–169.
292 D. B. Axworthy, J. M. Reno, M. D. Hylarides, R. W. Mallett, L. J. Theodore, L. M. Gustavson, F.-M. Su, L. J. Hobson, P. L. Beaumier and A. R. Fritzberg, *Proc. Natl. Acad. Sci. U. S. A.*, 2000, **97**, 1802–1807.

293 R. Rossin, S. M. van den Bosch, W. ten Hoeve, M. Carvelli, R. M. Versteegen, J. Lub and M. S. Robillard, *Bioconjugate Chem.*, 2013, **24**, 1210–1217.
294 R. Rossin, T. Läppchen, S. M. van den Bosch, R. Laforest and M. S. Robillard, *J. Nucl. Med.*, 2013, **54**, 1989–1995.
295 R. Rossin, S. M. J. van Duijnhoven, T. Läppchen, S. M. van den Bosch and M. S. Robillard, *Mol. Pharmaceutics*, 2014, **11**, 3090–3096.
296 S. M. J. van Duijnhoven, R. Rossin, S. M. van den Bosch, M. P. Wheatcroft, P. J. Hudson and M. S. Robillard, *J. Nucl. Med.*, 2015, **56**, 1422–1428.
297 M. Altai, A. Perols, M. Tsourma, B. Mitran, H. Honarvar, M. Robillard, R. Rossin, W. ten Hoeve, M. Lubberink, A. Orlova, A. E. Karlström and V. Tolmachev, *J. Nucl. Med.*, 2016, **57**, 431–436.
298 B. M. Zeglis, K. K. Sevak, T. Reiner, P. Mohindra, S. D. Carlin, P. Zanzonico, R. Weissleder and J. S. Lewis, *J. Nucl. Med.*, 2013, **54**, 1389–1396.
299 A. Yazdani, H. Bilton, A. Vito, A. R. Genady, S. M. Rathmann, Z. Ahmad, N. Janzen, S. Czorny, B. M. Zeglis, L. C. Francesconi and J. F. Valliant, *J. Med. Chem.*, 2016, **59**, 9381–9389.
300 B. E. Cook, P. Adumeau, R. Membreno, K. E. Carnazza, C. Brand, T. Reiner, B. J. Agnew, J. S. Lewis and B. M. Zeglis, *Bioconjugate Chem.*, 2016, **27**, 1789–1795.
301 P. Adumeau, K. E. Carnazza, C. Brand, S. D. Carlin, T. Reiner, B. J. Agnew, J. S. Lewis and B. M. Zeglis, *Theranostics*, 2016, **6**, 2267–2277.
302 M. H. Choi, H. E. Shim, S.-J. Yun, H. R. Kim, S. Mushtaq, C. H. Lee, S. H. Park, D. S. Choi, D.-E. Lee, E.-B. Byun, B.-S. Jang and J. Jeon, *Bioorg. Med. Chem.*, 2016, **24**, 2589–2594.
303 S. A. Albu, S. A. Al-Karmi, A. Vito, J. P. K. Dzandzi, A. Zlitni, D. Beckford-Vera, M. Blacker, N. Janzen, R. M. Patel, A. Capretta and J. F. Valliant, *Bioconjugate Chem.*, 2016, **27**, 207–216.
304 H. L. Evans, Q.-D. Nguyen, L. S. Carroll, M. Kaliszczak, F. J. Twyman, A. C. Spivey and E. O. Aboagye, *Chem. Commun.*, 2014, **50**, 9557–9560.
305 J. P. Meyer, J. L. Houghton, P. Kozlowski, D. Abdel-Atti, T. Reiner, N. V. Pillarsetty, W. W. Scholz, B. M. Zeglis and J. S. Lewis, *Bioconjugate Chem.*, 2016, **27**, 298–301.
306 N. K. Devaraj, G. M. Thurber, E. J. Keliher, B. Marinelli and R. Weissleder, *Proc. Natl. Acad. Sci. U. S. A.*, 2012, **109**, 4762–4767.
307 B. Nichols, Z. Qin, J. Yang, D. R. Vera and N. K. Devaraj, *Chem. Commun.*, 2014, **50**, 5215–5217.
308 M. M. Herth, V. L. Andersen, S. Lehel, J. Madsen, G. M. Knudsen and J. L. Kristensen, *Chem. Commun.*, 2013, **49**, 3805–3807.
309 O. Keinänen, E. M. Mäkilä, R. Lindgren, H. Virtanen, H. Liljenbäck, V. Oikonen, M. Sarparanta, C. Molthoff, A. D. Windhorst, A. Roivainen, J. J. Salonen and A. J. Airaksinen, *ACS Omega*, 2017, **2**, 62–69.
310 W. Ren, A. Ji, M. X. Wang and H. W. Ai, *ChemBioChem*, 2015, **16**, 2007–2010.
311 G. Zhang, J. Li, R. Xie, X. Fan, Y. Liu, S. Zheng, Y. Ge and P. R. Chen, *ACS Cent. Sci.*, 2016, **2**, 325–331.
312 E. Arbely, J. Torres-Kolbus, A. Deiters and J. W. Chin, *J. Am. Chem. Soc.*, 2012, **134**, 11912–11915.
313 D. P. Nguyen, M. Mahesh, S. J. Elsässer, S. M. Hancock, C. Uttamapinant and J. W. Chin, *J. Am. Chem. Soc.*, 2014, **136**, 2240–2243.
314 C. Streu and E. Meggers, *Angew. Chem., Int. Ed.*, 2006, **45**, 5645–5648.
315 T. Volker, F. Dempwolff, P. L. Graumann and E. Meggers, *Angew. Chem., Int. Ed.*, 2014, **53**, 10536–10540.
316 H. W. Ai, J. W. Lee and P. G. Schultz, *Chem. Commun.*, 2010, **46**, 5506–5508.
317 M. I. Sanchez, C. Penas, M. E. Vazquez and J. L. Mascarenas, *Chem. Sci.*, 2014, **5**, 1901–1907.
318 G. Y. Tonga, Y. Jeong, B. Duncan, T. Mizuhara, R. Mout, R. Das, S. T. Kim, Y. C. Yeh, B. Yan, S. Hou and V. M. Rotello, *Nat. Chem.*, 2015, **7**, 597–603.
319 H. T. Hsu, B. M. Trantow, R. M. Waymouth and P. A. Wender, *Bioconjugate Chem.*, 2016, **27**, 376–382.
320 K. K. Sadhu, E. Lindberg and N. Winssinger, *Chem. Commun.*, 2015, **51**, 16664–16666.
321 P. K. Sasmal, S. Carregal-Romero, W. J. Parak and E. Meggers, *Organometallics*, 2012, **31**, 5968–5970.
322 Y. Chen, A. S. Kamlet, J. B. Steinman and D. R. Liu, *Nat. Chem.*, 2011, **3**, 146–153.
323 F. Song, A. L. Garner and K. Koide, *J. Am. Chem. Soc.*, 2007, **129**, 12354–12355.
324 A. L. Garner, F. Song and K. Koide, *J. Am. Chem. Soc.*, 2009, **131**, 5163–5171.
325 R. M. Yusop, A. Unciti-Broceta, E. M. Johansson, R. M. Sanchez-Martin and M. Bradley, *Nat. Chem.*, 2011, **3**, 239–243.
326 M. Santra, S. K. Ko, I. Shin and K. H. Ahn, *Chem. Commun.*, 2010, **46**, 3964–3966.
327 J. T. Weiss, J. C. Dawson, K. G. Macleod, W. Rybski, C. Fraser, C. Torres-Sanchez, E. E. Patton, M. Bradley, N. O. Carragher and A. Unciti-Broceta, *Nat. Commun.*, 2014, **5**, 3277.
328 J. T. Weiss, J. C. Dawson, C. Fraser, W. Rybski, C. Torres-Sanchez, M. Bradley, E. E. Patton, N. O. Carragher and A. Unciti-Broceta, *J. Med. Chem.*, 2014, **57**, 5395–5404.
329 J. Li, J. Yu, J. Zhao, J. Wang, S. Zheng, S. Lin, L. Chen, M. Yang, S. Jia, X. Zhang and P. R. Chen, *Nat. Chem.*, 2014, **6**, 352–361.
330 J. Wang, B. Cheng, J. Li, Z. Zhang, W. Hong, X. Chen and P. R. Chen, *Angew. Chem., Int. Ed.*, 2015, **54**, 5364–5368.
331 J. Wang, S. Zheng, Y. Liu, Z. Zhang, Z. Lin, J. Li, G. Zhang, X. Wang, J. Li and P. R. Chen, *J. Am. Chem. Soc.*, 2016, **138**, 15118–15121.
332 R. Friedman Ohana, S. Levin, M. G. Wood, K. Zimmerman, M. L. Dart, M. K. Schwinn, T. A. Kirkland, R. Hurst, H. T. Uyeda, L. P. Encell and K. V. Wood, *ACS Chem. Biol.*, 2016, **11**, 2608–2617.
333 M. Santra, D. Ryu, A. Chatterjee, S. K. Ko, I. Shin and K. H. Ahn, *Chem. Commun.*, 2009, 2115–2117, DOI: 10.1039/b900380k.

334 A. A. Kislukhin, V. P. Hong, K. E. Breitenkamp and M. G. Finn, *Bioconjugate Chem.*, 2013, **24**, 684–689.
335 M. Taki, S. Iyoshi, A. Ojida, I. Hamachi and Y. Yamamoto, *J. Am. Chem. Soc.*, 2010, **132**, 5938–5939.
336 P. K. Sasmal, S. Carregal-Romero, A. A. Han, C. N. Streu, Z. Lin, K. Namikawa, S. L. Elliott, R. W. Koster, W. J. Parak and E. Meggers, *Chembiochem*, 2012, **13**, 1116–1120.
337 H. Y. Au-Yeung, E. J. New and C. J. Chang, *Chem. Commun.*, 2012, **48**, 5268–5270.
338 J. Kim and C. R. Bertozzi, *Angew. Chem., Int. Ed.*, 2015, **54**, 15777–15781.
339 R. van Brakel, R. C. Vulders, R. J. Bokdam, H. Grull and M. S. Robillard, *Bioconjugate Chem.*, 2008, **19**, 714–718.
340 K. Gorska, A. Manicardi, S. Barluenga and N. Winssinger, *Chem. Commun.*, 2011, **47**, 4364–4366.
341 J. B. Pawlak, G. P. Gential, T. J. Ruckwardt, J. S. Bremmers, N. J. Meeuwenoord, F. A. Ossendorp, H. S. Overkleeft, D. V. Filippov and S. I. van Kasteren, *Angew. Chem., Int. Ed.*, 2015, **54**, 5628–5631.
342 S. S. Matikonda, D. L. Orsi, V. Staudacher, I. A. Jenkins, F. Fiedler, J. Y. Chen and A. B. Gamble, *Chem. Sci.*, 2015, **6**, 1212–1218.
343 Y. Ge, X. Fan and P. R. Chen, *Chem. Sci.*, 2016, **7**, 7055–7060.
344 I. Khan, P. F. Agris, M. V. Yigit and M. Royzen, *Chem. Commun.*, 2016, **52**, 6174–6177.
345 J. M. Mejia Oneto, I. Khan, L. Seebald and M. Royzen, *ACS Cent. Sci.*, 2016, **2**, 476–482.
346 J. Li, S. Jia and P. R. Chen, *Nat. Chem. Biol.*, 2014, **10**, 1003–1005.
347 E. Agustin, P. N. Asare Okai, I. Khan, M. R. Miller, R. Wang, J. Sheng and M. Royzen, *Chem. Commun.*, 2016, **52**, 1405–1408.
348 A. K. Steiger, Y. Yang, M. Royzen and M. D. Pluth, *Chem. Commun.*, 2017, **53**, 1378–1380.
349 X. Fan, Y. Ge, F. Lin, Y. Yang, G. Zhang, W. S. Ngai, Z. Lin, S. Zheng, J. Wang, J. Zhao, J. Li and P. R. Chen, *Angew. Chem., Int. Ed.*, 2016, **55**, 14046–14050.
350 A. Hamasaki, R. Ducray and D. L. Boger, *J. Org. Chem.*, 2006, **71**, 185–193.
351 D. L. Boger and S. M. Sakya, *J. Org. Chem.*, 1988, **53**, 1415–1423.
352 E. Jimenez-Moreno, Z. Guo, B. L. Oliveira, I. S. Albuquerque, A. Kitowski, A. Guerreiro, O. Boutureira, T. Rodrigues, G. Jimenez-Oses and G. J. Bernardes, *Angew. Chem., Int. Ed.*, 2017, **56**, 243–247.
353 K. Neumann, S. Jain, A. Gambardella, S. Walker, E. Valero, A. Lilienkampf and M. Bradley, *Chembiochem*, 2016, **18**, 91–95.
354 H. Wu, S. C. Alexander, S. Jin and N. K. Devaraj, *J. Am. Chem. Soc.*, 2016, **138**, 11429–11432.
355 C. A. DeForest and K. S. Anseth, *Nat. Chem.*, 2011, **3**, 925–931.
356 R. M. Desai, S. T. Koshy, S. A. Hilderbrand, D. J. Mooney and N. S. Joshi, *Biomaterials*, 2015, **50**, 30–37.
357 D. L. Alge, M. A. Azagarsamy, D. F. Donohue and K. S. Anseth, *Biomacromolecules*, 2013, **14**, 949–953.
358 S. Hong, J. Carlson, H. Lee and R. Weissleder, *Adv. Healthcare Mater.*, 2016, **5**, 421–426.
359 V. X. Truong, M. P. Ablett, S. M. Richardson, J. A. Hoyland and A. P. Dove, *J. Am. Chem. Soc.*, 2015, **137**, 1618–1622.
360 K. Kawamoto, S. C. Grindy, J. Liu, N. Holten-Andersen and J. A. Johnson, *ACS Macro Lett.*, 2015, **4**, 458–461.
361 H. Zhang, K. T. Dicker, X. Xu, X. Jia and J. M. Fox, *ACS Macro Lett.*, 2014, **3**, 727–731.
362 C. F. Hansell, P. Espeel, M. M. Stamenovic, I. A. Barker, A. P. Dove, F. E. Du Prez and R. K. O'Reilly, *J. Am. Chem. Soc.*, 2011, **133**, 13828–13831.
363 S. Liu, H. Zhang, R. A. Remy, F. Deng, M. E. Mackay, J. M. Fox and X. Jia, *Adv. Mater.*, 2015, **27**, 2783–2790.
364 O. Salata, *J. Nanobiotechnol.*, 2004, **2**, 3.
365 U. Resch-Genger, M. Grabolle, S. Cavaliere-Jaricot, R. Nitschke and T. Nann, *Nat. Methods*, 2008, **5**, 763–775.
366 H. S. Han, N. K. Devaraj, J. Lee, S. A. Hilderbrand, R. Weissleder and M. G. Bawendi, *J. Am. Chem. Soc.*, 2010, **132**, 7838–7839.
367 H. S. Han, E. Niemeyer, Y. Huang, W. S. Kamoun, J. D. Martin, J. Bhaumik, Y. Chen, S. Roberge, J. Cui, M. R. Martin, D. Fukumura, R. K. Jain, M. G. Bawendi and D. G. Duda, *Proc. Natl. Acad. Sci. U. S. A.*, 2015, **112**, 1350–1355.
368 A. A. Ghazani, C. M. Castro, R. Gorbatov, H. Lee and R. Weissleder, *Neoplasia*, 2012, **14**, 388–395.
369 A. A. Ghazani, S. McDermott, M. Pectasides, M. Sebas, M. Mino-Kenudson, H. Lee, R. Weissleder and C. M. Castro, *Nanomedicine*, 2013, **9**, 1009–1017.
370 A. A. Ghazani, M. Pectasides, A. Sharma, C. M. Castro, M. Mino-Kenudson, H. Lee, J. A. Shepard and R. Weissleder, *Nanomedicine*, 2014, **10**, 661–668.
371 J. B. Haun, C. M. Castro, R. Wang, V. M. Peterson, B. S. Marinelli, H. Lee and R. Weissleder, *Sci. Transl. Med.*, 2011, **3**, 71ra16.
372 D. Issadore, J. Chung, H. Shao, M. Liong, A. A. Ghazani, C. M. Castro, R. Weissleder and H. Lee, *Sci. Transl. Med.*, 2012, **4**, 141ra192.
373 D. Issadore, H. J. Chung, J. Chung, G. Budin, R. Weissleder and H. Lee, *Adv. Healthcare Mater.*, 2013, **2**, 1224–1228.
374 H. Shao, J. Chung, L. Balaj, A. Charest, D. D. Bigner, B. S. Carter, F. H. Hochberg, X. O. Breakefield, R. Weissleder and H. Lee, *Nat. Med.*, 2012, **18**, 1835–1840.
375 J. Rho, J. Chung, H. Im, M. Liong, H. Shao, C. M. Castro, R. Weissleder and H. Lee, *ACS Nano*, 2013, **7**, 11227–11233.
376 H. J. Chung, K. L. Pellegrini, J. Chung, K. Wanigasuriya, I. Jayawardene, K. Lee, H. Lee, V. S. Vaidya and R. Weissleder, *PLoS One*, 2015, **10**, e0133417.
377 M. Liong, M. Fernandez-Suarez, D. Issadore, C. Min, C. Tassa, T. Reiner, S. M. Fortune, M. Toner, H. Lee and R. Weissleder, *Bioconjugate Chem.*, 2011, **22**, 2390–2394.
378 H. J. Chung, T. Reiner, G. Budin, C. Min, M. Liong, D. Issadore, H. Lee and R. Weissleder, *ACS Nano*, 2011, **5**, 8834–8841.
379 G. Budin, H. J. Chung, H. Lee and R. Weissleder, *Angew. Chem., Int. Ed.*, 2012, **51**, 7752–7755.
380 S. S. Agasti, R. H. Kohler, M. Liong, V. M. Peterson, H. Lee and R. Weissleder, *Small*, 2013, **9**, 222–227.

381 J. B. Haun, N. K. Devaraj, B. S. Marinelli, H. Lee and R. Weissleder, *ACS Nano*, 2011, **5**, 3204–3213.
382 V. M. Peterson, C. M. Castro, H. Lee and R. Weissleder, *ACS Nano*, 2012, **6**, 3506–3513.
383 F. Emmetiere, C. Irwin, N. T. Viola-Villegas, V. Longo, S. M. Cheal, P. Zanzonico, N. Pillarsetty, W. A. Weber, J. S. Lewis and T. Reiner, *Bioconjugate Chem.*, 2013, **24**, 1784–1789.
384 J. Li, M. Li, L. L. Zhou, S. Y. Lang, H. Y. Lu, D. Wang, C. F. Chen and L. J. Wan, *J. Am. Chem. Soc.*, 2016, **138**, 7448–7451.
385 J. Zhu, J. Hiltz, M. A. Mezour, V. Bernard-Gauthier, R. B. Lennox and R. Schirrmacher, *Chem. Mater.*, 2014, **26**, 5058–5062.
386 J. Zhu, J. Hiltz, R. B. Lennox and R. Schirrmacher, *Chem. Commun.*, 2013, **49**, 10275–10277.